Università degli Studi di Ferrara

DOTTORATO DI RICERCA IN
"SCIENZE CHIMICHE"

CICLO XXXVI

COORDINATORE
Prof. Massi Alessandro

New approaches on CO_2 reutilization for cyclic carbonates synthesis: catalysis and process intensification

Settore Scientifico Disciplinare

CHIM/06

Dottoranda

Rovegno Caterina

Tutore

Prof. Massi Alessandro

Co-tutori

Dr. Dambruoso Paolo

Prof.ssa Polo Eleonora

Anni 2020-2023

Table of contents

1. Introduction

1.1 Global scenario

Climate changes are affecting the population with increasing frequency and seriousness of extreme events every year. Considering only the European territory, the number of intense climate events (*e.g.* severe wind gusts, heavy snowfalls/snowstorms, ice accumulations, avalanches, damaging lightning strikes) dramatically grew in the last twenty-three years, as it has been reported in Figure 1 and in Table 1, showing data from the *European Severe Weather Database* (ESWD)[1] drafted by the *European Severe Storms Laboratory* (ESSL).

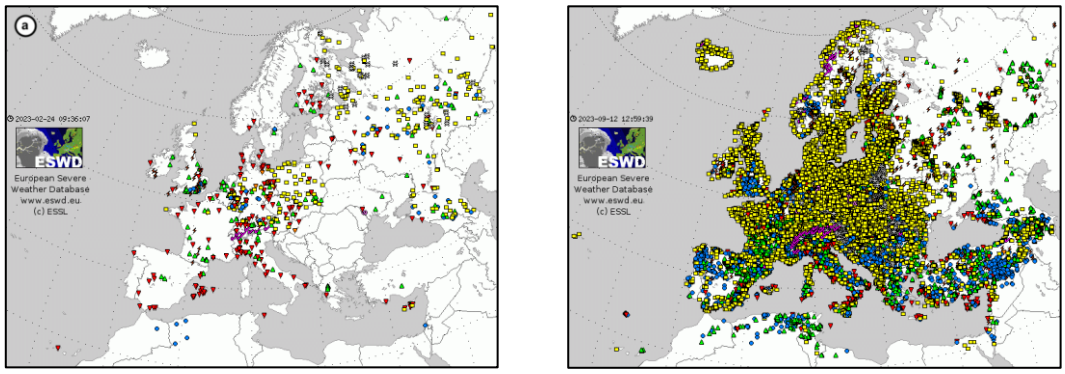

Figure 1 Geographic localization of severe climate events recorded in Europe and reported by the ESWD[1] in the period: a) 1st January 2000 - 31st December 2000 (on the left); b) 1st January 2023 - 31st August 2023 (on the right).

Table 1 Extreme climate events recorded in Europe, reported by the ESWD[1].

Period of time	Number of extreme climates events[a]
1st January 2000 - 31st December 2000	836
1st January 2005 - 31st December 2005	1917
1st January 2010 - 31st December 2010	6266
1st January 2015 - 31st December 2015	15463
1st January 2020 - 31st December 2020	25933
1st January 2023 - 31st August 2023	37287

[a] Data concerning all the severe events recorded in all the European states have been considered.

[1] https://eswd.eu

Due to the significative ocean rise predicted in the next eighty years[2], *i.e.* up to a meter rising by 2100, coastal cities are particularly exposed to the effects of climate changes. However, not only the cities near the seas risk suffering serious consequences[3]: the glaciers melting, unfortunately, is expected to cause the formation of new dry areas. The increasing desertification phenomenon will affect particularly the Himalayan region, impacting on the agriculture and, consequently, on food and resources availability.

According to the *Hindu Kush Himalaya Assessment* [1], even by respecting the most ambitious objectives on limiting the increase in global temperature, around a third of the Himalayan glaciers will however disappear. Due to this phenomenon, incalculable and devastating consequences are hypothesized for twenty million agricultural workers and a significant loss of food production will be unavoidable. The direct consequence of this circumstance will be the establishment of new migratory routes from the Himalayan region and other affected areas, which, according to experts' opinion, in turn they will cause around a billion "climate immigrants".

Climate changes are, without any doubt, a global plague with direct effects on food production and availability, on migration flows, on public health and, finally, on the world peace. In fact, all these effects could culminate in tensions between states and, consequently, lead to conflicts between them.

Krakowka *et al*. reported that environmental conflicts can be considered an ancient phenomenon, because they have been documented since the old China empire and, in the past, they caused the collapse of the Anasazi and the Akkadian [2]. Recent examples in Rwanda and Somalia seem to indicate an increasingly imminent environmental problem that could degenerate into new and violent conflicts. These cited examples are just a small part of the conflicts that could occur in the next future as a consequence of climate changes.

Scientific evidences unequivocally identify CO_2 as one of the gases responsible for the greenhouse effect, which is directly related to global warming, climate changes and which interfere with environmental security [3]. For these reasons, carbon dioxide emissions into the atmosphere play a fundamental role on the path that

[2] https://www.stimson.org/2019/climate-and-ocean-risk-vulnerability-index-corvi/
[3] https://www.stimson.org/2020/environmental-security-april-news-update/

connects human economic activities to the risk of new conflicts between states (Figure 2). To prevent events such as conflicts and wars, with catastrophic consequences on the well-being of populations, the reduction of carbon dioxide levels in the atmosphere is a primary objective to be pursued.

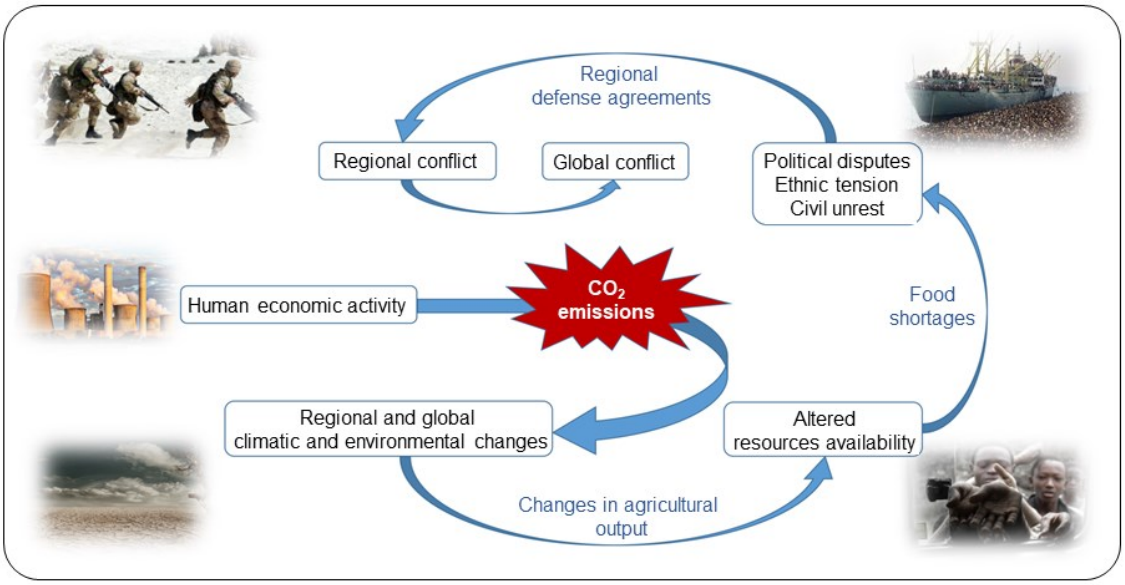

Figure 2 Correlation between human economic activities and the risk of military conflicts due to the increase in CO_2 levels in the atmosphere.

While the European Union is engaged in an important plan to reduce greenhouse gases emissions by 2030[4], the international scientific community is involved in many projects dedicated to the storage of carbon and its subsequent reuse with the aim of reducing the CO_2 emitted into the atmosphere, using it for the synthesis of fuels or high added-value chemicals [4].

[4] Anna Wojtowicz. Common energy policy of the EU–origins, objectives and stages of development. https://repozytorium.bg.ug.edu.pl, 2020

1.2 Importance of CO_2 reutilization

As anticipated in the previous section, in the last years, all around the world scientists have been focused on the identification and study of several new Carbon capture and storage (CCS) and Carbon capture and utilization (CCU) approaches, with the common objective to enhance the efficiency of carbon dioxide capture, storage and its reuse as a feedstock [5]. Indeed, CCU methodologies are currently attracting a lot of interest both from academia and process industry [6], despite the important challenges due to the high carbon dioxide chemical stability, *i.e.* kinetic and thermodynamic stability which is an intrinsic factor, and the demand for the development of innovative process if compared with those already established by the petrochemical industry. The primary goal of this branch of the research is to find new solutions which are low cost and highly efficient, both from an energetic and instrumentations point of view. For this reason, in order to overcome the energetic and environmental issues [7,8], CCU approaches should be designed to use carbon dioxide as a feedstock in mild conditions, *i.e.* ambient or moderately high temperature and pressure (<100 °C, <10 atm) [9–11], and by using catalysts which are as sustainable and as low cost as possible, avoiding noble metals based catalysts and promoting non-noble metal catalysts [9] and organocatalysts [10,11], in particular if they are highly recyclable.

While many different types of solid and liquid sorbents for CO_2 are under study and used in many CCS approaches [12], CCU methods work on the valorisation of captured carbon dioxide as a C1-building block to produce high added-value chemicals, so to compensate the energy consumption and costs related to the CO_2 capture and transport [13]. In fact, CO_2 can be used as a C1-building block in many approaches, as shown in Figure 3.

First of all, it can be fully reduced to produce hydrocarbons, with various carbon chain lengths, for energy storage, usable as fuels for all the purposes in everyday life. Then, carbon dioxide can react with hydrogen in partial reductions to prepare several classes of molecules which can be exploited in organic synthesis and many other fields, such as carbonylic and carboxylic compounds, alcohols, ethers and methylated amines. Finally, CO_2 can react with epoxides in incorporation reactions to obtain cyclic carbonates and polycarbonates, which are both fundamental chemicals in the industry [14–18]: while polycarbonates are used for the production of advanced materials with optical properties, cyclic carbonates are widely used as

high boiling point aprotic solvents [19,20], as electrolytes in secondary batteries [21,22] and as intermediates for the synthesis of fine chemicals and pharmaceuticals [23].

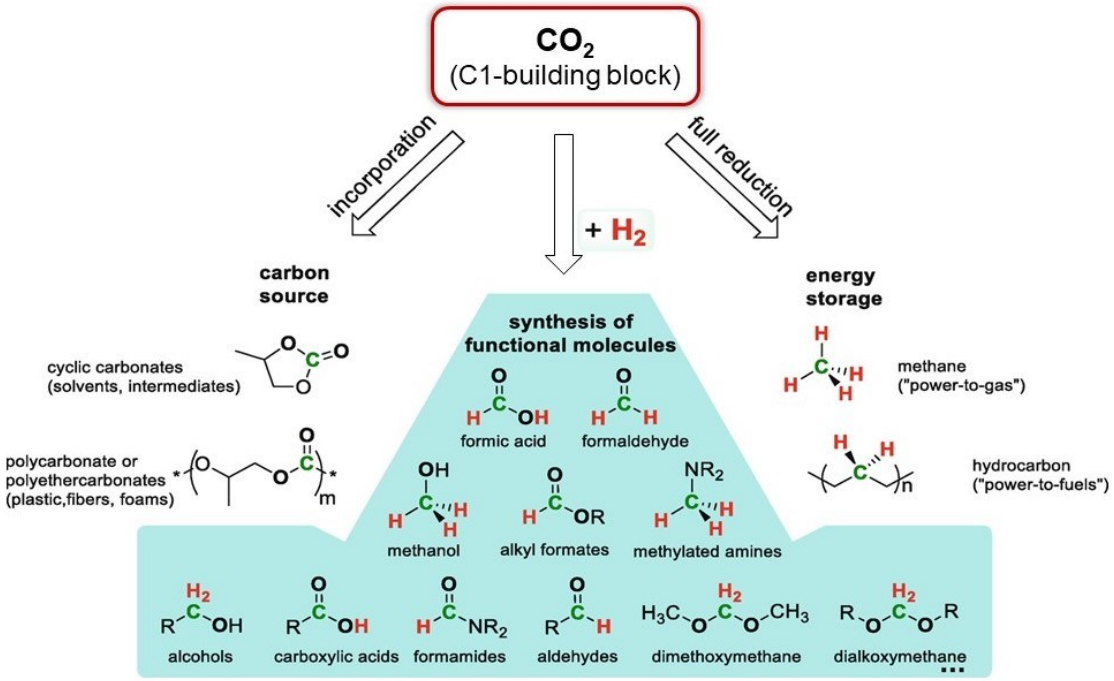

Figure 3 Three routes to re-use carbon dioxide as a C1-building block to produce high added-value chemicals.

1.3 The model reaction in the literature

In the framework described in the previous sections of this introduction, my research project has been focused on the investigation of new methodologies for incorporation reactions of the CO_2 on epoxides to produce cyclic carbonates in several different mild conditions. Cyclic carbonates, as already highlighted in Section 1.2, have considerable applicative importance which is reflected in the wide spectrum of use. In particular, they are exploited to obtain excellent aprotic polar solvents, electrolytes in batteries [24], intermediates for fine chemicals, polymeric products, intermediates for drugs [25] and precursors for polycarbonates [15].

The reaction chosen as a model to perform the studies was the styrene oxide conversion into styrene carbonate (Scheme 1).

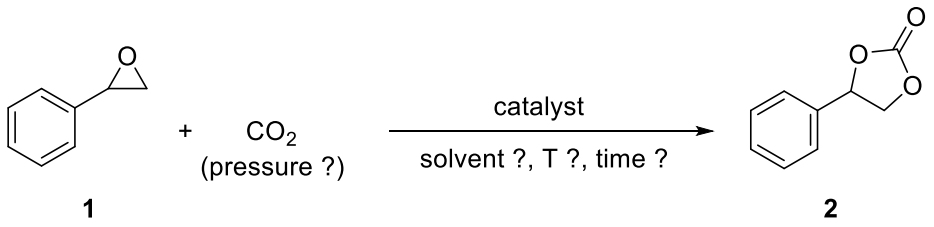

Scheme 1 Model reaction of carbon dioxide incorporation into styrene oxide to produce styrene carbonate.

This reaction has been widely reported in the literature as a model reaction for many studies, because of the moderate stability of styrene oxide, due to the phenylic ring, if compared with other epoxides.

Studying the catalytic carbonation of epoxides through the identified model reaction, our objective was to identify sustainable and innovative catalytic mild procedures in the realm of CCU approaches. To pursue this objective the catalyst should have been selected as a trade-off between cheapness, recyclability and catalytic performances. A wide series of homogeneous and heterogeneous catalytic systems have been reported in the literature for the model reaction, including metal complexes, quaternary onium salts, ionic liquids, organocatalytic systems, alkali metal salts, metal oxides and simple alkaline salts [9–11,26–30]. All of them can be divided into two main groups, based on their functionalities: some of them are Lewis bases, some other are made of combined Lewis acids and bases. Among the latter, it is possible to distinguish between metal-based and metal-free catalysts. Nevertheless, among all these classes of catalysts, only few of them can be used in

mild conditions, *i.e.* without high temperature and pressure requirements, and can be recycled trough straightforward purification procedures [7,8,31].

In this scenario, ionic liquids (ILs) based on quaternary ammonium, imidazolium and pyridinium salts emerged for their feasible features, *i.e.* nonflammability, low volatility, thermal stability, and flexible structure adaptability [32–37]. In details, relevant structural catalyst's features have been identified by a deep analysis of literature reports on ammonium and imidazolium salts. First, the role played by the counterion is reported to be fundamental for the catalytic activity: the conversion rate increases by passing from chloride to bromide counterion, and it increases even more by using iodide as the counterion [38]. So, the more nucleophilic is the counterion, the higher the obtained conversion can be. Moreover, the catalysis study performed by J. Sun *et al.* [38], has shown that, in the case of ammonium salts playing the role of catalysts, the substitution with butylic groups is able to lead to a higher conversion if compared with the same catalyst with ethylic substituents. Finally, it has been reported that by introducing hydroxyl groups as pendants on the IL moiety, the conversion can be significantly increased without altering the selectivity on the target product formation [38]. This phenomenon is the result of the effect of the hydrogen bonding between the hydroxyl groups on the catalyst and the oxygen atom of the epoxide, to promote the ring-opening process due to the halide nucleophilic attack (Scheme 2) [39–45].

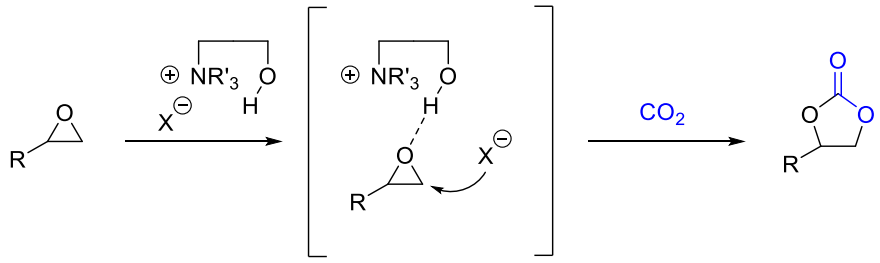

Scheme 2 Bifunctional ILs catalytic mechanism.

Also pyridinium salts [46] have been exploited as catalysts in the synthesis of cyclic carbonates. In this case the used catalyst has been immobilized on silica nanoparticles and it showed a satisfying activity. Based on the previous studies that we analyse, it could be very interesting to see that an hydroxyethylic pendant, if added to the catalyst, could increase its efficiency. Furthermore, because this example of solid nanocatalyst, which emerged from the literature study, seemed promising, the consequent decision of trying a semi-heterogeneous catalysis, *i.e.* heterogeneous conditions with the catalyst having nanometric dimensions (d<100

nm), for the model reaction was obvious. In this case, the carbonate yield will be slightly affected by the heterogenicity of the system, but there are many advantages connected to operating in these conditions (see Section 1.5): nanocatalysts can be recovered, recycled and reused, to minimize wastes.

On the basis of what has emerged from the literature, a set of novel polyhydroxylated ILs, *i.e.* ammonium, imidazolium and pyridinium organocatalysts, have been proposed in this thesis to work as catalysts for the synthesis of styrene oxide from styrene carbonate and the same catalytic systems have been immobilized on nanoparticles surfaces to investigate semi-heterogeneous catalysis (Chapter 4 and 5). The selected ILs, whose details and catalytic activity has been described in Chapter 4, were very promising but required some synthetic steps that imply an expense in terms of time, purification steps, solvents waste and, consequently, money. For this reason, these catalysts, especially the nanocatalysts (Chapter 5), are feasible mainly for the in-batch bulk synthesis of cyclic carbonates or for the in-flow synthesis in very small scale. Consequently, for the larger scale experiments in aerosol continuous flow reactor, described in Chapter 6, a deeper literature study has been necessary. Because of the very large amount of catalyst required for the study, the aim was to find catalysts which were cheap and very easy to be prepared. Fortunately, a wide amount of ILs can be used for the purpose and some of them, like triethylammonium iodide, which can be prepared *in situ*, and N-methyl-3-hydroxypiridinium iodide, which required a facile synthetic step, respected the requirements and are very easy to be prepared in large scale, in addition to offering encouraging catalytic performances [47,48].

All the catalysts which operate in mild conditions reported in this section until now can be grouped in the class of metal-free catalysts, while in the literature can be found other interesting catalytic systems which are metal-based and they still don’t require extreme conditions. The triethylene glycol-potassium iodide (TEG/KI) complex is an example of this kind of catalytic system. This latter has been reported by Kaneko *et al.* [49] as a low-cost catalyst, recyclable, sustainable and very easy to be prepared without any synthetic effort from cheap and readily available commercial chemicals, which exhibit a good catalytic activity at ambient pressure and moderate temperatures through a bifunctional activation mechanism [50].

1.4 Flow chemistry and aerosol to enhance productivity

This thesis project had the goal to exploit carbon dioxide for the synthesis of cyclic carbonates, in particular styrene carbonate, with the purpose to investigate new catalysts performances, the application of new methodologies for process intensification and their synergistic effects.

The reaction chosen as the model reaction, *i.e.* the styrene oxide conversion into styrene carbonate using CO_2, is a biphasic gas-liquid transformation which has intrinsic efficiency problems related to mass transfer phenomena in heterogeneous systems [51]. Considering the most active catalyst, that instantaneously consumes all dissolved CO_2, the bottleneck of this process is the speed of CO_2 absorption in the liquid phase: a faster CO_2 absorption results in a quicker process. This rate-limiting phenomenon happens because the limits imposed by mass transfer have effects on the kinetics of this class of reactions and their performances depends on the amount of gas dissolved in the liquid phase. In fact, from a thermodynamic point of view, carbon dioxide solubility, as a gas, is regulated by Henry's law, *i.e.* it depends on the features of the liquid, on the partial pressure of CO_2 and on the temperature [52,53]. Instead, from a kinetic point of view, the absorption rate of CO_2 at the interface between the gas and the liquid depends on the ratio between the surface area (SA) and the liquid volume, following Fick's law (Eq. 1) [54].

$$\frac{d[CO_{2(sol)}]}{dt} = K_L \times \frac{SA}{V} \times \left([CO_{2(sol)}]_{sat} - [CO_{2(sol)}]\right) \qquad \textbf{(Eq. 1)}$$

where:

- $[CO_{2(sol)}]$ is the concentration of CO_2 in the solution;
- $[CO_{2(sol)}]_{sat}$ is the saturation concentration of CO_2 in the solution;
- K_L is the mass-transfer coefficient for the liquid;
- SA is the gas-liquid interface surface;
- V is the volume of the liquid.

In this scenario in which the focus is on a mass-transfer limited reaction, a process intensification it is necessary to enhance the efficiency of the reactions and the productivity of the system. In fact, by moving from a classical discontinuous reactor to a segmented flow tubular reactor (PFR type, Plug Flow reactor) and finally to an aerosol reactor, it can be possible to overcome the mass transfer limit. It has been already explained that the parameter which is determining for the kinetics of a gas-

liquid biphasic reaction is the dissolution rate of the reactive gas in the liquid in which the reaction occurs. The value of this parameter can be changed, with the consequence of improving the system efficiency, by moving to a plug flow or an aerosol reactor.

According to Fick's law (Eq. 1), the dissolution rate of the reactive gas directly depends on the ratio between the surface area of the gas-liquid interface and the volume of the liquid phase. In gas-liquid reactions conducted in tubular reactors operating with a segmented flow, the SA/V ratio can increase by an order of magnitude compared to that characterizing a classic reactor for discontinuous bulk reactions [54]. Furthermore, based on the diameter of the microdroplets, if we consider each microdroplet of the aerosol as a microreactor itself (Figure 4), the calculated SA/V ratio will be very high and so the gas dissolution speed can increase up to 50-500 times by switching from a conventional discontinuous reactor to an aerosol one [55]. In fact, there are evidences in the literature that microdroplets generated in microfluidic channels [56], microemulsions and aerosols [57,58] behave as microreactors, *i.e.* confined and high SA/V units, with peculiar features at the droplet interface, (*e.g.* pH alteration, accumulation of reagents, effective diffusion, concentration effect by fast solvent evaporation) [59].

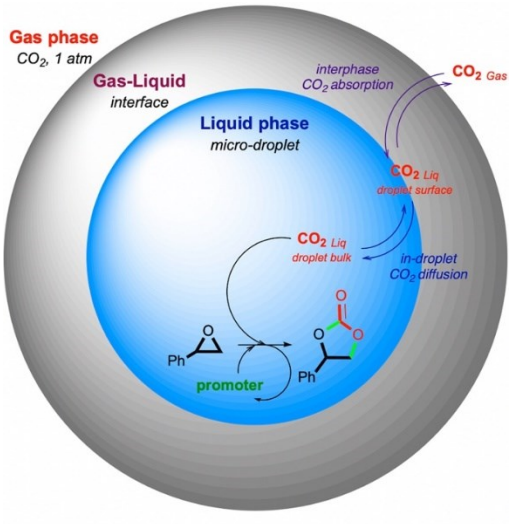

Figure 4 Absorption mechanism of CO_2 in the liquid microdroplet [60].

The use of these new technologies, *i.e.* going from a classic bulk system to an aerosol one or even more to a PFR reactor or a continuous flow aerosol reactor, allows the significant improvement of the productivity of the system. In fact, flow chemistry has recently proven great potential as enabling technology for process

intensification of gas-liquid reactions of CO_2 [61–80]. In literature have been reported several examples of continuous PFR type reactors and their advantages compared to traditional batch systems (for bulk reactions) and CSTR (Continuous Stirred Tank Reactor) type systems. The advantages include a better temperature control and enhanced mass transfer, as reported by M. D. Johnson in his book [81]. Nowadays, PFR type reactors are mainly used in the fine chemical industry, where gases such as H_2, O_2 and CO are used as reagents with conventional heating systems, while studies carried out with CO_2 and this type of reactors are less frequent [75]. Besides the enhanced kinetics of mass-transfer, there are additional advantages of flow conditions in CCU strategies like the better heat transfer, safety of the process and its reliability, better control of the pressure of the system, facile scale-up [82,83].

Aerosol reactors have recently appeared in the literature as a valuable tool, attracting the interest of the scientific community for the degree of innovation they can introduce. Regarding biphasic gas-liquid reactions in aerosol, very few (but very promising) examples are present in the literature, *e.g.* photochemical oxidation with reactive gases [84] and in general aerobic oxidations [55,85,86], singlet oxygen photooxidations [87] and the formation of carbamic acids from amines using CO_2 as nebulization gas [88]. Despite this latter study has been performed at the analytical scale with an electrosonic spray ionization (ESSI) source, it helped to elucidate the mechanism of CO_2 activation at the gas-liquid interface and of the enhanced kinetics in aerosol if compared with bulk, thus paving the way for the development of innovative and highly effective CCS and CCU strategies. The other examples of reactions in aerosol involve the gas phase acting exclusively as an inert carrier. Even in these cases, it is very interesting that reactions in aerosols proceed faster than reactions in classical batch reactors with inert gas [56], not only due to the increase in mass-transfer, but also because of an intrinsic physico-chemical phenomenon [87]. The literature data regarding aerosol reactions encouraged us to perform a comparative study of the model reaction, using different catalytic systems which were easy to prepare and sustainable, in aerosol *vs.* in a classical bulk reactor, with the final goal to detect the enhancement in the production rate of the styrene carbonate due to microdroplets conditions.

1.5 Why TANGO Project?

In the scenario portrayed in the previous sections of this introduction, in which it is fundamental to find and explore new CCU approaches using efficient and sustainable processes, TANGO project has been conceived. TANGO[5] means "Technology Against climate chaNge to mitiGate CO_2 envirOnmental security threats" and it consist in a project funded by the NATO Science for Peace and Security (SPS) program. The project is a collaboration between European and extra-European partners, whose specific expertises are fundamental for the success of the project. The partners involved, in details, are Dr. Dambuoso's group at the ISOF-CNR (Bologna), Prof. Massi's group at the University of Ferrara, Prof. Peddis's group at the University of Genova, Prof. Leblebici's group at the KU Leuven in Belgium, Prof. Lahcini's group at the Cadi Ayyad University (Marrakech) in Morocco.

TANGO project was born with the main objective to identify a new sustainable approach on CO_2 utilization through productive, fast and selective reactions, developing a highly efficient process.

In the literature have been reported several examples of synthetic approaches to the use of carbon dioxide, with different features, including reactions carried out with homogeneous or heterogeneous catalysts, or which use photo- or electro-catalysis.

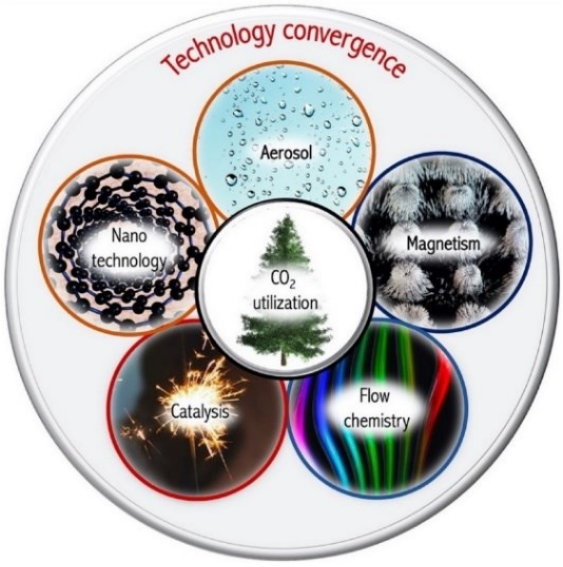

Figure 5 Technology convergence approach of TANGO project.

As an alternative to the solutions proposed in the literature, TANGO pursues an approach of convergence between different technologies, how it has been depicted in Figure 5, in order to validate an effective protocol for the reduction of greenhouse

[5] http://www.tangoproject.eu

gases based on the conversion of CO_2 into molecules with high added value, using efficient, productive and sustainable procedures.

Inspired by Green Chemistry principles[6], the objective of this project is to face CO_2 exploitation efficiency, productivity and sustainability challenges, introducing and validating innovative approaches, like continuous flow, aerosol and approaches which use recyclable catalysts immobilized on magnetic nano-supports. To pursue this goal, the convergence of various technologies must be implemented and tested on a valuable model reaction (Scheme 3).

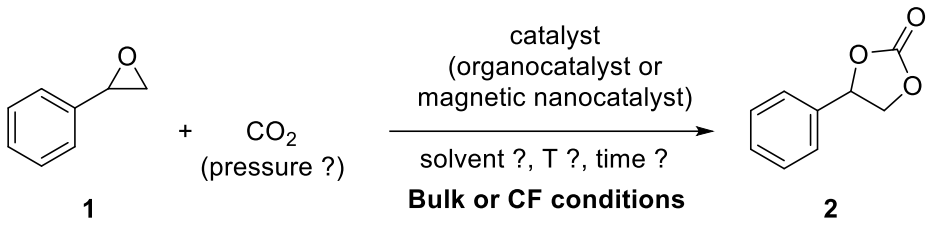

Scheme 3 Model reaction to which TANGO project refers.

In particular, referring to the catalytic conversion of a generic epoxide to the corresponding carbonate, the project intends to deepen the processes related to the production of cyclic carbonates using carbon dioxide as a reactive gas.

Furthermore, the combination of nanotechnology and magnetism applied to catalysis mingles the advantages of both homogeneous and heterogeneous catalysis with an easy recover of the catalyst. In fact, while homogeneous catalysts exhibit high reaction efficiencies by offering the maximum possible proximity among starting materials and the catalyst but paying severe recovery limitations, heterogeneous catalysis promotes process efficiency through physical separation/recovery methods like centrifugation and filtration, in turn, negatively affecting reactions speed. However, it has been found that MNPs have a tendency to aggregate into large clusters which can limit their application in many cases. The use of superparamagnetic nanoparticles appears to be an adequate solution to this last problem, especially combining it with the coating of their surfaces with appropriate inert supports. Magnetism will afford a profitable separation technology exploiting static magnetic fields properties.

[6] https://www.acs.org/greenchemistry/principles/12-principles-of-green-chemistry.html

In this way, the production of cyclic carbonates from epoxides and CO_2 will be investigated by means of both new organocatalysts and innovative semi-heterogeneous catalysts suitably prepared by immobilizing privileged catalytically active functional groups on the outer surface of magnetic core-shell nanoparticles, implementing traditional catalysis with nanotechnology and obtaining nanocatalysts. For this reason, the study of different supports for their immobilization was of fundamental importance: metal-organic structures, porous polymers with metal functional groups (metal-POPs), covalent organic structures without metals (COFs), cellulose and chitosan have been described as systems for heterogeneous catalysis, while polymers and silica-based materials have been designed to immobilize the active species containing the catalytic site [89]. The literature study identified silica as the best inert support (shell of the core-shell MNPs) for our purpose. Silica-coated nanoparticles, in fact, have been exploited for various applications, ranging from nanomedicine to electronics, up to catalysis as inert supports. Furthermore, numerous advantages are found in semi-heterogeneous catalysis: the high surface area, the magnetic recovery, the easy functionalization (attachment of the catalyst to the silica-based surface) and the high stability at high temperatures. The silica shell also guarantees high chemical stability and resistance to degradation of the nanoparticle [90]. The dimensions and geometries of the catalyst supports influence the progress of the reaction, as the performance increases proportionally to the surface area. Numerous and consolidated silica coating techniques for MNPs are reported in the literature, which allow different shapes, dimensions and compositions to be obtained, depending on the different procedure [91]. Considering all this, nanocatalysts are considered as semi-heterogeneous catalysis systems [92]. In the figure below (Figure 6) the core-shell magnetic nanocatalysts that will be studied in TANGO have been schematically represented.

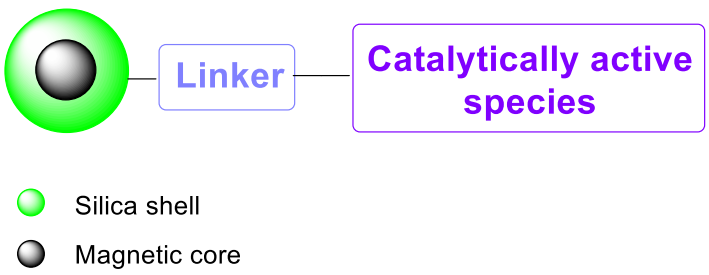

Figure 6 General scheme of the obtained nanocatalysts through the immobilization of the catalytically active species on core-shell MNPs.

Regarding the nanocatalysts magnetic cores, a strong interest has been generated around these metallic nanoparticles (usually composed of magnetite, *i.e.* iron oxide with a spinel structure, or cobalt-ferrite) due to their numerous applications, including catalysis and the magnetic transport of medicines [93].

Among the prepared organocatalysts, the most performing one resulting from propaedeutic bulk studies will be exploited in a plug-flow reactor. Furthermore, this catalyst will be also prepared in its nanocatalyst version, allowing semi-heterogeneous studies of the model reaction, thus providing a novel process window to maximize process intensification through continuous reactor operation and catalyst recovery by application of external magnetic fields.

As an outcome, this project intends to offer to the scientific and industrial communities an innovative carbon dioxide exploitation approach. This novel paradigm will merge into a research breakthrough at the forefront of various independently developed technology realms, paving the way for a circular, efficient, highly productive and sustainable utilization of carbon dioxide. This innovative approach will be easily extended to a wide range of CO_2-based reactions and to the entire realm of gas-liquid biphasic transformation as well.

2. Aim of the thesis

Considering the scenario described in Chapter 1, the zero-waste (% Atom Economy = 100%) insertion of CO_2 into epoxides to obtain cyclic carbonates is emerging as a strategic transformation for the chemical process industry. In fact, it has been estimated that it can be able to consume, together with the dry reforming of methane, up to the 25 % of the total waste of carbon dioxide produced every year [10]. For this reason, the aim of this thesis is to develop new methodologies to prepare cyclic carbonates exploiting CO_2, which can be considered at the same time sustainable and efficient. To this purpose, new catalysts have been prepared and their performances have been evaluated by using them both in batch and continuous flow apparatus for process intensification. Considering the advantages of using new technologies like magnetic nanocatalysis, flow chemistry or microdroplets conditions and the related literature, it appeared to be very promising to exploit the integration of all these different technologies, which can synergistically cooperate, to improve the speed, selectivity and productivity in gas-liquid reactions, in this case, using CO_2. In this context, it is very important to independently study all these new methodologies in order to create a detailed scenario in which an implemented methodology can be identified and designed. The model reaction of styrene oxide carbonation to yield styrene carbonate (Scheme 1) have been used to test the catalysts efficiency and to compare them in all the research works described in the following chapters.

In details, in Chapter 3 it has been reported the kinetic study of the model reaction performed by using a potassium iodide/triethylene glycol (KI/TEG) complex to catalyse the obtaining of styrene carbonate in several conditions (Scheme 4).

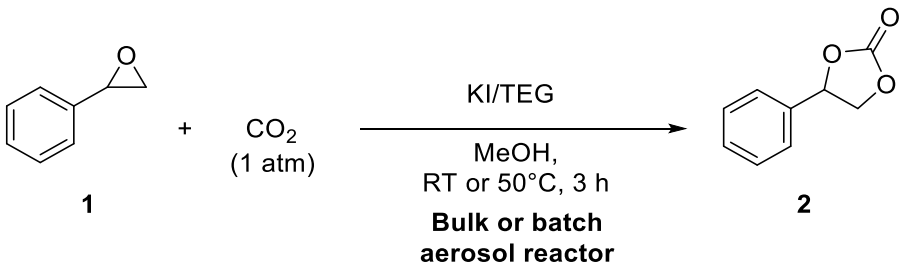

Scheme 4 Reaction studied in the research work reported in Chapter 3.

In the exploration, the results obtained in bulk and in a batch aerosol reactor have been compared both at room temperature and at 50°C, as a proof of concept for the

advantages of microdroplets conditions in mass-transfer limited gas-liquid biphasic transformations.

In Chapter 4 and Chapter 5 have been reported research works inserted in the context of TANGO project.

In particular, as it is depicted in Scheme 5, in Chapter 4 it has been reported the preparation and the use of five different ionic liquids as organocatalysts for the styrene oxide conversion into styrene carbonate. The catalysts have been synthesized, fully characterized and then tested on the model reaction.

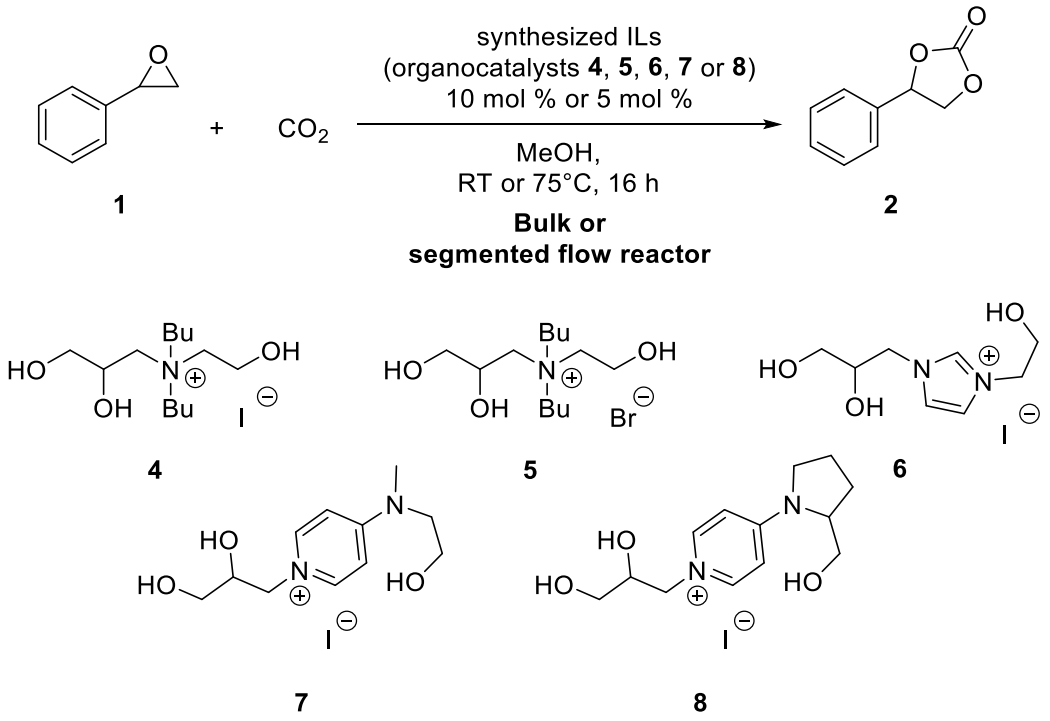

Scheme 5 Reaction studied in the research work reported in Chapter 4.

The best performing catalyst, then, has been used to obtain a collection of different cyclic carbonates from their corresponding epoxides (Figure 7), expanding the scope of the research. Furthermore, following our interest in the development of efficient technology platforms for the intensification of gas-liquid reactions [94,95], the selected catalyst has been used to promote cyclic carbonates obtaining in segmented flow conditions in a plug-flow reactor, with the detection of significant improvements in terms of reaction rate and productivity passing from a bulk reactor to flow chemistry.

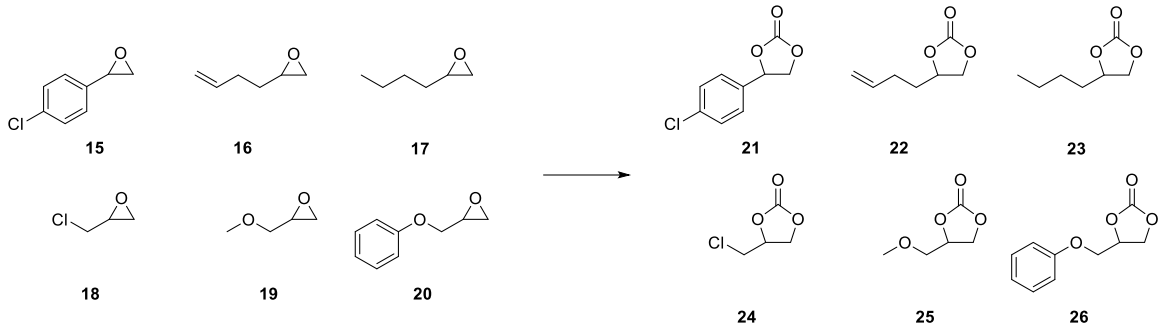

Figure 7 Substrates and products of the scope extension performed in Chapter 4.

Subsequently, in Chapter 5, the catalytically active moiety of the previously identified best performing ionic liquid, has been immobilized on silica core-shell magnetic nanoparticles, to obtain nanocatalysts. The objective of this TANGO activity was to compare the catalysts efficiency in homogeneous and semi-heterogeneous conditions. Two classes of nanocatalysts (with two different cores composition) have been prepared through a multi-step synthesis, and fully characterized using a wide variety of analytic techniques to confirm that the prepared objects had the required characteristics: superparamagnetism, diameters less than 100 nm, and all the functionalities required for the catalytic activity. Then, the performances of the prepared nanocatalysts have been evaluated on the model reaction in a classical bulk reactor (Scheme 6).

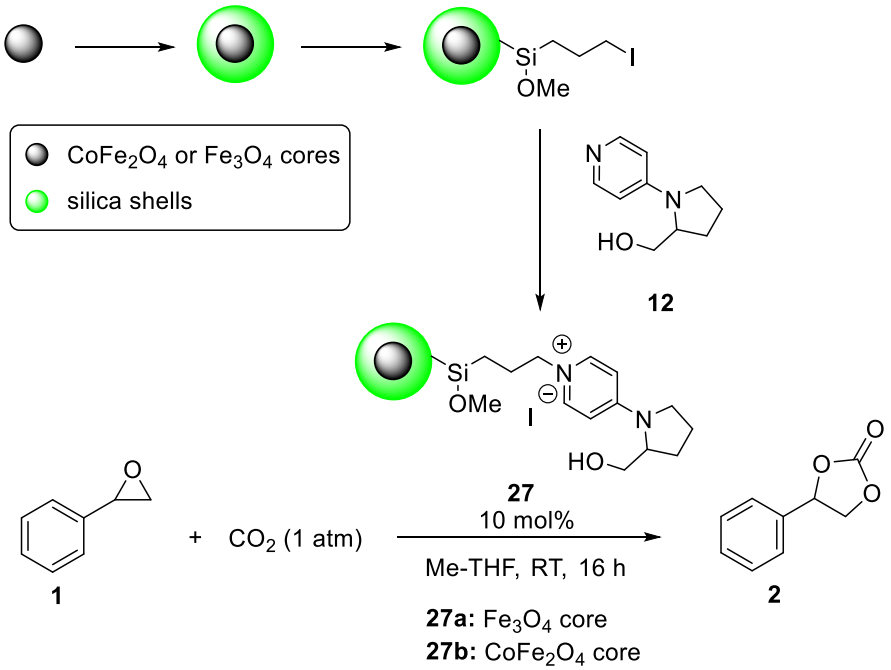

Scheme 6 Model reaction in semi-heterogeneous conditions, studied in Chapter 5.

Finally, in the last research work of this thesis (Chapter 6), an aerosol continuous flow set-up has been assembled and exploited to explore the beneficial effects of microdroplets conditions on styrene carbonate synthesis. A lot of parameters are involved while performing reactions in this kind of custom-made reactor and, for this reason, each of them has been studied and optimized, and they have been reported in Scheme 7.

A fast screening of the abovementioned operative conditions has been performed with a ready accessible catalyst identified in the literature, an ionic liquid introduced as organocatalyst for the model reaction.

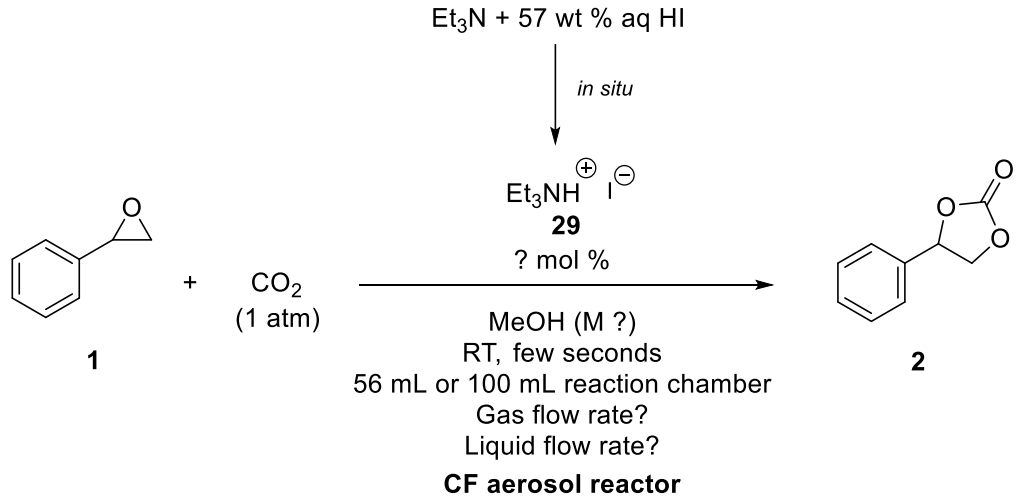

Scheme 7 Aerosol reaction explored in the research work reported in Chapter 6.

Guided by the principles of Green Chemistry[7], the final aim of this thesis is, therefore, to explore new optimized processes that maximize the efficiency of the conversion of epoxides into cyclic carbonates exploiting CO_2 as a feedstock, and to recover and recycle the used catalyst at the end of the reaction.

[7] https://www.acs.org/greenchemistry/principles/12-principles-of-green-chemistry.html

3. Efficiency in CO_2 utilization strategies: The case of styrene carbonate synthesis in microdroplets conditions using KI/TEG catalytic system

3.1 Introduction and aim of the research

The first catalyst explored to study the model reaction of carbonation of styrene oxide (Scheme 1) was the triethylene glycol (TEG)/potassium iodide (KI) system. In particular, in this chapter is presented a comparative kinetic study of the TEG/KI catalysed reaction in microdroplets conditions, with the resulting advantages of aerosol previously discussed in Section 1.4. The results of this study have been published in the Journal of CO_2 Utilization [60].

As previously anticipated, the model reaction selected for this study was the carbonation of styrene oxide **1** to produce styrene carbonate **2**. The TEG/KI complex **3**, reported in the literature by Kaneko *et. al* [49] (Scheme 8) matched all prerequisites we set at the basis of our research, *i.e.* low-cost, practicality, recyclability, sustainability and good catalytic activity through a described bifunctional activation mechanism [50].

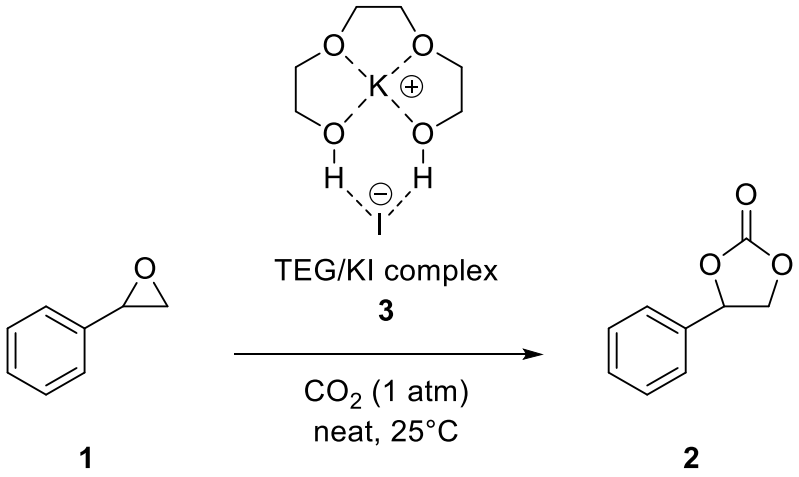

Scheme 8 The model reaction as reported by Kaneko *et al.* [49].

3.2 Discussion of the results

Although that reported in literature [49] seemed a promising starting point to pursue our research goal, it was necessary to adapt the procedure for an easy handling of the reaction mixture. In fact, the complex 1:1 TEG/KI in methanol has been initially obtained as a homogeneous solution but the addition of compound **1** resulted in a heterogeneous slurry, unsuitable for our aerosol reactor. For this reason, it was necessary to study how the variation of the TEG/KI ratio affected the obtaining of a fully homogeneous reaction mixture and, consequently, allowed an efficient ultrasonic nebulization. Stepwise additions of TEG resulted in reducing the KI precipitated. In the end it has been identified a 4.3 TEG/KI ratio as the optimized condition to obtain a clear and homogeneous solution.

The second optimized reaction parameter was the molar percentage of the catalyst (complex **3**) in respect of the styrene oxide **1**. Investigation efforts allowed the identification of the mass-transfer limited reaction conditions. In fact, if the rate limiting step of the reaction was the CO_2 transfer across the gas-liquid interface, the rate of conversion of the styrene oxide into the styrene carbonate was no longer dependent on the catalyst amount. In order to identify the mass-transfer limited reaction conditions, the **1**/**3** ratio was varied in batch experiments conducted in-bulk mode (Table 2).

Table 2 Bulk experiments to achieve mass-transfer limited conditions in the model reaction (Scheme 8).

Entry	**1** (mmol)	KI (mol %)	**3** (KI/TEG) ratio	**2** yield (%)[a]
1	3.5	25	4.3	36
2	3.5	50	4.3	52
3	3.5	75	4.3	51
4	3.5	100	4.3	49

[a] Detected by pre-saturated quantitative ^{1}H NMR experiments on the crude reaction mixture.

After some experimentation using the previously optimized 4.3 TEG/KI ratio (entries 1-4), it resulted that the yield of styrene carbonate (51 %) remained almost unchanged at catalytic complex loadings higher than 0.50 mol %. Nonetheless,

equimolar KI/SO ratio has been used in the further experiments to ensure the operation under mass-transfer limited conditions (entry 4).

Disappointingly, because of viscosity constraints, any attempt to nebulize the identified reaction mixture failed with our homemade ultrasonic nebulizer (Section 3.3.6). The reaction mixture dilution with an appropriate solvent appeared a suitable solution for viscosity tuning to allow the actual nebulization of the mixture. The chosen solvent was methanol because it is classified as a green solvent [96], it is easy to be recycled through distillation and its capability to dissolve CO_2 is relevant [52]. Furthermore, methanol easily dissolved styrene oxide, thus obtaining homogeneous mixture with the catalytic complex.

From this point forward, a three-hours reaction time was arbitrarily set for our kinetic study, matching the need to have both a fast screening and a reliable data acquisition.

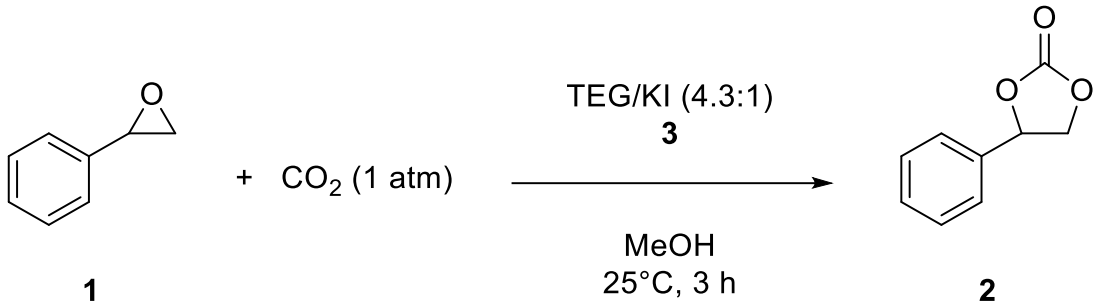

Scheme 9 The model reaction with optimized catalytic complex ratio.

The third optimized parameter was the methanol volume, taking into account both the need of an effective nebulization of the reaction mixture (adequately viscous solution) and the solubilization at the proper concentration of all reagents. In Table 3 are reported the styrene oxide to styrene carbonate conversion data achieved in 3 hours reaction time. This exploration allowed the optimization of the MeOH/TEG ratio. The optimal compromise between actual nebulization and styrene oxide conversion into styrene carbonate was found with the 2.5:1 MeOH/TEG volumetric ratio (entry 6). In these conditions, the amount of methanol was reduced to the minimum compatible with an effective nebulization, avoiding further dilution, negatively affecting the reaction outcome in terms of the styrene carbonate yield at 7.00 MeOH/TEG ratio, 9 % carbonate yield was registered (entries 7-8).

Table 3 Three-hours aerosol experiments to optimize MeOH/TEG ratio in the previously optimized catalytic conditions (4.3 TEG/KI optimized ratio).

Entry	KI (mol %)	MeOH/TEG (v/v)	SC yield (%)[a]	UN[b]
5	100	1.25	26	No
6	100	2.50	23	Yes
7	100	5.00	15	Yes
8	100	7.00	9	Yes

[a] Detected by pre-saturated quantitative ^{1}H NMR experiments on the crude reaction mixture. [b] Effective ultrasonic nebulization (UN) in the homemade reactor.

The comparative kinetic study of styrene oxide carbonation in bulk *vs.* aerosol conditions has been performed by using, for the microdroplets experiments, the homemade reactor described in Section 3.3.6. This reactor has been built using commercially available components, which ensured an easy experimental reproducibility. The aerosol generation has been performed by sonicating the liquid phase in the bottom part of the reactor. Some pictures of the adopted reactor are shown in Figure 8.

In the case of high temperature (50°C) reactions, the set-up has been integrated with one or two IR lamps orthogonal to the aerosol reaction chamber, in order to heat the microdroplets, and with a thermographic camera for the real-time monitoring of the reaction temperature (Section 3.3.7).

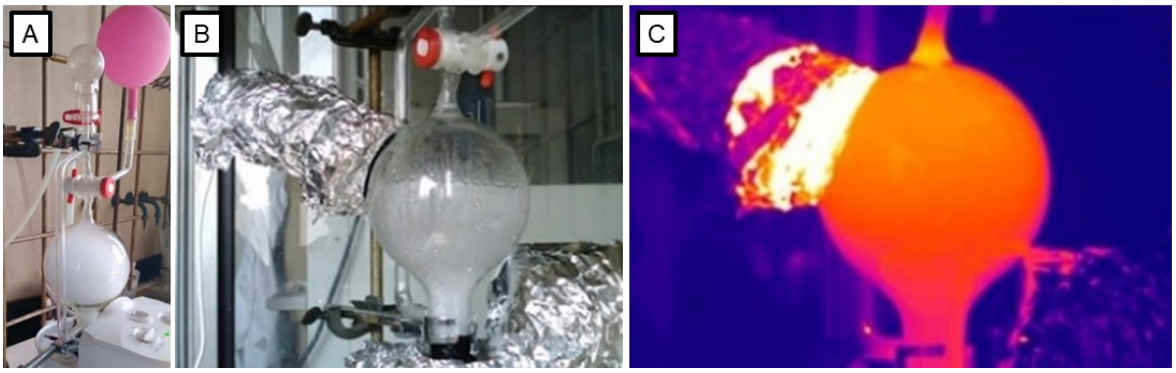

Figure 8 UN set-up for the aerosol carbonation of the styrene oxide. In detail: A) the set-up nebulizing the crude at 25°C; B) the nebulized mixture warmed at 50°C with one 100 W IR lamp; C) real-time monitoring of the reaction temperature with the thermo-camera.

To evaluate the acceleration of reactions performed in microdroplets conditions, the model styrene carbonate synthesis in optimized conditions has been performed under mass transfer limited conditions in bulk and in the homemade batch aerosol reactor. The correlation between the reaction acceleration and the ratio between the gas-liquid surface area and the liquid volume (SA/V) at the gas-liquid interphase, has been studied through kinetic experiments conducted in four different conditions, in which the SA/V has been progressively increased: non-stirred bulk (calculated SA/V value of 130 m^2/m^3 [8]), magnetically stirred bulk (SA/V value of 10^3 m^2/m^3 [54]), sonicated bulk and aerosol conditions (SA/V value of 10^4-10^6 m^2/m^3 [97]). The sonication effect in bulk experiments has been also investigated to normalize the results obtained in aerosol by the effect of ultrasounds-related physico-chemical phenomena that occurs in the liquid phase.

The results of the kinetic study at 25°C obtained in the four different conditions are shown in terms of styrene carbonate yield in the following Figure 9.

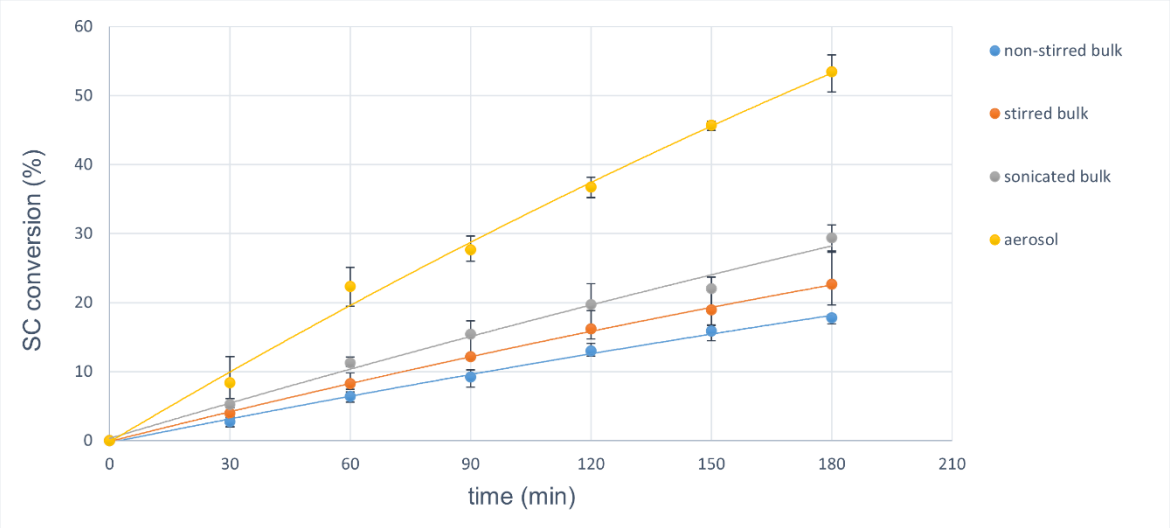

Figure 9 Kinetic profiles of model reaction at 25°C in non-stirred bulk, stirred bulk, sonicated bulk and aerosol. All reactions were performed in triplicates and the error bars has been reported as min-max range of measured values. Averaged experimental data have been fitted with a 2nd grade polynomial curve.

Each of the three bulk reactions has been monitored every 30 minutes by sampling an aliquot of the mixture and analyzing it through pre-saturated quantitative ^{1}H NMR. In the case of microdroplets reactions, it was impossible to sample the aerosol and, for this reason, the results shown have been acquired by performing six different reactions with increasing reaction times (*i.e.* 30, 60, 90, 120, 150 and 180 minutes).

Observing the curves in Figure 9 it is possible to see an increase in term of styrene carbonate yield passing from a non-stirred system (18 % yield in 3 hours) to a stirred one (23 % yield in 3 hours). This behavior was obviously expected, and it is due to the corresponding SA/V increase caused by reaction mixture stirring. The effect of sonication on the reactive system improved a little bit more the yield (29 % yield in 3 hours), if compared with the classical magnetically stirred bulk. Aerosol conditions were able to further increase the styrene oxide conversion into carbonate, giving a 54 % yield. This result corresponded to a 1.9 apparent acceleration factor (AAF) *vs.* the sonicated bulk reaction. The AAF has been calculated as AAF = $[SC]_{aerosol}/[SC]_{sonicated\ bulk}$, *i.e.* the ratio between the carbonate yield in microdroplets conditions and in the sonicated bulk, both after 3 hours. This AAF has been named apparent acceleration factor because it is not calculated on the basis of kinetic constants. Instead, our AAF is calculated using experimentally obtained yields and it approximates the actual AF (acceleration factor), which would be calculated using the kinetic variables which changed passing from bulk conditions to microdroplets one.

The performances of our homemade aerosol set-up have been also investigated for longer reaction's time, achieving 73% styrene carbonate yield in 6 hours.

These results were promising because the effect of enhancement due to aerosol conditions depends on the intrinsic features of the reaction under investigation, as it has been reported in the literature [98]. In the chosen model reaction for this investigation, it can be assumed that the increase in the carbonate yield is due to the faster CO_2 absorption in the liquid phase which positively affected the catalyst efficiency, overcoming mass-transfer limitations.

It has been widely reported in the literature that the carbonation of epoxides is deeply affected by the temperature [6] and, for this reason, the model reaction has been also investigated at 50°C, both in sonicated bulk and microdroplets conditions. The aerosol experiments were performed at 50°C thanks to the heating power of one or two IR lamps. In the meantime, the temperature of the sprayed aerosol has been monitored using a thermo-camera, which gave us a precise measure of the temperature in the different areas of the aerosol chamber (Figure 10).

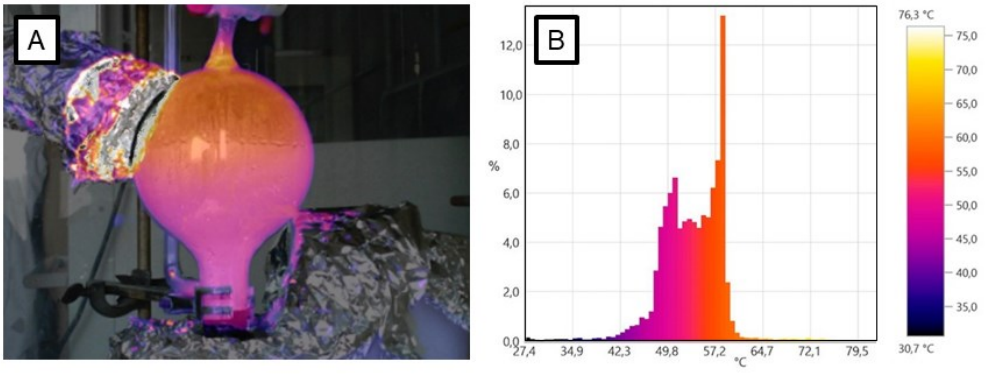

Figure 10 Thermo-camera real-time monitoring of the reaction temperature in the aerosol chamber. In detail: A) thermo-image of the microdroplets warmed at 50°C (averaged temperature); B) temperature profile of the aerosol chamber.

The results obtained at 50°C (averaged temperature) are shown in the following Figure 11. The bulk reaction has been monitored every 30 minutes by sampling an aliquot of the mixture and by analyzing it through pre-saturated quantitative ^{1}H NMR. In the case of microdroplets reaction, it was impossible to sample the aerosol and, for this reason, the results shown have been acquired by performing six different reactions with increasing reaction times (*i.e.* 30, 60, 90, 120, 150 and 180 minutes).

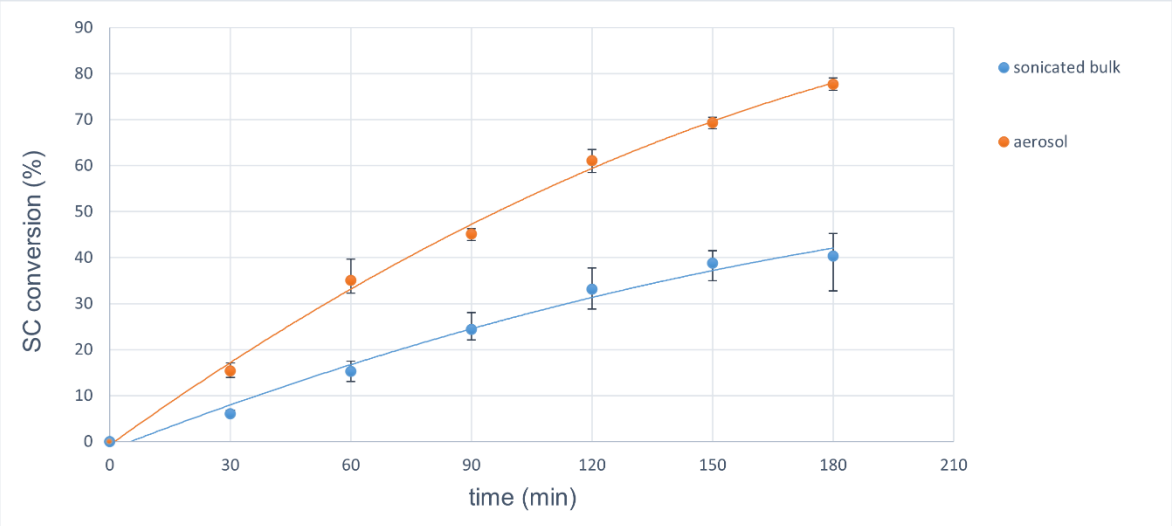

Figure 11 Kinetic profiles of model reaction at 50°C in sonicated bulk and aerosol using the previously reported heated set-up (Figure 8 B and C). All reactions were performed in triplicates and the error bars has been reported as min-max range of measured values. Averaged experimental data have been fitted with a 2nd grade polynomial curve.

Observing the curves, it is possible to see a significative increase in term of styrene carbonate yield passing from sonicated bulk conditions (40 % yield in 3 hours) to aerosol (78 % yield in 3 hours). With these results we were able to confirm the enhancement effect of both aerosol conditions and temperature on the model reaction. The AAF (AAF = $[SC]_{aerosol}/[SC]_{sonicated\ bulk}$) calculated for the reaction at 50°C was 1.95, confirming the twofold acceleration due to aerosol effect observed at 25°C.

All results obtained in this investigation, both at 25°C and 50°C allowed us to hypothesize a reaction mechanism (Scheme 10) which was in accordance with the two mechanistic hypotheses proposed by Kaneko *et al.* [49] and Butera *et al.* [50].

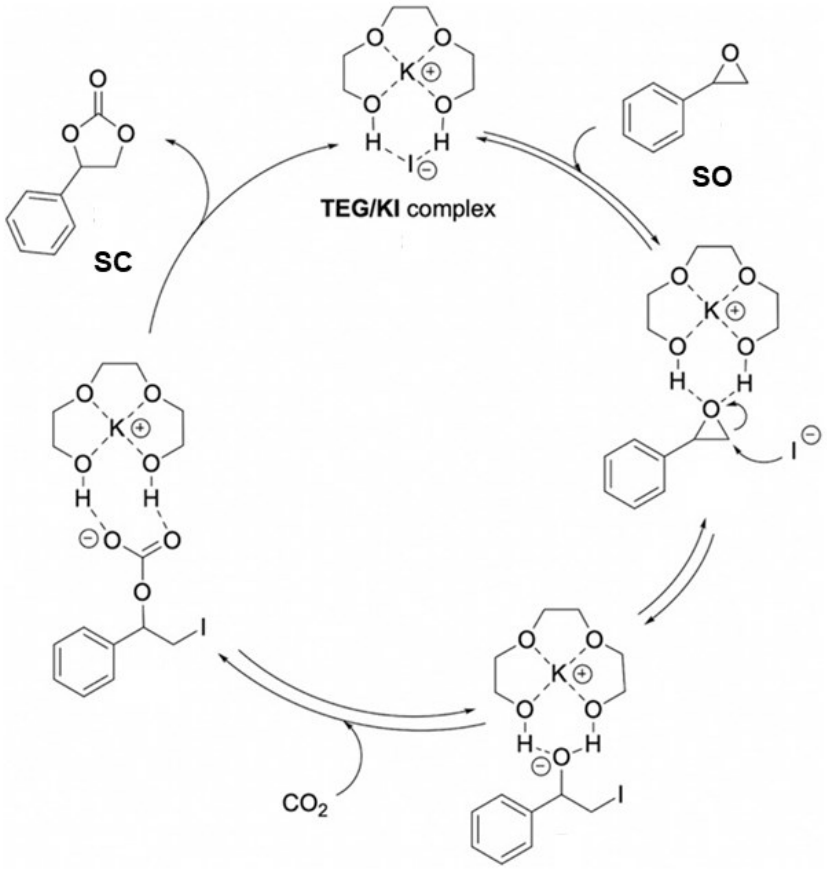

Scheme 10 The proposed mechanism, in agreement with the mechanistic hypotheses proposed by Kaneko *et al.* [49] and Butera *et al.* [50].

3.3 Experimental section

3.3.1 Materials

Styrene oxide (>98%) was purchased from TCI Europe N.V.; methanol (HPLC grade, ≥99,9%), triethylene glycol (≥99.0%) and potassium iodide (≥99.0%) were purchased from Merck; $CDCl_3$ (99.8%) was purchased from CortecNet. All chemicals were used without any further purification.

3.3.2 Optimized reaction mixtures preparation

The homogeneous reaction mixtures were prepared by stirring (950 rpm) in a 10 mL vial for 30 minutes at RT a mixture of styrene oxide (SO, 0.4 mL, 3.5 mmol, 1 eq), potassium iodide (KI, 0.581 mg, 3.5 mmol, 1 eq), triethylene glycol (TEG, 2 mL, 15 mmol, 4.3 eq), and methanol (MeOH, 5 mL) as the solvent.

3.3.3 Reaction procedures

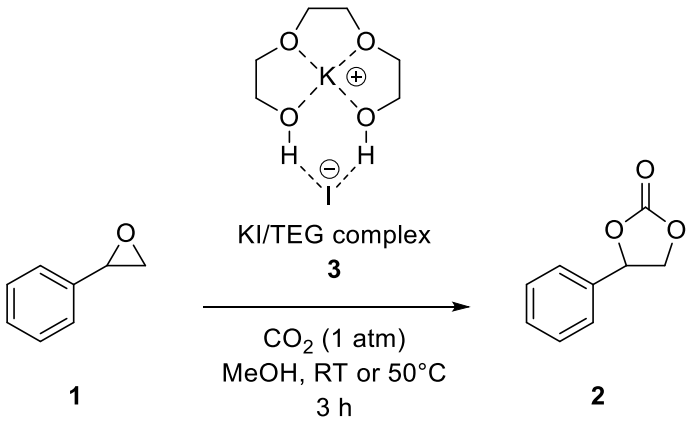

Compound	Molecular formula	Molecular weight
Styrene oxide (SO)	C_8H_8O	120.15 g/mol
Potassium iodide	KI	166.0028 g/mol
TEG	$C_6H_{14}O_4$	150.17 g/mol
Styrene carbonate (SC)	$C_9H_8O_3$	164.16 g/mol

The reactions of the prepared homogeneous mixtures with CO_2 have been performed following four different procedures, all of them in batch reactors: non-stirred bulk reaction, stirred bulk reaction, sonicated bulk reaction and microdroplets (aerosol) reaction. All procedures have been repeated in triplicates and the averaged data values have been reported.

3.3.3.1 Not-stirred bulk procedure

The previously prepared homogeneous mixture has been transferred in a 25 mL round-bottom flask, connected to a 1 L chromatography reservoir equipped with a gas connector on top. After three vacuum/CO_2 cycles, the mixture has been allowed to react in the gas-liquid reaction, both at 25°C or at 50°C, for 3 hours in CO_2 environment. Every 30 minutes the mixture has been sampled and the samples have been preserved to be analyzed to produce the kinetic curve of the reaction.

After 3 hours of reaction the solvent has been evaporated and the resulting crude has been purified and characterized as described in Section 3.3.4 and Section 3.3.5.

3.3.3.2 Stirred bulk procedure

The previously prepared homogeneous mixture has been transferred in a 25 mL round-bottom flask equipped with a magnetic stirrer, connected to a 1 L chromatography reservoir equipped with a gas connector on top. After three vacuum/CO_2 cycles, the mixture has been stirred (600 rpm) for 3 hours in CO_2 environment, both at 25°C or at 50°C. Every 30 minutes the mixture has been sampled and the samples have been preserved to be analyzed to produce the kinetic curve of the reaction.

After 3 hours of reaction the solvent has been evaporated and the resulting crude has been purified and characterized as described in Section 3.3.4 and Section 3.3.5.

3.3.3.3 Sonicated bulk procedure

The previously prepared homogeneous mixture has been transferred in a 25 mL round-bottom flask, connected to a 1 L chromatography reservoir equipped with a gas connector on top. The round-bottom flask has been dipped into the water bath of an ultrasonic medical nebulizer (Yuwell 402B). The flask hasn't been centered on the nebulizer piezoelectric to avoid the nebulization of the reacting mixture. After three vacuum/CO_2 cycles, the mixture was sonicated at the specified temperature (25°C or 50°C) for 3 hours in CO_2 environment. Every 30 minutes the mixture has been sampled and the samples have been preserved to be analyzed to produce the kinetic curve of the reaction.

After 3 hours of reaction the solvent has been evaporated and the resulting crude has been purified and characterized as described in Section 3.3.4 and Section 3.3.5.

3.3.3.4 Aerosol procedure

The previously prepared homogeneous mixture has been transferred into the custom-made aerosol reactor (described in Section 3.3.6), equipped with a gas connector on top. The bottom of the reactor has been dipped into the water bath of an ultrasonic medical nebulizer (Yuwell 402B), centering it on the nebulizer piezoelectric to allow the nebulization of the reacting mixture. After three vacuum/CO_2 cycles, the reaction mixture was nebulized and maintained at the specified temperature (see Section 3.3.7), both at 25°C or at 50°C, for 30, 60, 90, 120, 150 or 180 minutes in CO_2 environment.

After the end of the reaction, the reactor has been turned upside down and dipped in a melting ice bath to allow the microdroplets condensation. Then, the solvent has been evaporated and the resulting crude has been purified and characterized as described in Section 3.3.4 and Section 3.3.5.

3.3.4 Products purification

Each of the reaction crudes has been diluted with 20 mL of a 1:1 EtOAc/H_2O mixture and then extracted with three aliquots of EtOAc. Products have been concentrated from the organic phase and purified through automatized flash chromatography (Chromatographic method: CombiFlash RF 200 LC system; stationary phase: silica 120, CV = 192 mL; flow rate: 85 mL/min; elution method: 1 CV isocratic 100% Cy, 1 CV gradient to 10% EtOAc, 3 CV isocratic 10% EtOAc, 1 CV gradient to 20% EtOAc, 3 CV isocratic 20% EtOAc, 5 CV gradient to 100% EtOAc, 2 CV isocratic 100% EtOAc).

3.3.5 Products characterization

The products characterization has been performed *via* NMR spectroscopy, using an Agilent DD2 NMR system, equipped with a 11.7 T (500 MHz) PremiumCompact+ superconducting magnet and an Agilent OneNMR probe. All the isolated products have been fully characterized by NMR spectroscopy through ^{1}H NMR, ^{13}C NMR, ^{1}H-^{1}H COSY, ^{1}H-^{13}C HSQC and ^{1}H-^{13}C HMBC experiments performed in $CDCl_3$. Also, kinetic data have been acquired *via* NMR spectroscopy, performing pre-saturated quantitative ^{1}H NMR experiments in $CDCl_3$ for each collected sample (one every 30 minutes of reaction for each reaction).

3.3.5.1 Styrene oxide (1)

^{1}H NMR (500 MHz, $CDCl_3$) δ 7.39-7.30 (m, 5 H, AR), δ 3.88 (dd, 1 H, CH, $J_{CH\text{-}CH2}$ = 3.96 Hz, $J_{CH\text{-}CH2'}$ = 2.67 Hz), δ 3.16 (dd, 1 H, CH_2, $J_{CH2\text{-}CH2'}$ = 5.46 Hz, $J_{CH2\text{-}CH}$ = 4.16 Hz), δ 2.82 (dd, 1 H, CH_2', $J_{CH2'\text{-}CH2}$ = 5.50 Hz, $J_{CH2'\text{-}CH}$ = 2.58 Hz).

^{13}C NMR (125 MHz, $CDCl_3$) δ 137.55 (AR_{ipso}), δ 128.42 (AR_{meta}), δ 128.10 (AR_{para}), δ 125.42 (AR_{ortho}), δ 52.27 (CH), δ 51.11 (CH_2).

3.3.5.2 Styrene carbonate (2)

^{1}H NMR (500 MHz, $CDCl_3$) δ 7.46-7.36 (m, 5 H, AR), δ 5.68 (t, 1 H, CH, $J_{CH\text{-}CH2}$ = $J_{CH\text{-}CH2'}$ = 8.01 Hz), δ 4.81 (t, 1 H, CH_2, $J_{CH2\text{-}CH2'}$ = $J_{CH2\text{-}CH}$ = 8.40 Hz), δ 4.35 (t, 1 H, CH_2', $J_{CH2'\text{-}CH2}$ = $J_{CH2'\text{-}CH}$ = 8.29 Hz).

^{13}C NMR (125 MHz, $CDCl_3$) δ 154.77 (OCOO), δ 135.76 (AR_{ipso}), δ 129.68 (AR_{meta}), δ 129.18 (AR_{para}), δ 125.82 (AR_{ortho}), δ 77.94 (CH), δ 71.11 (CH_2).

3.3.6 Aerosol reactor

The homemade aerosol apparatus (Figure 12), adapted from the Heated Ultrasonic Nebulization (HUN) system reported by Zare *et. al* [97], consisted of a 25 mL cylindrical nebulization chamber that has been bottom-capped with a 0.2 mm thick aluminum foil, tightly held by a plastic screw cap. A 1 L reaction chamber, with a three-ways tap on top for gas and vacuum connection and microdroplets condensation, has been connected above the nebulization chamber. The nebulization chamber has been dipped into the water bath of the Yuwell 402B medical ultrasonic nebulizer (UN) and centered on the piezoelectric transducer to allow the aluminum foil vibration and so the nebulization of the reaction mixture. The temperature of the water bath of the UN has been regulated at 25°C or 50°C, depending on the reaction, and maintained at that temperature for the entire reaction time.

In the case of 50°C reactions, the aerosol has been maintained at that temperature using one or two 100 W IR lamps. At the end of each reaction, the reactor has been turned upside down and dipped in a melting ice bath to allow the microdroplets condensation and the crude recovering.

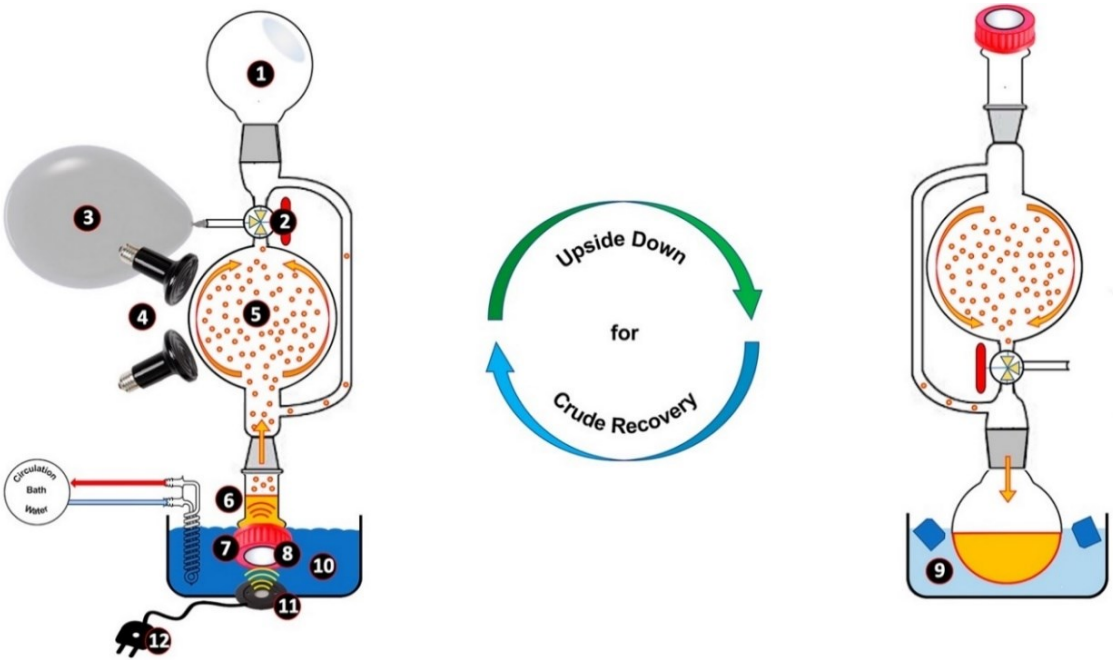

Figure 12 Homemade aerosol reactor used for styrene carbonate synthesis in microdroplets conditions, consisting of: 1) collecting flask; 2) three-ways tap; 3) CO_2 balloon; 4) IR lamps; 5) 1 L aerosol reaction chamber; 6) nebulization chamber; 7) plastic screw cap; 8) aluminium foil; 9) melting ice bath for the condensation of the microdroplets. Yuwell 402B ultrasonic nebulizer consisting of: 10) water bath; 11) piezoelectric transducer; 12) plug for power supply.

3.3.7 Monitoring of the reaction temperature

The temperature during of all the reactions have been measured and monitored using a Testo thermal imaging camera (Testo 890 Thermal Imager). The used thermo-camera allowed a thermal sensitivity of 0.04 °C (40 mK) in the temperature measuring range of 0°C to +650°C and it produced images with a SuperResolution option (1280 × 960 pixels accounting for overall 1.228.800 pixels). The thermographic analyses have been performed with Testo IRSoft software (version 4.8).

3.4 Conclusions

These results for the first time demonstrated the beneficial kinetic effects on reactions conducted in aerosol, considered as an innovative methodology to increase the styrene oxide conversion into its corresponding cyclic carbonate. This carbonation of an epoxide has been selected as a model reaction in the realm of CO_2-utilization strategies, which are considered a fundamental research topic nowadays.

The batch approach used in this research work allowed a lower CO_2 consumption during the experiments, if compared to a continuous flow process.

The aerosol set-up with the ultrasonic nebulization system used in this research work has demonstrated to be efficient for our purpose, although it was home-made. Indeed, during the kinetic studies it has been observed a twofold acceleration in microdroplets conditions *vs.* sonicated bulk, both at 25°C and 50°C. Furthermore, the experiments at 50°C confirmed the dependency of the model reaction on the temperature, affording a higher yield when the reaction was performed at higher temperature.

The very mild conditions in which the model reaction has been performed, together with the encouraging results obtained, confirmed the aerosol to be a promising, innovative and powerful tool in the continuous efforts to efficiently exploit carbon capture and utilization (CCU) approaches. Furthermore, the achieved results paved the way to expand this methodology by using diverse and more efficient catalytic system on the synthesis of cyclic carbonates (see the following chapters) or to extend the innovative technology to the entire realm of gas-liquid biphasic reactions, which are normally constrained by mass-transfer limitation phenomena.

4. Efficiency in Carbon Dioxide Fixation into Cyclic Carbonates: Operating Bifunctional Polyhydroxylated Pyridinium Organocatalysts in Segmented Flow Conditions

4.1 Introduction and aim of the research

The research work reported in this chapter, which is part of TANGO project (see Section 1.5), has been carried out as a collaboration between Dr. Paolo Dambruoso's group at ISOF-CNR in Bologna and Prof. Alessandro Massi's group at the University of Ferrara. The results obtained have been published on Molecules [99].

As it has been highlighted in the introduction of this thesis, TANGO project pursues the goal to find innovative strategies to face the CO_2 utilization problem (CCU), always taking in account Green Chemistry principles [96]. In this scenario, it is extremely relevant to introduce new efficient catalysts. Various metal-based ionic liquids (ILs) have been recently reported in the literature [32–35], showing good to excellent yields and selectivities, typically by the application of high CO_2 pressures (up to 50 bar). For this reason, TANGO project prepared a set of ILs for the fixation of CO_2 on styrene oxide to obtain styrene carbonate (Figure 13), with the aim to evaluate their catalytic efficiencies and identify the most performing one.

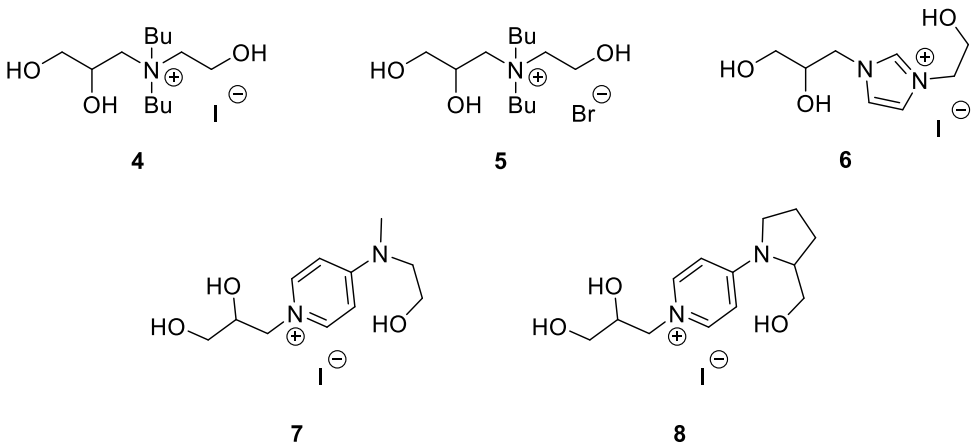

Figure 13 Set of prepared target ILs used as organocatalysts.

Common structural feature of the novel catalysts was the presence of three hydroxyl pendants, because it has been demonstrated in the literature that this kind of substitution increases the catalytic efficiency in both the cases of ammonium and imidazolium salts [38], as a result of the synergistic effect of hydrogen bonding with

the oxygen atom of epoxides, which effectively contributes to the ring-opening process promoted by the halide nucleophilic attack (Scheme 11) [38,100–105].

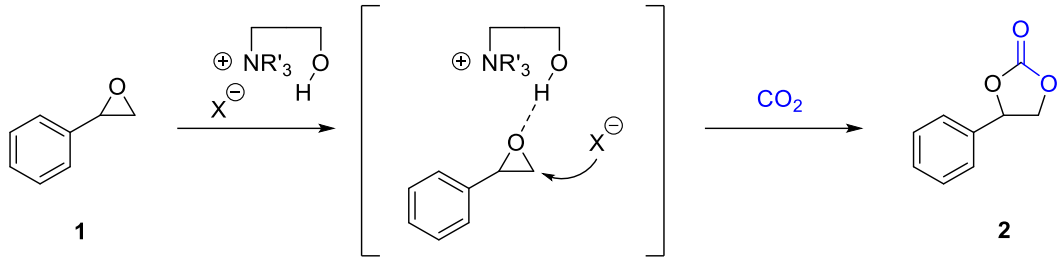

Scheme 11 Bifunctional ILs catalytic mechanism.

The first two organocatalysts, *i.e.* **4** and **5**, have been chosen to explore the influence of the counterion on the catalytic mechanism and to confirm that iodide salts are the best performing. In fact, in the same already cited article [38], it has been reported that the epoxide conversion increased by passing from chloride to bromide counterion, suggesting that the more nucleophilic is the counterion, the higher is the obtained conversion. For this reason, by using a more nucleophilic counterion, as iodide, it might result in improved carbonate yield. Furthermore, also pyridinium salts, *i.e.* **7** and **8**, have been chosen for the study, because of their known ability to catalyse this kind of reactions [46]. In this case, the two catalysts exhibit diverse rigidity in their substituents. Indeed, the purpose was to study if the rotation around a bond in the ammino-substituent of the pyridine ring could affects or not the catalytic activity.

With the goal to obtain a solid and efficient catalytic system, once the best performing catalyst has been chosen, the method has been validated on the carbonation of other terminal epoxides.

Furthermore, keeping in mind that one of TANGO goals is the process intensification, segmented flow chemistry has been introduced to increase the productivity of the system. In fact, flow chemistry has recently been proven to have great potential in biphasic gas-liquid reactions of CO_2 [41,61–67,69,70,72–80,106], because of its ability to improve mass transfer rate across the interphase, which is often the rate-limiting step of CO_2 reactions. Aside from enhanced kinetics, additional advantages of flow conditions in CCU strategies are the improved heat transfer, safety, process reliability, easy control of pressure, facile scaling-up by extending the period of product collection [82,83].

4.2 Discussion of the results

4.2.1 Organocatalysts synthesis

The syntheses of organocatalysts precursors **9**, **10**, **11** and **12** have been performed at ISOF-CNR, while the preparations of the five ionic liquids **4**, **5**, **6**, **7** and **8** have been executed at the University of Ferrara.

The synthesis of organocatalyst **4** has been performed in two steps: the epoxide ring-opening with dibutylamine and then the quaternarization, obtaining the polyhydroxylated ammonium iodide target salt (Scheme 12).

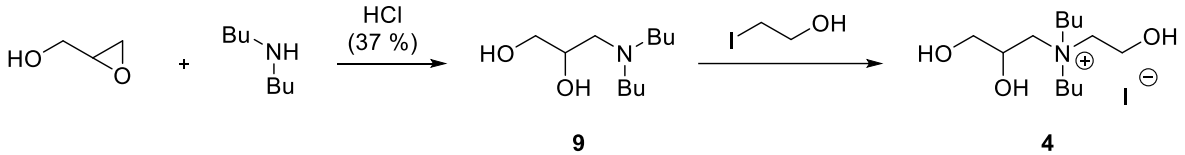

9 **4**

Scheme 12 Two-steps synthesis of compound **4**.

The first attempt to obtain compound **9** occurred with the reaction of glycidol and dibutylamine 1:1 at 100°C for 2 hours with methanol as the solvent, because of the very low amount of volume of reagents used [107].

In these conditions the reaction afforded the product with a significative contamination of unreacted dibutylamine, either by using an excess of epoxide, because of the side reaction of glycidol with the solvent. To avoid side reactivity, THF has been used instead of methanol to perform the target reaction, with an excess of epoxide (3:1 *vs.* dibutylamine) because of the difficult separation of the eventual unreacted dibutylamine from the mixture. In these conditions, the attempt to increase the **9** yield has been performed by adding concentrated hydrochloric acid (37 % v/v) to the mixture to enhance the epoxide ring-opening and to obtain a good yield (72 % after purification) by refluxing the mixture overnight.

Once precursor **9** has been obtained, it has been refluxed in ethanol with 2-iodoethanol following the standard procedure for the N-alkylation of tertiary amines. This procedure afforded an inseparable mixture of two products (Scheme 13), *i.e.* **4** (32 %) and the side product **13** (68 %).

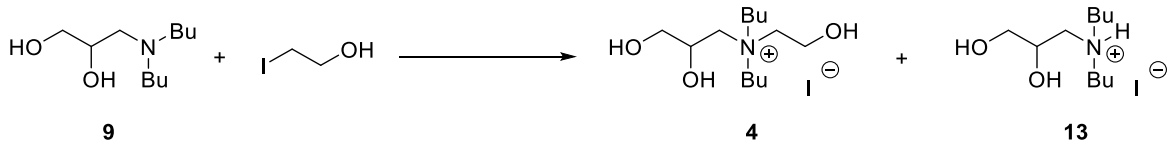

Scheme 13 Synthesis of compound **4** and side reaction path.

Decreasing the temperature to 60°C improved the selectivity toward **4**, but it negatively affected the conversion (see Table 4). Similarly, by using different polar aprotic solvents, *i.e.* DMF and THF, and by changing the temperature, the same disappointing results have been obtained (entries 4-5). The production of **13** has been explained by hydriodic acid elimination from iodoethanol promoted by precursor **9**. The target organocatalyst **4** has been finally prepared in 48 hours without any solvent, at 75°C, in quantitative yield (entry 8).

Table 4 Optimization of the synthesis of organocatalyst **4**.

Entry [a]	Solvent	Temperature (°C)	**4** (%)[b]	**13** (%)[b]
1	EtOH	reflux	32	68
2	EtOH	60	21	<5
3	DMF	80	24	76
4	DMF	70	18	27
5	THF	reflux	41	59
6	neat	25	<5	-
7	neat	60	49	-
8	neat	75	>95	-

[a] Conditions: **9** (2.5 mmol), 2-iodoethanol (2.5 mmol). [b] Detected with ^{1}H NMR of the crude reaction mixture with durene as internal standard.

The optimized procedure to obtain the alkylammonium salt **4** has been used also to obtain organocatalyst **5** using 2-bromoethanol for quaternarization (Scheme 14), with the aim of verifying the effect of halide variation on the catalytic efficiency on styrene oxide ring-opening.

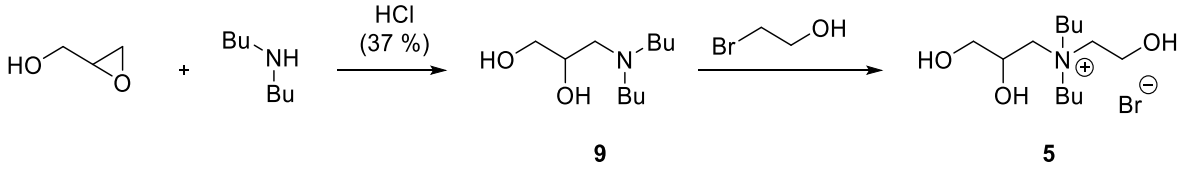

Scheme 14 Two-steps synthesis of compound **5**.

The same procedure has been also used to obtain the bifunctional organocatalyst **6** from precursor **10**, whose synthesis was based on a reported methodology, but it has been modified for the specific purpose [108] (Scheme 15). To obtain compound **10**, the reaction has been performed with N,N-diisopropylethylamine (DIPEA) as a basic catalyst to promote the selective N-epoxide ring-opening and using acetonitrile as the reaction solvent .

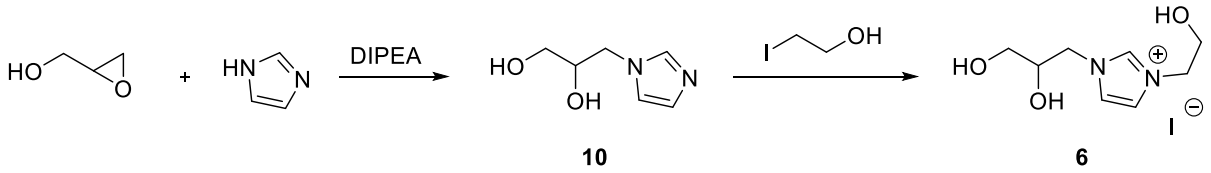

10 **6**

Scheme 15 Two-steps synthesis of compound **6**.

The synthesis of the organocatalyst **7** and **8**, has been performed in two steps: the coupling of chloropyridine hydrochloride and excess of secondary amine (cyclic or not cyclic depending on the specific case, in which the hydroxyalkyl chain had a different degree of free rotation) at 120°, in 24 hours under magnetic stirring or 3 hours in microwave, and the N-alkylation of pyridine to add the polyhydroxylated moiety. Additionally, another preliminary step was required to synthesize the alkylating agent **14** from glycidol (see Scheme 16).

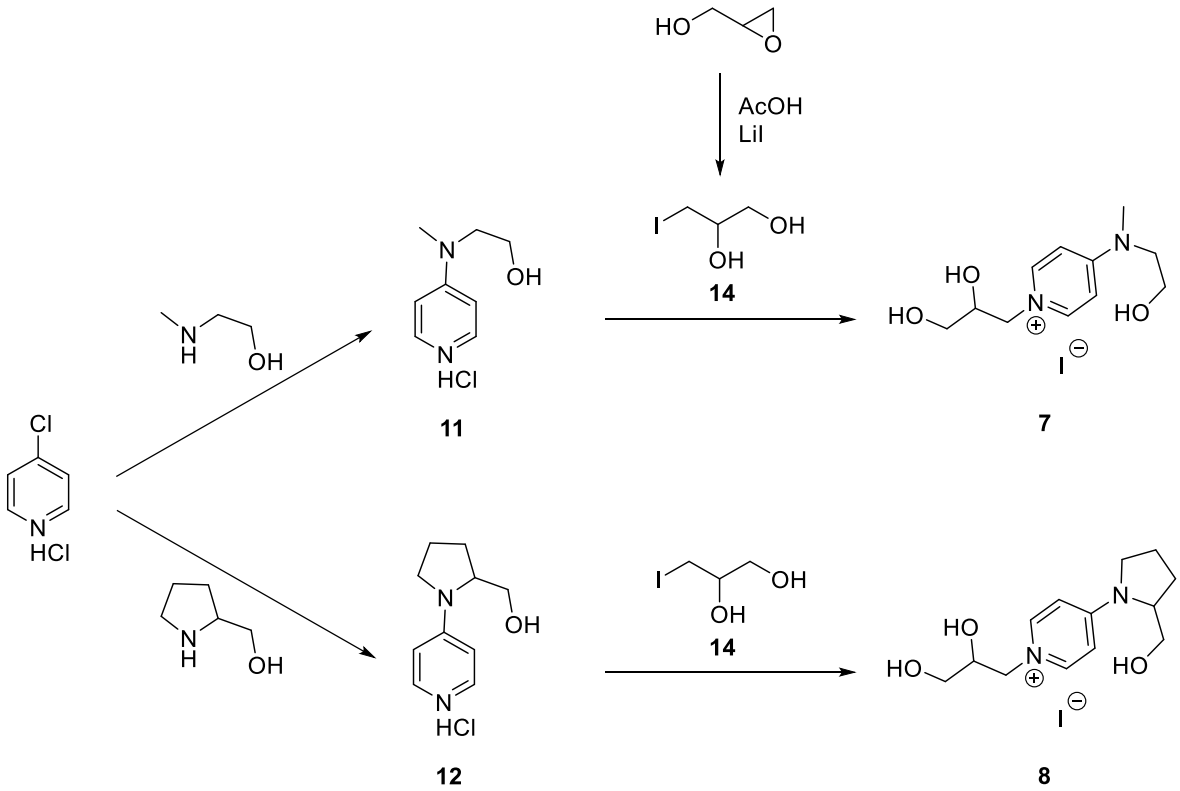

Scheme 16 Synthesis of pyridinium iodide salts **7** and **8**.

In fact, compound **14** has been identified for the introduction of 1,2-propanediol group on the organocatalysts precoursors **11** and **12**. Although its synthesis has been reported in the literature as typically performed in three steps from glycerol [109], in this research work, the regioselective conversion of glycidol into compound **14** (75 % yield) has been performed using lithium iodide and AcOH in 30 minutes at RT [110].

The two polyhydroxylated pyridinium salts **7** and **8** have been finally obtained by N-alkylation with iodide **14** under the previously optimized neat conditions.

4.2.2 Identification of the best performing organocatalyst on the styrene oxide carbonation under bulk conditions

The experimental activities described in this section have been performed by the research group at the University of Ferrara.

To identify the best performing catalyst on epoxides carbonations among the synthesized bifunctional organocatalysts **4**, **5**, **6**, **7** and **8**, they have been tested in bulk conditions on the model reaction of conversion of styrene oxide into styrene carbonate (Scheme 17).

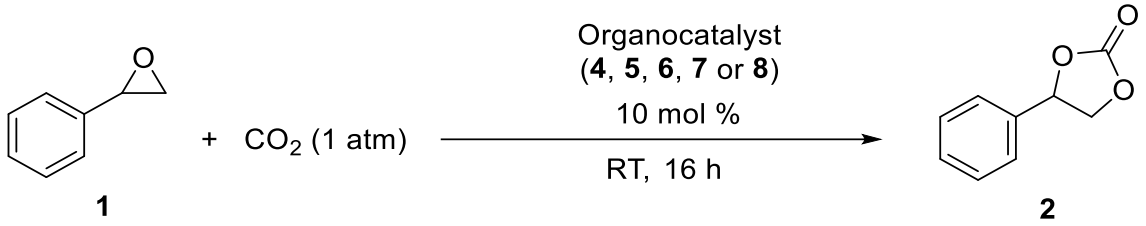

Scheme 17 Styrene oxide carbonation with organocatalysts **4**, **5**, **6**, **7** or **8**.

Results obtained in 16 hours at room temperature and ambient pressure are shown in Table 5. In accordance with the order of nucleophilicity of halide anions and their ability to coordinate the acidic hydrogen of the reaction intermediate involved in the catalytic mechanism (see Scheme 11) [10], iodide alkylammonium salt **4** afforded a higher carbonate yield if compared with bromide alkylammonium salt **5** (entries 1-2).

Table 5 Screening of organocatalyst **4**, **5**, **6**, **7** and **8** activities.

Entry [a]	Catalyst	Conversion (%)[b]	Selectivity (%)[b]	**2** (%)[b]
1	**4**	30	>99	30
2	**5**	5	>99	5
3	**6**	27	>99	27
4	**7**	35	>99	35
5	**8**	44	>99	44

[a] Conditions: SO (2.00 mmol), CO_2 (1 atm, balloon), neat conditions. [b] Detected with ^{1}H NMR of the crude reaction mixture with durene as internal standard.

Based on conversion and selectivity data reported in the table, among the iodide salts **4**, **6**, **7** and **8**, the polyhydroxylated pyridinium organocatalyst **8** has been identified as the most efficient promoter to obtain styrene carbonate from styrene oxide (entry 5). This result highlighted the importance of some rigidity in the hydroxyalkyl chain for transition state stabilization (entry 4-5).

4.2.3 Optimization study using catalyst 8 under bulk conditions

The experimental activities described in this section have been performed by the research group at the University of Ferrara.

Once organocatalyst **8** has been identified as the best performing one, several conditions were screened, to improve the process productivity. The results obtained are shown in the following Table 6.

Table 6 Optimization study using organocatalyst **8** under bulk conditions.

Entry [a]	**8** (mol %)	Temperature (°C)	Time (h)	Conversion (%)[b]	Selectivity (%)[b]	SC (%)[b]
1	10	25	16	44	>99	44
2	10	50	16	62	>99	62
3	10	75	16	>95	>99	>95
4	5	75	16	>95	>99	>95
5	2	75	16	74	>99	74
6	5	75	12	88	>99	88
7 [c]	5	75	16	15	>99	15
8 [d]	5	75	16	48	>99	48
9 [e]	5	75	16	92	>99	92

[a] Conditions: SO (2.00 mmol), CO_2 (1 atm, balloon), neat conditions. [b] Detected with ^{1}H NMR of the crude reaction mixture with durene as internal standard.
[c] Additive: DMF (5.00 mmol). [d] Additive: H_2O (50 mol %). [e] Additive: EtOH (50 mol %).

In particular, by increasing the temperature up to 75°C, the quantitative conversion of styrene oxide into styrene carbonate has been obtained in 16 hours (entries 1-3). The same promising result has been obtained by halving the amount of catalyst to 5 mol % (entry 4), while by using 2 mol % of catalyst **8** the conversion decreased (entry 5). Also, a shorter reaction time, *i.e.* 12 hours instead of 16 hours, negatively affected the reaction outcome, leading to 88 % of conversion (entry 6).

Although the performances achieved (entry 4) greatly satisfied our expectations, operating in those conditions initially afforded a heterogeneous slurry, unsuitable for our process intensification purposes. Accordingly, the use of some additives has

been considered to obtain an optimized process in homogeneous conditions. Although previous literature findings [104] suggested the use of DMF and H_2O as additives in our SO carbonation, any attempt of their exploitation resulted in a significative conversion decrease (entries 7-8). Conversely, when EtOH (50 mol%) was used as an additive to obtain a full solubilization of catalyst **8**, the conversion was only minimally affected (entry 9).

In the optimized conditions (entry 4), the productivity (P) of the process in bulk conditions has been calculated using Eq. 2.

(Eq. 2)

$$P = \frac{\text{mol(product)}}{\text{time} \times \text{mol(catalyst)}} = 1.2 \; \frac{\text{mmol(SC)}}{h^{-1} \times \text{mmol(}\mathbf{8}\text{)}}$$

At the end of the reaction, the recyclability of the organocatalyst **8** has been explored. The catalyst has been recovered from the mixture, after the synthesis of styrene carbonate, by adding EtOAc to allow the precipitation of the catalyst and the collection of the product by centrifugation. The catalyst has been recovered and recycled over six reactions, obtaining just a low decrease (~ 3 %) in terms of conversion after the fifth recycle, mainly due to the partial loss of catalyst during the recovery and washing steps. The results are reported in the following Table 7.

Table 7 Recycling experiment using optimized conditions (entry 4).

Entry [a]	Run	**2** yield (%)[b]
1	1	95
2	2	95
3	3	95
4	4	93
5	5	92
6	6	92

[a] Conditions: SO (2.00 mmol), CO_2 (1 atm, balloon), neat conditions. [b] Detected with ^1H NMR of the crude reaction mixture with durene as internal standard.

4.2.4 Substrate scope extension study using catalyst 8

The experimental activities described in this section have been performed by the research group at the University of Ferrara.

The efficiency of the optimized method has been tested through a substrate scope extension study, using several terminal epoxides shown in Figure 14.

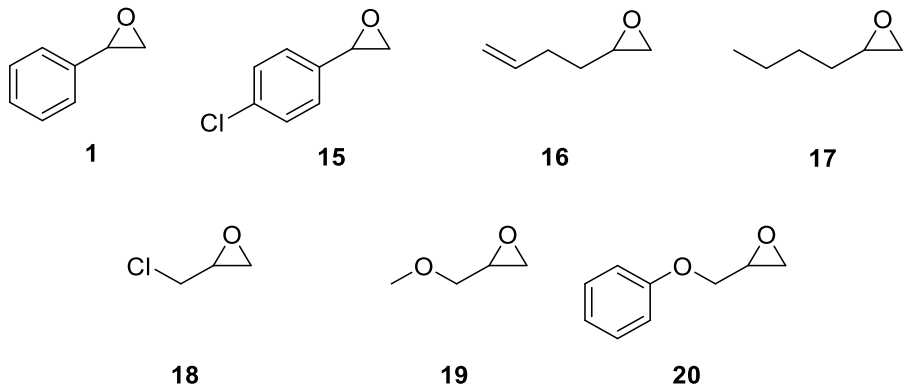

Figure 14 Substrates for scope extension.

The study has been performed at 75°C and ambient pressure in 16 hours and the results are reported in Table 8. Not only styrene oxide and its derivative could efficiently react in the optimized conditions (entries 1-2), but also the other epoxides presenting an alkyl chain can be converted into their corresponding cyclic carbonates in good to excellent yields (entries 3-7).

Table 8 Substrates scope study.

Entry [a]	Substrate	**8** (mol %)	Conversion (%)[b]	Selectivity (%)[b]
1	**1**	5	>95	>99
2	**15**	5	85	>99
3	**16**	5	>95	>99
4	**17**	5	80	>99
5	**18**	5	85	>99
6	**19**	5	95	>99
7	**20**	5	87	>99

[a] Conditions: SO (2.00 mmol), CO_2 (1 atm, balloon), neat conditions. [b] Detected with ^{1}H NMR of the crude reaction mixture with durene as internal standard.

4.2.5 Segmented flow experiments using catalyst 8 on the cyclic carbonates preparation from epoxides

The experimental activities described in this section have been performed by the research group at the University of Ferrara.

The optimized conditions to carry out styrene carbonate synthesis in a homogeneous reaction mixture, which have been reported in Section 4.2.3, were used to explore the process intensification of cyclic carbonates synthesis, exploiting flow techniques [111–123]. In particular, the reactions have been performed in the segmented flow set-up described in Section 4.3.5, which consisted of a 4.42 mL spiral capillary reactor (FEP tubing; 0.75 mm ID) immersed in a bath regulated at 75°C. The coil was connected to a pump and a CO_2 cylinder through a T junction, where the gas and liquid streams were mixed. The exact CO_2 amount was delivered by a mass-flow controller (MCF), while a back-pressure regulator (BPR) constantly kept the system at 8.5 atm of CO_2 pressure. To identify a stable flow regime, liquid and gas flow rates have been initially variated, always keeping a molar excess of CO_2 over styrene oxide. The residence time (t_r) has been calculated as the ratio of reactor volume by the total gas and liquid flow rates.

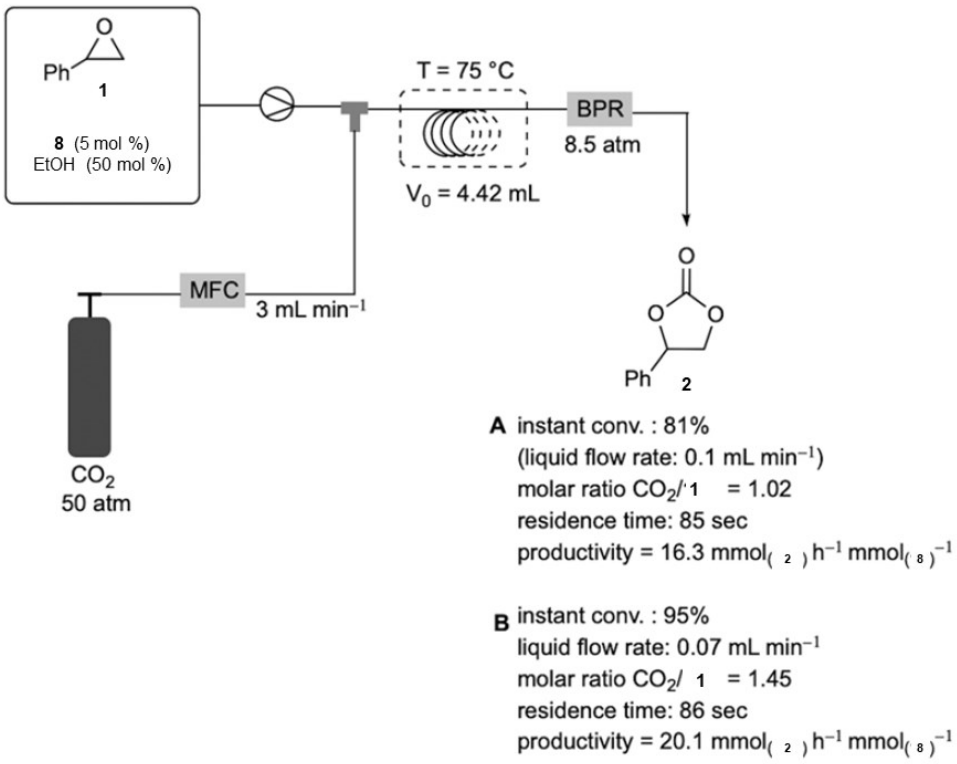

Figure 15 Production of styrene carbonate under segmented flow conditions.

Two sets of conditions have been identified to be optimized with a constant CO_2 flow rate of 3.00 mL/min and liquid flow rates of 0.10 mL/min (conditions A, CO_2/styrene oxide molar ratio of 1.02) and 0.07 mL/min (conditions B, CO_2/styrene oxide molar ratio of 1.45), as it has been reported in Figure 15.

After the steady-state regime has been reached, *i.e.* 2 minutes after the beginning of the experiment, conditions A provided an instant conversion of styrene oxide into styrene carbonate of 81 % in just 85 seconds of t_r, which result corresponded to a process productivity (P) of 16.3 $\frac{\text{mmol(SC)}}{\text{h}^{-1} \times \text{mmol}(\mathbf{8})}$, calculated using Eq. 2. Furthermore, by using conditions B, *i.e.* a lower liquid flow rate, the conversion increased up to > 95 % in 86 seconds of t_r, corresponding to a process productivity of 20.1 $\frac{\text{mmol(SC)}}{\text{h}^{-1} \times \text{mmol}(\mathbf{8})}$. This last obtained value of productivity was about 17 times higher than the one measured in the optimized bulk experiment reported in Section 4.2.3. This process efficiency improvement can be explained by the enhanced mass transfer of CO_2 at the gas-liquid interphase, due to the increased pressure (thermodynamic effect) and segmented flow regime (kinetic effect due to the increased gas/liquid surface to volume ratio).

After the segmented flow conditions have been optimized, the same method has been applied to the substrates **15**, **16**, **17**, **18**, **19** and **20**, represented in Figure 14, to produce their corresponding carbonates **21**, **22**, **23**, **24**, **25** and **26** (Figure 16).

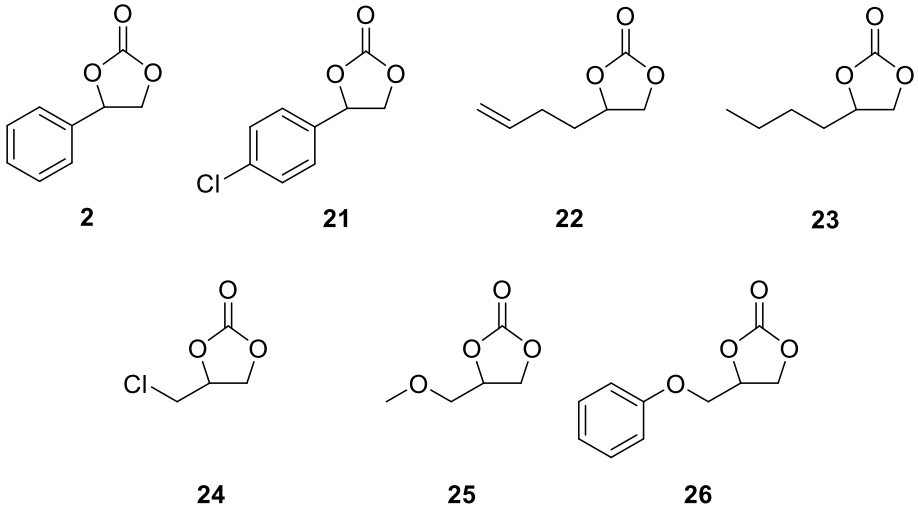

Figure 16 Cyclic carbonates.

The very promising results obtained have been reported in Table 9, in which are shown productivity values in the range of 17.2-20.1 $\frac{\text{mmol(SC)}}{\text{h}^{-1} \times \text{mmol}(\mathbf{8})}$.

Table 9 Production of cyclic carbonates under segmented flow conditions.

Entry [a]	Substrate	**8** (mol %)	Conversion (%)[b]	P[c]
1	**1**	5	>95	20.1
2	**15**	5	90	18.0
3	**16**	5	>95	20.0
4	**17**	5	86	17.2
5	**18**	5	91	18.1
6	**19**	5	>95	20.0
7	**20**	5	92	18.4

[a] Conditions: SO (2.00 mmol), EtOH (50 mol %), CO_2 (8.5 atm), T=75°C, t_r=86 s, CO_2 flow rate: 3 mL/min, liquid flow rate: 0.07 mL/min. conditions. [b] Instant conversion in the steady-state regime has been determined with ^{1}H NMR analysis. [c] Productivities (P) have been measured in $\frac{\text{mmol(SC)}}{\text{h}^{-1} \times \text{mmol}(\mathbf{8})}$.

4.3 Experimental Section

4.3.1 Materials

All the used reagents were commercially available at TCI Europe N.V., Merck or Fluorochem and they have been purchased depending on the availability and the best price. $CDCl_3$ (99.8%) and DMSO-d_6 were purchased from CortecNet. All chemicals were used without any further purification.

4.3.2 Characterization methods

4.3.2.1 Nuclear magnetic resonance (NMR)

The products characterization has been performed *via* NMR spectroscopy, using an Agilent DD2 NMR system, equipped with a 11.7 T (500 MHz) PremiumCompact+ superconducting magnet and an Agilent OneNMR probe. All the isolated products have been fully characterized by NMR spectroscopy through ^{1}H NMR, ^{13}C NMR, ^{1}H-^{1}H COSY, ^{1}H-^{13}C HSQC and ^{1}H-^{13}C HMBC experiments performed in $CDCl_3$.

4.3.2.2 High resolution mass spectrometry (HRMS)

High resolution mass spectra have been recorded in positive ions mode, using an instrument *Agilent 6520 HPLC-Chip Q/TF-MS 229 nanospray*.

4.3.3 Organocatalysts synthesis

4.3.3.1 Synthesis of 3-(dibutylamino)propane-1,2-diol (9)

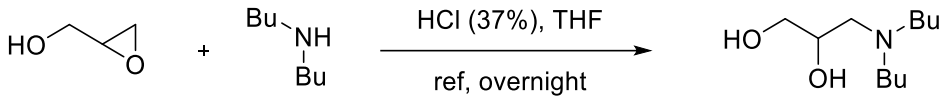

9

Compound	Molecular formula	Molecular weight
Glycidol	$C_3H_6O_2$	74.08 g/mol
Dibutylamine	$C_8H_{19}N$	129.25 g/mol
Hydrochloric acid (37%)	HCl	36.46 g/mol
9	$C_{11}H_{25}NO_2$	203.33 g/mol

Glycidol (15.0 mmol, 3 eq) in THF (10 mL), HCl 37% (1 mL) and dibutylamine (5.0 mmol, 1 eq) have been added to a round bottom flask with a refrigerator on top. The mixture has been stirred and refluxed overnight. Once the dibutylamine was completely reacted, the product has been purified by acid/base extraction with DCM. In particular, the reaction crude has been solubilized in DCM, then the organic phase has been extracted with a solution of HCl 1 M (pH = 1-2); the organic layer has been removed and the aqueous phase basified to pH = 13-14 using a solution 1 M of NaOH and re-extracted with DCM. The organic layer has been treated with anhydrous sodium sulphate, filtered and the solvent was evaporated by rotavapor and high vacuum pump, obtaining compound **9** as a yellow viscous oil (3.60 mmol, 72% yield).

^{1}H NMR (500 MHz, $CDCl_3$) δ 5.73-5.59 (m, 3 H, H1 + H2), δ 5.45 (dd, 1 H, , H1', J = 11.1, 4.5 Hz), δ 4.59-4.42 (m, 3 H, H3 + H4 + H8), δ 4.42-4.31 (m, 3 H, H3' + H4' + H8'), δ 3.47-3.33 (m, 4 H, H5 + H9), δ 3.33-3.18 (m, 4 H, H6 + H10), δ 2.87 (t, 6 H, H7 + H11, J = 7.4 Hz).

^{13}C NMR (125 MHz, $CDCl_3$) δ 67.3 (C2), δ 65.0 (C1), δ 57.0 (C3), δ 54.3 (C4 + C8), δ 29.2 (C5 + C9), δ 20.7 (C6 + C10), δ 14.1 (C7 + C11).

HRMS (ESI) m/z: $[M + H]^+$ calculated for $C_{11}H_{26}NO_2^+$ 204.1958, found 204.1952.

4.3.3.2 Synthesis of 3-(1H-imidazol-1-yl)propane-1,2-diol (10)

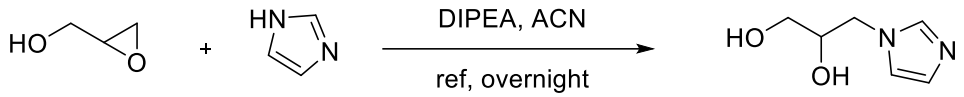

10

Compound	Molecular formula	Molecular weight
Glycidol	$C_3H_6O_2$	74.08 g/mol
imidazole	$C_3H_4N_2$	68.08 g/mol
N,N-diisopropylethylamine (DIPEA)	$C_8H_{19}N$	129.25 g/mol
10	$C_6H_{10}N_2O_2$	142.16 g/mol

Glycidol (15.0 mmol, 1.5 eq) in acetonitrile (10 mL), DIPEA (10.0 mmol, 1 eq) and imidazole (10 mmol, 1 eq) have been added to a round bottom flask with a refrigerator on top. The mixture has been stirred and refluxed overnight. Once the imidazole was completely reacted, purification took place by flash chromatography (Chromatographic method: CombiFlash RF 200 LC system; stationary phase: silica 120, CV = 192 mL; flow rate: 85 mL/min; elution method: from 100% A to 100% B in 45 CV, then 100% B in 10 CV; A: EtOAc + 2% NH_4OH, B: EtOAc/MeOH = 9/1 + 2% NH_4OH). The solvent was evaporated by rotavapor and high vacuum pump, obtaining compound **10** as a pale-yellow viscous oil (5.70 mmol, 57% yield).

^{1}H NMR (500 MHz, D_2O) δ 7.68 (s, 1 H, AR NCHN), δ 7.18 (s, 1 H, AR), δ 7.03 (s, 1 H, AR), δ 4.19 (dd, 1 H, H1, J = 13.7, 3.0 Hz), δ 4.06-3.98 (m, 2 H, H1' + H2), δ 3.60 (dd, 1 H, H3, J = 11.8, 5.0 Hz), δ 3.53 (dd, 1 H, H3', J = 11.8, 5.0 Hz).

^{13}C NMR (125 MHz, D_2O) δ 138.2 (AR NCN), δ 127.2 (AR), δ 120.5 (AR), δ 70.6 (C2), δ 62.4 (C3), δ 49.0 (C1).

HRMS (ESI) m/z: $[M + H]^+$ calculated for $C_6H_{11}N_2O_2^+$ 143.0815, found 143.0816.

4.3.3.3 Synthesis of 2-(Methyl(pyridin-4-yl)amino)ethan-1-ol (11)

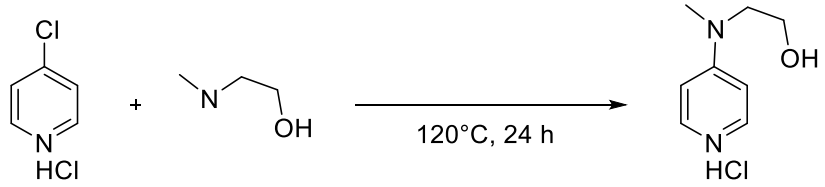

11

Compound	Molecular formula	Molecular weight
4-Chloropyridine hydrochloride	$C_5H_5Cl_2N$	150.00 g/mol
N-methylethanolamine	C_3H_9NO	75.11 g/mol
11	$C_8H_{12}N_2O$	152.20 g/mol

4-Chloropyridine hydrochloride (5.00 mmol, 1 eq) and N-methylethanolamine (62.5 mmol, 12.5 eq) have been added to a round bottom flask. The mixture has been stirred at 120°C for 24 hours and then the large excess of unreacted amine has been vacuum-evaporated. After 24 hours the crude was diluted in DCM and washed with a solution of K_2CO_3 1 M. The organic layer has been treated with anhydrous sodium sulphate, filtered and the solvent evaporated by rotavapor and high vacuum pump for additional 24 hours, obtaining compound **11** as a white amorphous solid (3.50 mmol, 70% yield).

^{1}H NMR (500 MHz, $CDCl_3$) δ 8.12 (dd, 2 H, AR NCH, J = 5.1, 1.6 Hz), δ 6.52 (dd, 2 H, AR, J = 5.1, 1.6 Hz), δ 3.83 (t, 2 H, CH_2OH, J = 5.7 Hz), δ 3.54 (t, 2 H, NCH_2, J = 5.7 Hz), δ 3.04 (s, 3 H, CH_3), δ 2.70 (broad s, 1 H, OH).

^{13}C NMR (125 MHz, $CDCl_3$) δ 149.0 (AR NC), δ 106.7 (AR), δ 59.6 (COH), δ 53.6 (NC), δ 38.2 (CH_3).

HRMS (ESI) m/z: $[M + H]^+$ calculated for $C_8H_{13}N_2O^+$ 153.1022, found 153.1024.

4.3.3.4 Synthesis of (1-(Pyridin-4-yl)pyrrolidin-2-yl)methanol (12)

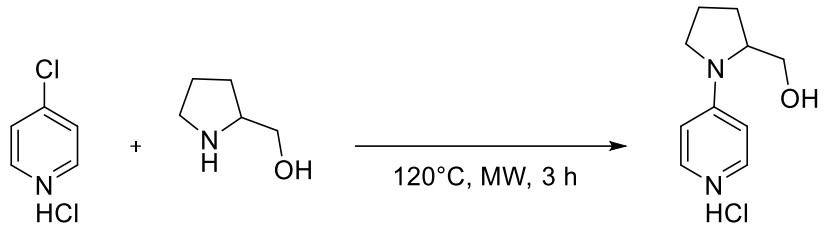

12

Compound	Molecular formula	Molecular weight
4-Chloropyridine hydrochloride	$C_5H_5Cl_2N$	150.00 g/mol
Prolinol	$C_5H_{11}NO$	101.15 g/mol
12	$C_{10}H_{14}N_2O$	178.24 g/mol

4-Chloropyridine hydrochloride (0.70 mmol, 1 eq) and prolinol (8.75 mmol, 12.5 eq) have been added to a 5 mL vial equipped with a magnetic stirrer. The vial was hermetically sealed and inserted into the microwave. The reaction mixture was stirred and irradiated for 3 hours at 120 °C, and then the large excess of unreacted prolinol has been vacuum-evaporated. After 24 hours the crude was diluted in DCM and washed with a solution of K_2CO_3 1 M. The organic layer has been treated with anhydrous sodium sulphate, filtered and the solvent was evaporated by rotavapor and high vacuum pump for additional 24 hours, obtaining compound **12** as a brown amorphous solid (0.70 mmol, >99% yield).

^{1}H NMR (500 MHz, $CDCl_3$) δ 8.16 (d, 2 H, AR NCH, J = 5.0 Hz), δ 6.48 (d, 2 H, AR, J = 5.0 Hz), δ 3.98-3.83 (m, 1 H, H2), δ 3.70 (dd, 1 H, J = 11.0, 4.2 Hz), δ 3.60 (dd, 1 H, J = 11.0, 6.9 Hz), δ 3.48-3.43 (m, 1 H), δ 3.28-3.08 (m, 1 H), δ 2.20-1.90 (m, 5 H).

^{13}C NMR (125 MHz, $CDCl_3$) δ 152.4 (AR_{ipso}), δ 149.6 (AR NC), δ 107.4 (AR), δ 62.6 (C1), δ 59.6 (C2), δ 48.1 (C5), δ 28.3 (C3), δ 23.2 (C4).

HRMS (ESI) m/z: $[M + H]^+$ calculated for $C_{10}H_{15}N_2O^+$ 179.1179, found 179.1181.

4.3.3.5 Synthesis of N-Butyl-N-(2,3-dihydroxypropyl)-N-(3-hydroxypropyl) butan-1-aminium iodide (4)

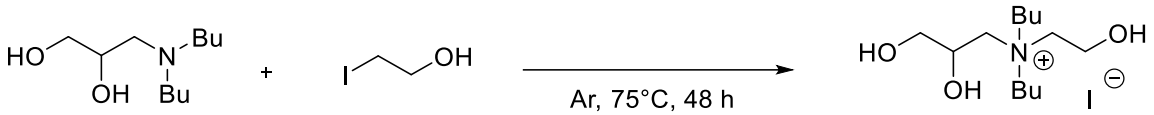

9 **4**

Compound	Molecular formula	Molecular weight
9	$C_{11}H_{25}NO_2$	203.33 g/mol
2-iodoethanol	ICH_2CH_2OH	171.97 g/mol
4	$C_{13}H_{30}NO_3^+I^-$	375.30 g/mol

Compound **9** (2.50 mmol) and 2-iodoethanol (2.50 mmol) have been added to a 10 mL vial equipped with a magnetic stir bar. Then, three vacuum/argon cycles have been performed and the vial has been put under argon atmosphere. The reaction mixture has been vigorously stirred for 48 hours at 75 °C. No purification steps were needed to obtain compound **4** as a very viscous brown liquid (2.12 mmol, 85 % yield).

^{1}H NMR (500 MHz, DMSO-d_6) δ 5.31 (d, 1 H, J = 5.3 Hz), δ 5.20 (t, 1 H, *J* = 5.3 Hz), δ 5.04 (t, 1 H, *J* = 5.3 Hz), δ 4.03-3.88 (m, 1 H), δ 3.87-3.71 (m, 2 H), δ 3.63-3.55 (m, 1 H), δ 3.50-3.35 (m, 6 H), δ 3.32-3.11 (m, 2 H), δ 3.01 (broad s, 1 H), δ 1.78-1.46 (m, 4 H), δ 1.36-1.17 (m, 4 H), δ 0.95-0.83 (m, 6 H).

^{13}C NMR (125 MHz, DMSO-d_6) δ 66.0, δ 64.1, δ 62.8, δ 61.8, δ 60.6, δ 59.8, δ 56.5, δ 55.0, δ 23.6, δ 19.6, δ 19.0, δ 13.9.

HRMS (ESI) m/z: $[M + H]^+$ calculated for $C_{13}H_{30}NO_3^+$ 248.2226, found 248.2232.

4.3.3.6 Synthesis of N-Butyl-N-(2,3-dihydroxypropyl)-N-(3-hydroxypropyl) butan-1-aminium bromide (5)

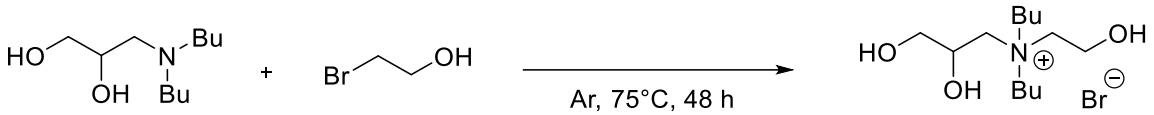

9 **5**

Compound	Molecular formula	Molecular weight
9	$C_{11}H_{25}NO_2$	203.33 g/mol
2-bromoethanol	$BrCH_2CH_2OH$	124.97 g/mol
5	$C_{13}H_{30}NO_3^+Br^-$	328.29 g/mol

Compound **9** (2.50 mmol) and 2-bromoethanol (2.50 mmol) have been added to a 10 mL vial equipped with a magnetic stir bar. Then, three vacuum/argon cycles have been performed and the vial has been put under argon atmosphere. The reaction mixture has been vigorously stirred for 48 hours at 75 °C. No purification steps were needed to obtain compound **5** as a very viscous brown liquid (2.12 mmol, 85 % yield).

^{1}H NMR (500 MHz, DMSO-d_6) δ 5.33 (d, 1 H, J = 5.2 Hz), δ 5.21 (t, 1 H, *J* = 5.2 Hz), δ 5.04 (t, 1 H, *J* = 5.2 Hz), δ 4.04-3.90 (m, 1 H), δ 3.89-3.73 (m, 2 H), δ 3.73-3.52 (m, 1 H), δ 3.50-3.34 (m, 6 H), δ 3.31-3.12 (m, 2 H), δ 3.03 (s, 1 H), δ 1.81-1.46 (m, 4 H), δ 1.38-1.16 (m, 4 H), δ 0.96-0.81 (m, 6 H).

^{13}C NMR (125 MHz, DMSO-d_6) δ 66.0, δ 64.1, δ 62.7, δ 61.8, δ 60.6, δ 59.8, δ 56.5, δ 55.0, δ 23.6, δ 19.6, δ 19.0, δ 13.9.

HRMS (ESI) m/z: $[M + H]^+$ calculated for $C_{13}H_{30}NO_3^+$ 248.2226, found 248.2229.

4.3.3.7 Synthesis of 1-(2,3-Dihydroxypropyl)-3-(2-hydroxyethyl)-1H-imidazol-3-ium iodide (6)

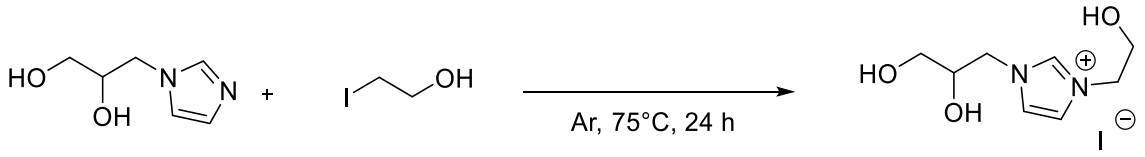

10 **6**

Compound	Molecular formula	Molecular weight
10	$C_6H_{10}N_2O_2$	142.16 g/mol
2-iodoethanol	ICH_2CH_2OH	171.97 g/mol
6	$C_8H_{15}N_2O_3^+I^-$	314.13 g/mol

Compound **10** (1.40 mmol) and 2-iodoethanol (1.40 mmol) have been added to a 10 mL vial equipped with a magnetic stir bar. Then, three vacuum/argon cycles have been performed and the vial has been put under argon atmosphere. The reaction mixture has been vigorously stirred for 24 hours at 75 °C. No purification steps were needed to obtain compound **6** as a very viscous brown liquid (1.23 mmol, 88 % yield).

^{1}H NMR (500 MHz, DMSO-d_6) δ 9.05 (s, 1 H), δ 7.69 (d, 2 H, J = 9.4 Hz), δ 5.29 (d, 1 H, J = 5.0 Hz), δ 5.14 (t, 1 H, J = 5.0 Hz), δ 4.93 (t, 1 H, J = 5.0 Hz), δ 4.30 (dd, 1 H, J = 13.8, 2.7 Hz), δ 4.21 (t, 2 H, J = 5.0 Hz), δ 4.07 (dd, 1 H, J = 13.8, 8.2 Hz), δ 3.83-3.68 (m, 3 H), δ 3.46-3.36 (m, 1 H), δ 3.26-3.17 (m, 1 H).

^{13}C NMR (125 MHz, DMSO-d_6) δ 137.2, δ 123.5, δ 122.8, δ 70.1, δ 63.2, δ 59.8, δ 52.6, δ 52.0.

HRMS (ESI) m/z: $[M + H]^+$ calculated for $C_8H_{15}N_2O_3^+$ 187.1077, found 187.1071.

4.3.3.8 Synthesis of 3-iodopropane-1,2-diol (14)

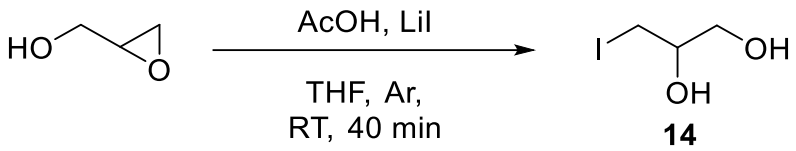

14

Compound	Molecular formula	Molecular weight
Glycidol	$C_3H_6O_2$	74.08 g/mol
Lithium iodide	LiI	133.85 g/mol
AcOH	$C_2H_4O_2$	60.05 g/mol
14	$C_3H_7IO_2$	201.99 g/mol

LiI (80.0 mmol, 10 g) has been added to a solution of glycidol (50.0 mmol) and acetic acid (150 mmol) in anhydrous THF (40 mL). The solution has been stirred in argon atmosphere for 40 min at RT. Then, the mixture has been diluted with distilled water and extracted with two aliquots of EtOAc (20 mL each). The organic layer has been treated with anhydrous sodium sulphate and filtered, and the solvent was removed using rotavapor. By following this procedure, compound **14** has been quantitatively obtained as a yellow amorphous solid (50.0 mmol).

^{1}H NMR (500 MHz, D_2O) δ 3.59-3-42 (m, 3 H), δ 3.25 (dd, 1 H, J = 10.8, 4.5 Hz), δ 3.15 (dd, 1 H, J = 10.8, 4.5 Hz).

^{13}C NMR (125 MHz, D_2O) δ 70.6, δ 64.4, δ 8.6.

HRMS (ESI) m/z: $[M + H]^+$ calculated for $C_3H_8IO_2^+$ 202.9563, found 202.9554.

4.3.3.9 Synthesis of 1-(2,3-Dihydroxypropyl)-4-((2-hydroxyethyl)(methyl) amino)pyridin-1-ium iodide (7)

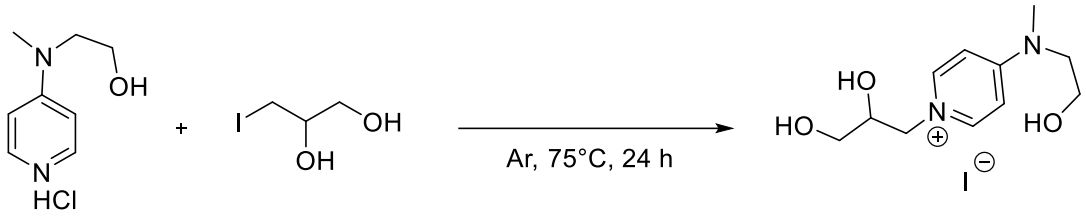

11 **14** **7**

Compound	Molecular formula	Molecular weight
11	$C_8H_{12}N_2O$	152.20 g/mol
14	$C_3H_7IO_2$	201.99 g/mol
7	$C_{11}H_{19}N_2O_3^+I^-$	354.19 g/mol

Compound **11** (0.25 mmol) and **14** (0.25 mmol) have been added to a 10 mL vial equipped with a magnetic stir bar. Then, three vacuum/argon cycles have been performed and the vial has been put under argon atmosphere. The reaction mixture has been vigorously stirred for 24 hours at 75 °C. No purification steps were needed to obtain compound **7** as a very viscous yellow liquid (0.25 mmol, quant.).

^{1}H NMR (500 MHz, DMSO-d_6) δ 8.13 (dd, 2 H, J = 12.5, 7.5 Hz), δ 7.12 (d, 1 H, J = 5.2 Hz), δ 6.96 (d, 1 H, J = 7.5 Hz), δ 5.24 (d, 1 H, J = 5.2 Hz), δ 4.92 (dd, 2 H, J = 12.0, 6.2 Hz), δ 4.27 (d, 1 H, J = 10.6 Hz), δ 4.01 (dd, 1 H, J = 13.6, 8.2 Hz), δ 3.73 (broad s, 1 H), δ 3.63 (s, 4 H), δ 3.53-3.40 (m, 2 H), δ 3.15 (s, 3 H).

^{13}C NMR (125 MHz, DMSO-d_6) δ 156.6, δ 143.5, δ 142.8, δ 108.0, δ 107.6, δ 70.6, δ 63.1, δ 60.0, δ 58.4, δ 54.2.

HRMS (ESI) m/z: $[M + H]^+$ calculated for $C_{11}H_{19}N_2O_3^+$ 227.1390, found 227.1380.

4.3.3.10 Synthesis of 1-(2,3-Dihydroxypropyl)-4-((2-hydroxyethyl)(methyl) amino)pyridin-1-ium iodide (8)

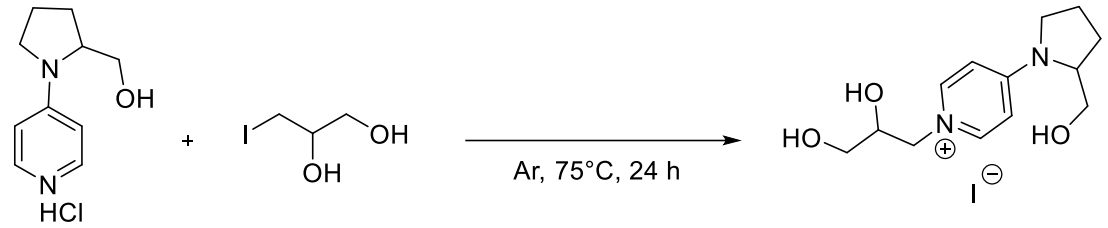

12 **14** **8**

Compound	Molecular formula	Molecular weight
12	$C_{10}H_{14}N_2O$	178.24 g/mol
14	$C_3H_7IO_2$	201.99 g/mol
8	$C_{13}H_{21}N_2O_3^+I^-$	380.23 g/mol

Compound **12** (0.25 mmol) and **14** (0.25 mmol) have been added to a 10 mL vial equipped with a magnetic stir bar. Then, three vacuum/argon cycles have been performed and the vial has been put under argon atmosphere. The reaction mixture has been vigorously stirred for 24 hours at 75 °C. No purification steps were needed to obtain compound **8** as a very viscous brown liquid (0.25 mmol, quant.).

^{1}H NMR (500 MHz, DMSO-d_6) δ 8.16 (t, 2 H, J = 6.3 Hz), δ 7.06 (dd, 1 H, J = 7.8, 2.8 Hz), δ 6.86 (dd, 1 H, J = 7.8, 2.8 Hz), δ 5.25 (d, 1 H, J = 5.4 Hz), δ 4.96 (dt, 2 H, J = 13.1, 5.4 Hz), δ 4.29 (d, 1 H, J = 12.3 Hz), δ 4.14 (d, 1 H, J = 5.1 Hz), δ 4.03 (dd, 1 H, J = 13.6, 7.8 Hz), δ 3.75 (broad s, 1 H), δ 3.58 (t, 1 H, J = 10.8 Hz), δ 3.51-3.35 (m, 4 H), δ 3.31-3.21 (m, 1 H), δ 2.23-1.71 (m, 4 H).

^{13}C NMR (125 MHz, DMSO-d_6) δ 154.0, δ 143.5, δ 142.9, δ 108.8, δ 108.4, δ 70.8, δ 63.2, δ 61.3, δ 61.1, δ 60.1, δ 49.2, δ 28.0, δ 22.8.

HRMS (ESI) m/z: $[M + H]^+$ calculated for $C_{13}H_{21}N_2O_3^+$ 253.1547, found 253.1551.

4.3.4 Organocatalysts efficiency tests on the carbonation of epoxides

4.3.4.1 Bulk tests of catalyst 4, 5, 6, 7 and 8 at RT on SO carbonation

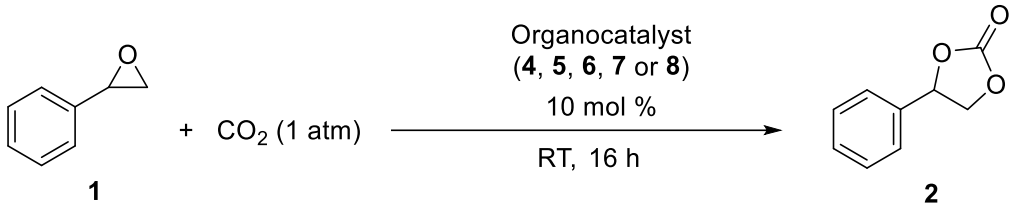

Compound	Molecular formula	Molecular weight
1	C_8H_8O	120.15 g/mol
4	$C_{13}H_{30}NO_3^+I^-$	375.30 g/mol
5	$C_{13}H_{30}NO_3^+Br^-$	328.29 g/mol
6	$C_8H_{15}N_2O_3^+I^-$	314.13 g/mol
7	$C_{11}H_{19}N_2O_3^+I^-$	354.19 g/mol
8	$C_{13}H_{21}N_2O_3^+I^-$	380.23 g/mol

In a 10 mL vial equipped with a small magnetic stir bar, 240 mg (2.00 mmol) of styrene oxide and 10 mol % of previously synthesized organocatalyst **4**, **5**, **6**, **7** or **8** have been added. The closed vial has been subjected to three vacuum/CO_2 cycles and finally filled with CO_2. The mixture has been stirred for 16 hours at RT. The crude mixture has been characterized through ^{1}H NMR (in $CDCl_3$), using an internal standard of durene, to quantify the styrene oxide conversion into styrene carbonate.

^{1}H NMR (500 MHz, $CDCl_3$): a) Styrene oxide **1**: δ 7.39-7.30 (m, 5 H, AR), δ 3.88 (dd, 1 H, CH, $J_{CH\text{-}CH2}$ = 3.96 Hz, $J_{CH\text{-}CH2'}$ = 2.67 Hz), δ 3.16 (dd, 1 H, CH_2, $J_{CH2\text{-}CH2'}$ = 5.46 Hz, $J_{CH2\text{-}CH}$ = 4.16 Hz), δ 2.82 (dd, 1 H, CH_2', $J_{CH2'\text{-}CH2}$ = 5.50 Hz, $J_{CH2'\text{-}CH}$ = 2.58 Hz); b) Styrene carbonate **2**: δ 7.46-7.36 (m, 5 H, AR), δ 5.68 (t, 1 H, CH, $J_{CH\text{-}CH2}$ = $J_{CH\text{-}CH2'}$ = 8.01 Hz), δ 4.81 (t, 1 H, CH_2, $J_{CH2\text{-}CH2'}$ = $J_{CH2\text{-}CH}$ = 8.40 Hz), δ 4.35 (t, 1 H, CH_2', $J_{CH2'\text{-}CH2}$ = $J_{CH2'\text{-}CH}$ = 8.29 Hz).

4.3.4.2 General procedure for cyclic carbonates synthesis from corresponding epoxides under bulk conditions using organocatalyst 8

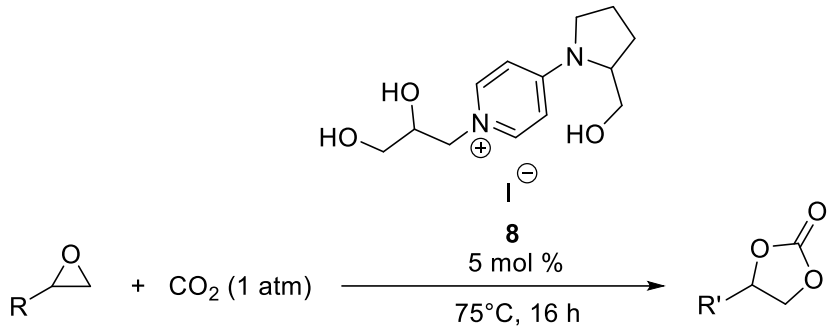

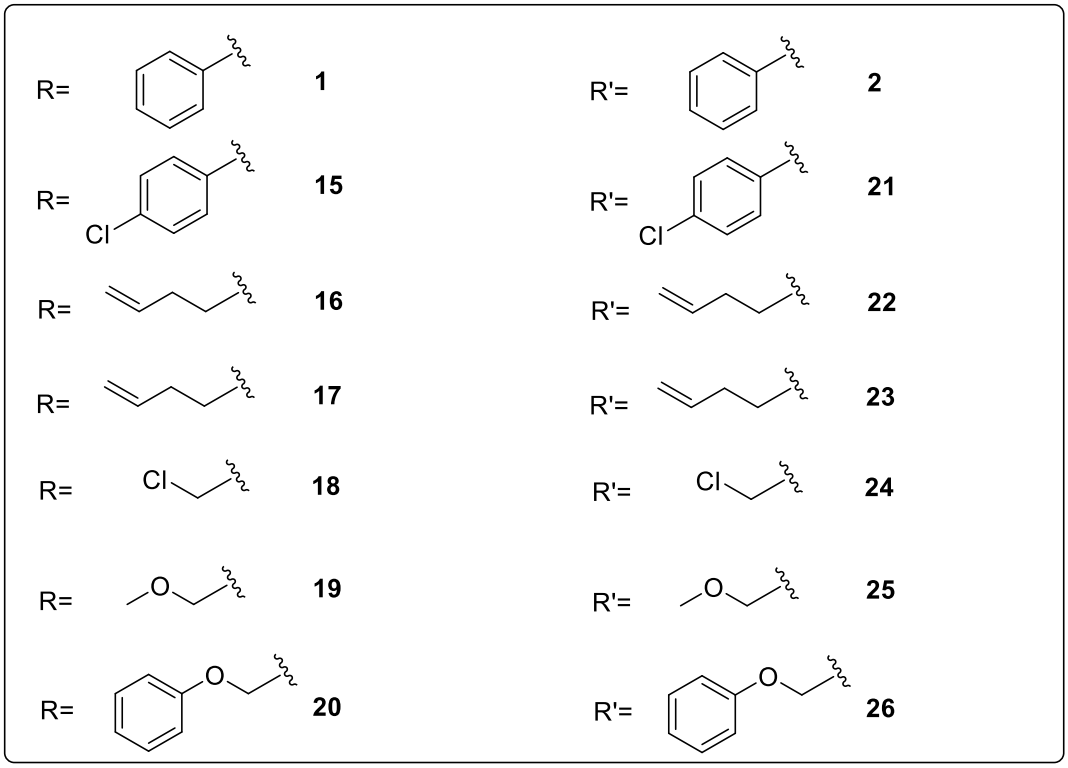

Compound	Molecular formula	Molecular weight
1	C_8H_8O	120.15 g/mol
15	C_8H_7ClO	154.59 g/mol
16	$C_6H_{10}O$	98.15 g/mol
17	$C_6H_{12}O$	100.16 g/mol
18	C_3H_5ClO	92.52 g/mol
19	$C_4H_8O_2$	88.11 g/mol
20	$C_9H_{10}O_2$	150.18 g/mol
8	$C_{13}H_{21}N_2O_3^+I^-$	380.23 g/mol

In a 10 mL vial equipped with a small magnetic stir bar, 2.00 mmol of epoxide (**1**, **15**, **16**, **17**, **18**, **19** or **20**) and 5 mol % of previously synthesized organocatalyst **8** have been added. The closed vial has been subjected to three vacuum/CO_2 cycles and finally filled with CO_2. The mixture has been stirred for 16 hours at 75°C.

Then, the reacted mixture has been diluted with EtOAc to precipitate the organocatalyst and centrifuged to recover the product, which has been purified using short column chromatography on silica gel (9:1 Cy/EtOAc). By using this procedure, the corresponding cyclic carbonate have been obtained in variable yields (**2** >95 % yield, **21** 85 % yield, **22** >95 % yield, **23** 80 % yield, **24** 85 % yield, **25** 95 % yield and **26** 87 % yield).

2: **^{1}H NMR (500 MHz, $CDCl_3$)** δ 7.46-7.36 (m, 5 H, AR), δ 5.68 (t, 1 H, CH, $J_{CH\text{-}CH2}$ = $J_{CH\text{-}CH2'}$ = 8.01 Hz), δ 4.81 (t, 1 H, CH_2, $J_{CH2\text{-}CH2'}$ = $J_{CH2\text{-}CH}$ = 8.40 Hz), δ 4.35 (t, 1 H, CH_2', $J_{CH2'\text{-}CH2}$ = $J_{CH2'\text{-}CH}$ = 8.29 Hz). **^{13}C NMR (125 MHz, $CDCl_3$)** δ 154.77 (OCOO), δ 135.76 (AR_{ipso}), δ 129.68 (AR_{meta}), δ 129.18 (AR_{para}), δ 125.82 (AR_{ortho}), δ 77.94 (CH), δ 71.11 (CH_2). **HRMS (ESI)** m/z: $[M + H]^+$ calculated for $C_9H_9O_3^+$ 165.0546, found 165.0539.

21: **^{1}H NMR (500 MHz, $CDCl_3$)** δ 7.43 (d, 2 H, J = 8.5 Hz), δ 7.31 (d, 2 H, J = 8.5 Hz), δ 5.66 (t, 1 H, *J* = 8.0 Hz), δ 4.80 (t, 1 H, J = 8.6 Hz), δ 4.31 (dd, 1 H, J = 8.6 Hz). **^{13}C NMR (125 MHz, $CDCl_3$)** δ 154.5, δ 135.8, δ 134.2, δ 129.5, δ 122.2, δ 77.0, δ 71.0. **HRMS (ESI)** m/z: $[M + H]^+$ calculated for $C_9H_8ClO_3^+$ 199.0156, found 199.0163.

22: **^{1}H NMR (500 MHz, $CDCl_3$)** δ 5.88-5.70 (m, 1 H), δ 5.15-5.01 (m, 2 H), δ 4.78-4.67 (m, 1 H), δ 4.53 (t, 1 H, *J* = *8.2* Hz), δ 4.08 (t, 1 H, *J* = *8.2* Hz), δ 2.34-2.10 (m, 2 H), δ 2,00-1.87 (m, 1 H), δ 1.83-1.71 (m, 1 H). **^{13}C NMR (125 MHz, $CDCl_3$)** δ 154.9, δ 136.0, δ 116.5, δ 76.3, δ 69.3, δ 33.1, δ 28.7. **HRMS (ESI)** m/z: $[M + H]^+$ calculated for $C_7H_{11}O_3^+$ 143.0703, found 143.0699.

23: **^{1}H NMR (500 MHz, $CDCl_3$)** δ 4.75-4.65 (m, 1 H), δ 4.52 (t, 1 H, *J* = 8.1 Hz), δ 4.07 (dd, 1 H, *J* = 8.1, 7.1 Hz), δ 1.88-1.76 (m, 1 H), δ 1.74-1.64 (m, 1 H), δ 1.48-1.31 (m, 4 H), δ 0.93 (t, 3 H, *J* = 7.1 Hz). **^{13}C NMR (125 MHz, $CDCl_3$)** δ 155.0, δ 77.0, δ 69.4, δ 33.6, δ 26.4, δ 22.2, δ 13.8. **HRMS (ESI)** m/z: $[M + H]^+$ calculated for $C_7H_{13}O_3^+$ 145.0859, found 145.0861.

24: **^{1}H NMR (500 MHz, $CDCl_3$)** δ 4.99-4.91 (m, 1 H), δ 4.59 (dd, 1 H, *J* = 8.9, 8.2 Hz), δ 4.41 (dd, 1 H, *J* = 8.9, 5.7 Hz), δ 3.84-3.68 (m, 2 H). **^{13}C NMR (125 MHz, $CDCl_3$)** δ 154.0, δ 74.2, δ 67.0, δ 43.5. **HRMS (ESI)** m/z: $[M + H]^+$ calculated for $C_4H_6ClO_3^+$ 137.0000, found 136.9998.

25: **^{1}H NMR (500 MHz, $CDCl_3$)** δ 4.85-4.75 (m, 1 H), δ 4.49 (t, 1 H, *J* = 8.4 Hz), δ 4.38 (dd, 1 H, *J* = 8.4, 6.1 Hz), δ 3.61 (qd, 2 H, *J* = 10.9, 3.9 Hz), δ 3.43 (s, 3 H). **^{13}C NMR (125 MHz, $CDCl_3$)** δ 154.9, δ 74.9, δ 71.4, δ 66.2, δ 59.7. **HRMS (ESI)** m/z: $[M + H]^+$ calculated for $C_4H_9O_4^+$ 133.0495, found 133.0489.

26: **^{1}H NMR (500 MHz, $CDCl_3$)** δ 7.31 (dd, 2 H, *J* = 8.2, 7.3 Hz), δ 7.02 (t, 1 H, *J* = 7.3 Hz), δ 6.91 (d, 2 H, *J* = 8.2 Hz), δ 5.09-4.98 (m, 1 H), δ 4.66-4.50 (m, 2 H), δ 4.20 (qd, 2 H, *J* = 10.5, 3.9 Hz), **^{13}C NMR (125 MHz, $CDCl_3$)** δ 157.7, δ 129.7, δ 122.0, δ 114.6, δ 74.0, δ 66.8, δ 66.2. **HRMS (ESI)** m/z: $[M + H]^+$ calculated for $C_{10}H_{11}O_4^+$ 195.0652, found 195.0660.

4.3.4.3 General procedure for cyclic carbonates synthesis from corresponding epoxides under segmented flow conditions using organocatalyst 8

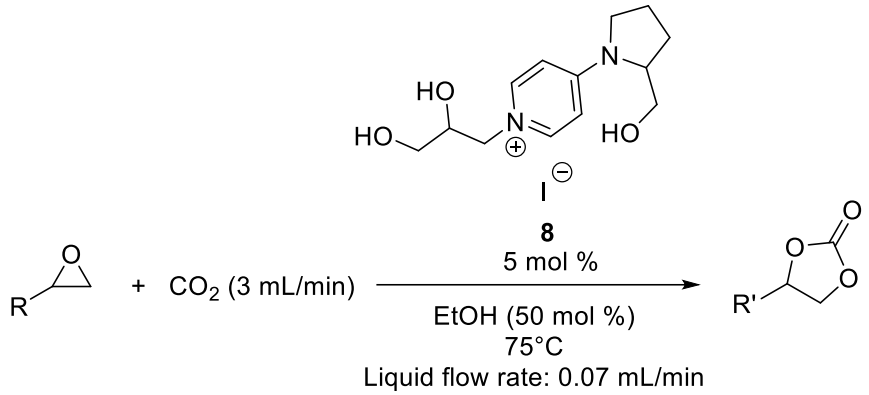

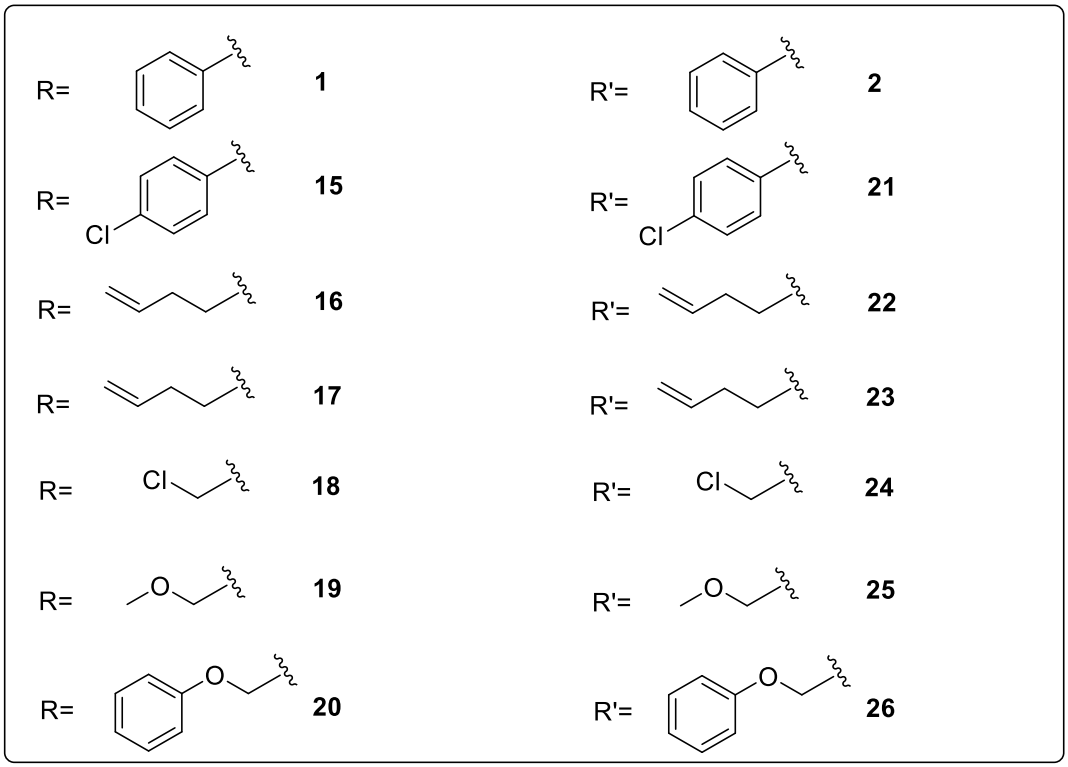

Compound	Molecular formula	Molecular weight
1	C_8H_8O	120.15 g/mol
15	C_8H_7ClO	154.59 g/mol
16	$C_6H_{10}O$	98.15 g/mol
17	$C_6H_{12}O$	100.16 g/mol
18	C_3H_5ClO	92.52 g/mol
19	$C_4H_8O_2$	88.11 g/mol
20	$C_9H_{10}O_2$	150.18 g/mol
8	$C_{13}H_{21}N_2O_3^+I^-$	380.23 g/mol

2.00 mmol of epoxide (**1**, **15**, **16**, **17**, **18**, **19** or **20**), 50 mol % of EtOH and 5 mol % of previously synthesized organocatalyst **8** have been mixed in the reservoir of the flow apparatus (10 mL vial) equipped with a small magnetic stir bar (Section 4.3.5). Then, the resulting solution has been pumped through the thermostated reactor at 75°C, using a 0.07 mL/min flow rate. Simultaneously, a CO_2 gas flow rate of 3 mL/min has been delivered. After 4 minutes from the injection, the crude mixture from the outlet stream has been collected and characterized through ^{1}H NMR (in $CDCl_3$), minute by minute for a total of 6 minutes using an internal standard of durene, for the evaluation of epoxides into their corresponding carbonates conversion. After 10 minutes, a further aliquot of the mixture has been collected and diluted with EtOAc to precipitate the organocatalyst and centrifuged to recover the product, which has been purified using short column chromatography on silica gel (9:1 Cy/EtOAc). By using this procedure, the corresponding cyclic carbonate have been obtained in variable yields (**2** >95 % yield, **21** 85 % yield, **22** >95 % yield, **23** 80 % yield, **24** 85 % yield, **25** 95 % yield and **26** 87 % yield).

2: **^{1}H NMR (500 MHz, $CDCl_3$)** δ 7.46-7.36 (m, 5 H, AR), δ 5.68 (t, 1 H, CH, $J_{CH\text{-}CH2}$ = $J_{CH\text{-}CH2'}$ = 8.01 Hz), δ 4.81 (t, 1 H, CH_2, $J_{CH2\text{-}CH2'}$ = $J_{CH2\text{-}CH}$ = 8.40 Hz), δ 4.35 (t, 1 H, CH_2', $J_{CH2'\text{-}CH2}$ = $J_{CH2'\text{-}CH}$ = 8.29 Hz). **^{13}C NMR (125 MHz, $CDCl_3$)** δ 154.77 (OCOO), δ 135.76 (AR_{ipso}), δ 129.68 (AR_{meta}), δ 129.18 (AR_{para}), δ 125.82 (AR_{ortho}), δ 77.94 (CH), δ 71.11 (CH_2). **HRMS (ESI)** m/z: $[M + H]^+$ calculated for $C_9H_9O_3^+$ 165.0546, found 165.0539.

21: **^{1}H NMR (500 MHz, $CDCl_3$)** δ 7.43 (d, 2 H, J = 8.5 Hz), δ 7.31 (d, 2 H, J = 8.5 Hz), δ 5.66 (t, 1 H, *J* = 8.0 Hz), δ 4.80 (t, 1 H, J = 8.6 Hz), δ 4.31 (dd, 1 H, J = 8.6 Hz). **^{13}C NMR (125 MHz, $CDCl_3$)** δ 154.5, δ 135.8, δ 134.2, δ 129.5, δ 122.2, δ 77.0, δ 71.0. **HRMS (ESI)** m/z: $[M + H]^+$ calculated for $C_9H_8ClO_3^+$ 199.0156, found 199.0163.

22: **^{1}H NMR (500 MHz, $CDCl_3$)** δ 5.88-5.70 (m, 1 H), δ 5.15-5.01 (m, 2 H), δ 4.78-4.67 (m, 1 H), δ 4.53 (t, 1 H, *J* = *8.2* Hz), δ 4.08 (t, 1 H, *J* = *8.2* Hz), δ 2.34-2.10 (m, 2 H), δ 2,00-1.87 (m, 1 H), δ 1.83-1.71 (m, 1 H). **^{13}C NMR (125 MHz, $CDCl_3$)** δ

154.9, δ 136.0, δ 116.5, δ 76.3, δ 69.3, δ 33.1, δ 28.7. **HRMS (ESI)** m/z: $[M + H]^+$ calculated for $C_7H_{11}O_3^+$ 143.0703, found 143.0699.

23: **^{1}H NMR (500 MHz, $CDCl_3$)** δ 4.75-4.65 (m, 1 H), δ 4.52 (t, 1 H, *J* = 8.1 Hz), δ 4.07 (dd, 1 H, *J* = 8.1, 7.1 Hz), δ 1.88-1.76 (m, 1 H), δ 1.74-1.64 (m, 1 H), δ 1.48-1.31 (m, 4 H), δ 0.93 (t, 3 H, *J* = 7.1 Hz). **^{13}C NMR (125 MHz, $CDCl_3$)** δ 155.0, δ 77.0, δ 69.4, δ 33.6, δ 26.4, δ 22.2, δ 13.8. **HRMS (ESI)** m/z: $[M + H]^+$ calculated for $C_7H_{13}O_3^+$ 145.0859, found 145.0861.

24: **^{1}H NMR (500 MHz, $CDCl_3$)** δ 4.99-4.91 (m, 1 H), δ 4.59 (dd, 1 H, *J* = 8.9, 8.2 Hz), δ 4.41 (dd, 1 H, *J* = 8.9, 5.7 Hz), δ 3.84-3.68 (m, 2 H). **^{13}C NMR (125 MHz, $CDCl_3$)** δ 154.0, δ 74.2, δ 67.0, δ 43.5. **HRMS (ESI)** m/z: $[M + H]^+$ calculated for $C_4H_6ClO_3^+$ 137.0000, found 136.9998.

25: **^{1}H NMR (500 MHz, $CDCl_3$)** δ 4.85-4.75 (m, 1 H), δ 4.49 (t, 1 H, *J* = 8.4 Hz), δ 4.38 (dd, 1 H, *J* = 8.4, 6.1 Hz), δ 3.61 (qd, 2 H, *J* = 10.9, 3.9 Hz), δ 3.43 (s, 3 H). **^{13}C NMR (125 MHz, $CDCl_3$)** δ 154.9, δ 74.9, δ 71.4, δ 66.2, δ 59.7. **HRMS (ESI)** m/z: $[M + H]^+$ calculated for $C_4H_9O_4^+$ 133.0495, found 133.0489.

26: **^{1}H NMR (500 MHz, $CDCl_3$)** δ 7.31 (dd, 2 H, *J* = 8.2, 7.3 Hz), δ 7.02 (t, 1 H, *J* = 7.3 Hz), δ 6.91 (d, 2 H, *J* = 8.2 Hz), δ 5.09-4.98 (m, 1 H), δ 4.66-4.50 (m, 2 H), δ 4.20 (qd, 2 H, *J* = 10.5, 3.9 Hz), **^{13}C NMR (125 MHz, $CDCl_3$)** δ 157.7, δ 129.7, δ 122.0, δ 114.6, δ 74.0, δ 66.8, δ 66.2. **HRMS (ESI)** m/z: $[M + H]^+$ calculated for $C_{10}H_{11}O_4^+$ 195.0652, found 195.0660.

4.3.5 The segmented flow apparatus

The segmented flow reactor used has been self-assembled in all its components (Figure 17). The amount of gaseous CO_2 in the apparatus was controlled by the mass flow controller (MFC) and mixed with the liquid phase in a T-mixer. The reactor consisted of a 4.42 mL spiral capillary (FEP tubing; 0.75 mm internal diameter; length 10 m) placed inside a thermostated bath. The liquid flow rate was controlled by a HPLC pump, while the back-pressure regulator (BPR) maintained a constant pressure of CO_2 (8.5 atm) throughout the system.

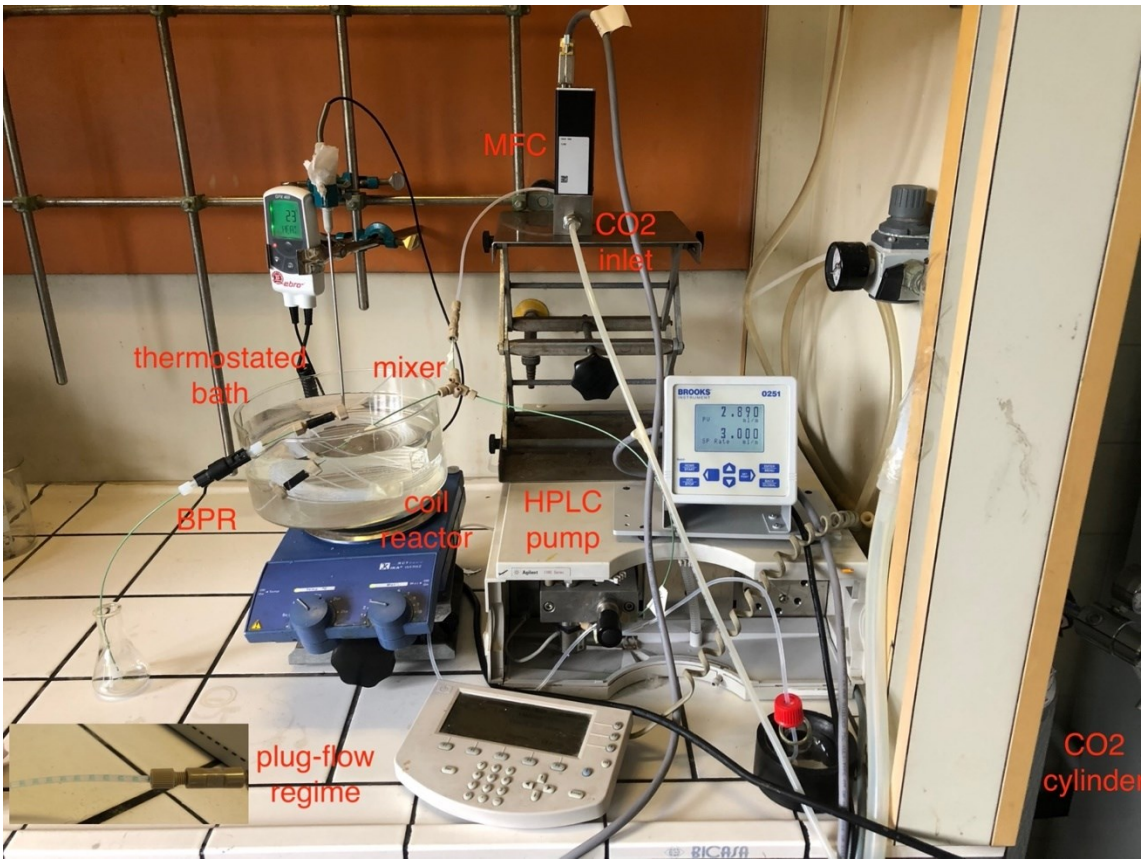

Figure 17 Segmented flow apparatus.

4.4 Conclusions

The goal of the research reported in this chapter was to investigate the chemical efficiency of the carbonation of terminal epoxides with CO_2 to produce the corresponding cyclic carbonates, using innovative organocatalysts.

To pursue the aim, a set of ionic liquids have been synthesized and tested for the styrene carbonate synthesis from styrene oxide in homogeneous conditions. After compound **8** has been identified as the best performing catalyst, the reaction conditions have been optimized to produce styrene carbonate quantitatively (> 95 % yield at 75°C in 16 hours).

Then, the same procedure has been applied for the synthesis of six other cyclic carbonates from their corresponding epoxides, obtaining good to excellent yields.

Furthermore, a process intensification study has been performed by translating the bulk reaction into a segmented flow set-up, obtaining the increase of the process productivity up to 17 times if compared with bulk process, as a result of the improved CO_2 mass transfer at the gas-liquid interface, due to the moderate increase in pressure (8.5 atm) and the segmented flow regime.

These very promising results paved the way for further studies of the bifunctional catalyst **8** in semi-heterogeneous conditions (see Chapter 5) and suggested that flow methodology might represent a new opportunity for further advancements in process intensification of CO_2 exploitation for cyclic carbonates synthesis.

5. Synthesis of the core-shell magnetic nanocatalysts and test of their activity as catalysts for the styrene oxide carbonation

5.1 Introduction and aim of the research

In this chapter the results of some activities of TANGO project (see Section 1.5) will be presented. As it has been highlighted in the introduction of this thesis, TANGO project pursues the goal to find innovative strategies to face the CO_2 utilization problem (CCU), always taking in account Green Chemistry principles [96]. In this context, it is extremely relevant to introduce new efficient and recyclable catalysts. For this reason, TANGO project had decided to immobilize on nanometric magnetic supports with a core-shell structure, obtaining **27**, the catalytic species identified in Chapter 4 as the best performing on the model reaction (**8**). As shown in Figure 18, the active catalytic species immobilized on **27**, targeted as elected nanocatalyst in this research work, lacks an additional secondary alcohol in respect of the homogeneous counterpart **8**. The synthesis of nanocatalyst **28**, that should have been the immobilized version of **8** was abandoned because of synthetic constraints.

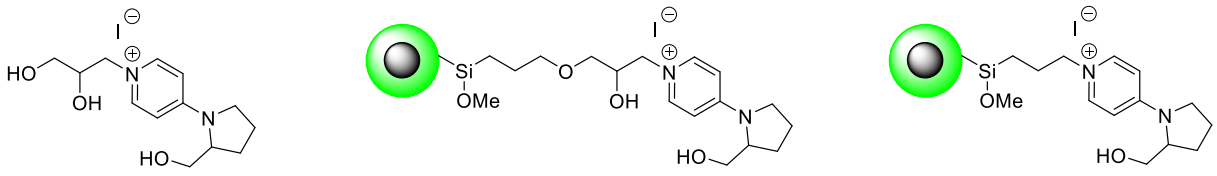

8 **28** **27**

Figure 18 Best performing homogeneous catalyst for the styrene oxide carbonation, identified in Chapter 4 and the corresponding immobilized one **27**.

The nanometric size of the particles allowed to operate in semi-heterogeneous catalysis conditions, *i.e.* heterogeneous catalysis with the catalytic species having a diameter smaller than 100 nm. These magnetic nanoparticles (MNPs) were structured with an inner magnetic core, which ensured an easy and efficient recovery and recycling, and an external silica shell which acted as an inert support for the immobilization of the catalytically active species. The magnetic properties of MNPs were extremely important for the innovative process and they were conferred by specific magnetic materials used for the preparation of the cores. Among many known magnetic materials, TANGO project decided to focus on two superparamagnetic materials [93], *i.e.* magnetite (Fe_3O_4) and cobalt-ferrite

($CoFe_2O_4$), with the aim to compare their performances and to identify the best performing material in the recovery process.

The general synthetic scheme followed to obtain the targeted core-shell nanocatalysts **27** (**27a** and **27b**) has been represented in the following Scheme 18. The preparation of the target nanocatalysts required three steps, in which the magnetic cores have been first of all coated with silica, then the shell surface has been functionalized with a linker and finally the homogenous catalyst precursor **12** has been immobilized on MNPs surfaces through the reaction with the linker.

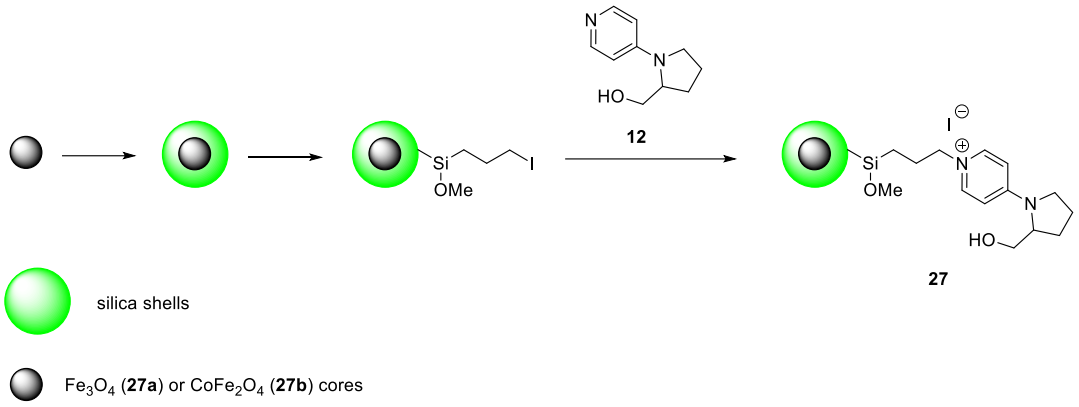

Scheme 18 General synthetic route adopted for the synthesis of catalyst **27**.

5.2 Discussion of the results

The two types of magnetic nanoparticles (Fe_3O_4 and $CoFe_2O_4$) used as nanocatalysts cores have been previously prepared by Prof. Davide Peddis's research group at the University of Genova. These nanoparticles, which had a diameter of 8-10 nm, have been supplied as colloids in toluene with a concentration of 5 mg/mL and with oleic acid as a stabilizer to prevent the formation of aggregates.

Before their synthetic elaboration, both the ferrofluids have been opportunely treated in order to obtain two new colloids suitable for further reactions, preparing two dispersions 0.8 mg/mL in cyclohexane (see Section 5.3.4.2).

5.2.1 Optimization of the nanocatalysts synthesis

The first step of nanocatalysts synthesis, *i.e.* the silica coating of the magnetic cores, needed to be optimized for the available ferrofluids because the success of the synthesis depended on the morphological features of the used sample (Scheme 19). To this aim, our starting point was the coating process described in literature by Cannas *et al.* [124] and it was the same for both cores (Fe_3O_4 and $CoFe_2O_4$).

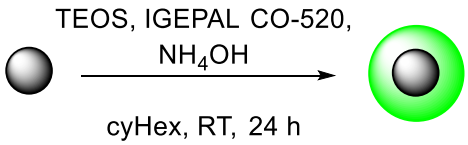

Scheme 19 Used procedure for the coating with silica of magnetic cores.

The optimization procedure, reported in the following Table 10, proceeded through the one by one variation of all the fundamentals parameters, in order to achieve the preparation of core-shell MNPs with good dimensional features, *i.e.* uniformly dispersed and with a silica shell thickness suitable for subsequent recovery at the end of the reaction, thus preserving adequate magnetic properties. In particular, the optimized parameters were: a) the volume of ferrofluid (*i.e.* Fe_3O_4 or $CoFe_2O_4$ 0.8 mg/mL in cyclohexane); b) the ratio between the added volumes of Igepal CO-520 and NH_4OH, where Igepal CO-520 was the surfactant used for the synthesis; c) the used volume of the ammonia aqueous solution (NH_4OH 30% in H_2O); d) the volume of tetraethyl orthosilicate (TEOS) added.

Table 10 Optimization of the parameters for the synthesis of the core-shell MNPs. In the following table, the optimized conditions have been highlighted in grey.

Optimized parameter	Entry	Ferrofluid volume [µL]	Igepal CO-520 [µL]	$\frac{\text{Igepal CO-520}}{NH_4OH}$	NH_4OH [µL]	TEOS [µL]
Fe_3O_4 or $CoFe_2O_4$ amount	1	250	430	12.29	35	20
	2	300	430	12.29	35	20
	3	350	430	12.29	35	20
$\frac{\text{Igepal CO-520}}{NH_4OH}$	4	350	335	9.57	35	20
	5	350	430	12.29	35	20
	6	350	525	15	35	20
NH_4OH volume	7	350	393	12.29	32	20
	8	350	430	12.29	35	20
	9	350	467	12.29	38	20
TEOS volume	10	350	467	12.29	38	15
	11	350	467	12.29	38	20
	12	350	467	12.29	38	25

After the optimized parameters have been identified by performing qualitative DLS analyses of each sample, the core-shell MNPs have been prepared using the optimized procedure (entry 10) and purified with a sequence of several EtOH washing and centrifugation cycles (see Section 5.3.2), which was always the same, also in the further synthetic steps.

The obtained coated MNPs have been characterized using several techniques to confirm the success of the synthesis and to check the required properties of the prepared material (see Section 5.2.2).

The second step of nanocatalysts synthesis was the core-shell MNPs post-grafting with 3-iodopropyl trimethoxysilane (Scheme 20), which allowed the insertion of a iodo-propylic linker on the MNPs surface to guarantee the further immobilization of the catalytically active species. Also in this case, it was necessary to optimize the synthetic conditions.

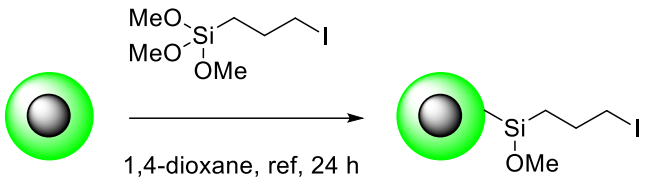

Scheme 20 Core-shell MNPs post-grafting with 3-iodopropyl trimethoxysilane.

The first unsuccessful attempt to disperse the MNPs in THF to perform the reaction, based on the procedure reported by Rahimi *et al.* [125], afforded a highly unstable colloid from which the MNPs spontaneously precipitated very fast.

In replacing THF with methanol, good MNPs dispersion properties were observed. However, the MeOH nucleophilicity negatively affected the outcome of this grafting step, resulting in the lack at XPS of any iodine signal on the obtained MNPs, probably because of methanol substitution of iodide occurred after 24h reflux, leading to a methoxy-substituted product.

After several attempts in finding the organic solvent matching our needs, 1,4-dioxane has been identified as the reaction solvent, because of its suitable properties, *i.e.* it is able to uniformly disperse MNPs, it has a boiling point of 101°C allowing the reaction to be performed at higher temperature if compared with other organic solvents, no reactivity with functional groups in the reaction mixture allowing the obtaining of the target product without any side products.

Using this optimized procedure, it was possible, after the purification of the products (see Section 5.3.2), to obtain post-grafted MNPs which have been characterized using several techniques, to confirm the success of the synthesis and to check the required properties of the prepared material (see Section 5.2.2).

A particular attention has been paid on the quantification of the grafting degree of the MNPs. The direct quantification of the iodine covalently bonded on the MNPs surface would permit to measure the parameter that was of interest for us. Unfortunately, this direct measurement was impossible with the analytic techniques available at ISOF-CNR (elemental analysis, ICP-MS, SS-NMR). The quantification of the carbon on the linker through elemental analysis (EA) wasn't reliable because the residual methoxylation degree of silicon, coming from 3-iodopropyl trimethoxysilane group, was unknown (1, 2 or a mixture of both residual methoxylic groups).

For all these reasons, it has been decided to adopt an indirect approach based on the hypothesis that, if the synthetic procedure was kept the same, the grafting degree of the MNPs remained the same by substituting 3-iodopropyl trimethoxysilane with 3-amminopropyl triethoxysilane in the reaction procedure (Scheme 21). The further quantification of the amount of nitrogen in the sample through EA, allowed us to estimate the parameter of our interest, *i.e.* the grafting degree of target MNPs. For this purpose, it has been performed the procedure reported in Scheme 21 to obtain the desired product to analyse.

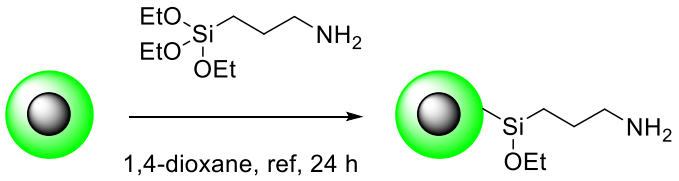

Scheme 21 Core-shell MNPs post-grafting with 3-amminopropyl trimethoxysilane finalized to the quantification of the functionalization degree obtained in the reaction in Scheme 20.

After the elemental analysis of the target sample, the functionalization degree of the MNPs has been calculated through the quantification of the EA nitrogen in the sample reported in Table 11.

Table 11 Weight percentage of each element in the sample, obtained by EA.

N (weight %)	C (weight %)	H (weight %)
1.89	9.06	2.13

The grafting level of the MNPs has been calculated to be 1.35 mmol of functional groups per gram of MNPs, by applying the following equation (Eq. 3).

$$\frac{N\,\%/_{14}}{N\ \text{atoms nr}} \times 10 = 1.35\ \text{mmol/g} \qquad \textbf{(Eq. 3)}$$

Based on the obtained result and assuming the reliability of the initial hypothesis, it was possible to estimate the amount of **12** necessary to saturate all the iodopropyl-groups on the surface of the MNPs, to perform the last synthetic step (Scheme 22) and to obtain the target nanocatalysts **27**, with both the two classes of magnetic cores (Fe_3O_4 or $CoFe_2O_4$).

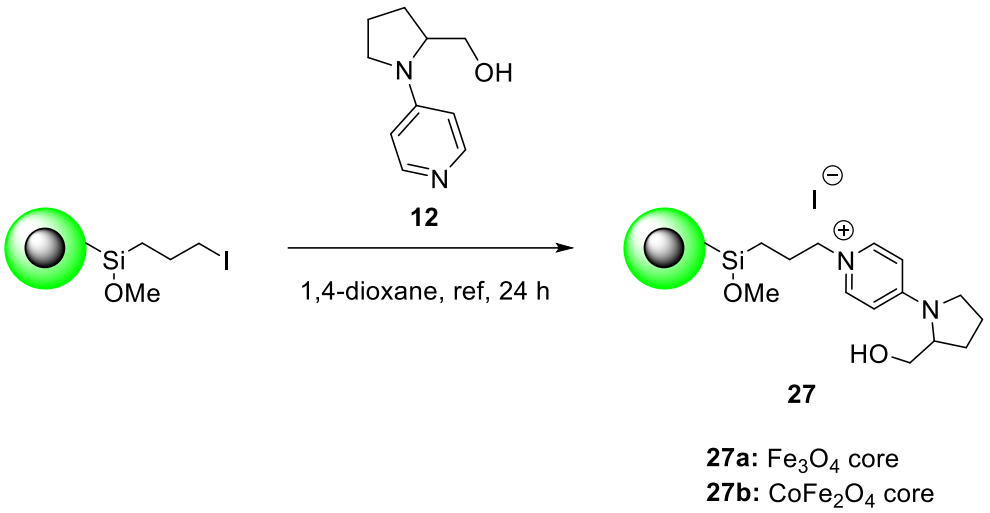

Scheme 22 Immobilization of the catalytic active species on core-shell MNPs surfaces.

This last synthetic step has been performed using similar conditions to those adopted for the post-grafting step (Scheme 21), in terms of solvent, temperature and reaction time. Compound **12** has been previously prepared following the procedure described in Section 4.3.3.4.

The prepared target nanocatalysts have been purified using the procedure described in Section 5.3.2 and their full characterization required several techniques, to confirm the success of the syntheses and to check the required properties of the prepared materials (see Section 5.2.2).

5.2.2 Characterization of the obtained nanocatalysts

After the two target nanocatalysts **27a** and **27b** have been successfully synthesized, they have been characterized in terms of both morphology and composition. The analytical techniques that have been used were:

a) Dynamic Light Scattering (DLS), which provided information about the hydrodynamic diameter and polydispersity of the nanoparticles;
b) Zeta Potential (Z_P), which provided information on the surface charge;
c) Infrared Spectroscopy (FTIR);
d) X-ray Photoelectron Spectroscopy (XPS), to have information on the surface elemental composition;
e) Elemental Analysis (EA), which allowed the quantification of nitrogen and carbon in the products after the functionalization;
f) Transmission Electron Microscopy (TEM);
g) Magnetic measurements, which provided information on the magnetization of the material after the contact with a magnetic field.

After each synthetic step, DLS measurements have been performed on upcoming MNPs to qualitatively evaluate the polydispersity level. The quantitative results of these analyses weren't actually useful for our purpose because the dimensional information that this technique is able to provide it's a hydrodynamic diameter, *i.e.* the diameter of the nanoparticle surrounded by a solvent shell, which thickness depends on the affinity of the MNPs surface with the used solvent.

Instead, Z_P measurements confirmed us the nanocatalysts positive surface charge, as expected because of the material's surface charge, on which pyridinium salts were immobilized.

IR spectra have been recorded after each synthesis step. However, just in the case of the first reaction*, i.e.* the magnetic cores coating, this analysis was relevant to confirm the success of the synthesis. Indeed, as is it shown in Figure 19, the IR spectrum of core-shell MNPs (green line) appears very different if compared both to the TEOS one (red line) and the cores spectrum (dark blue line). The polymer formation around the inner cores reflects on the spectrum because of broad signals. Furthermore, the Si-O stretching signals are visible between 800 and 1100 cm^{-1}.

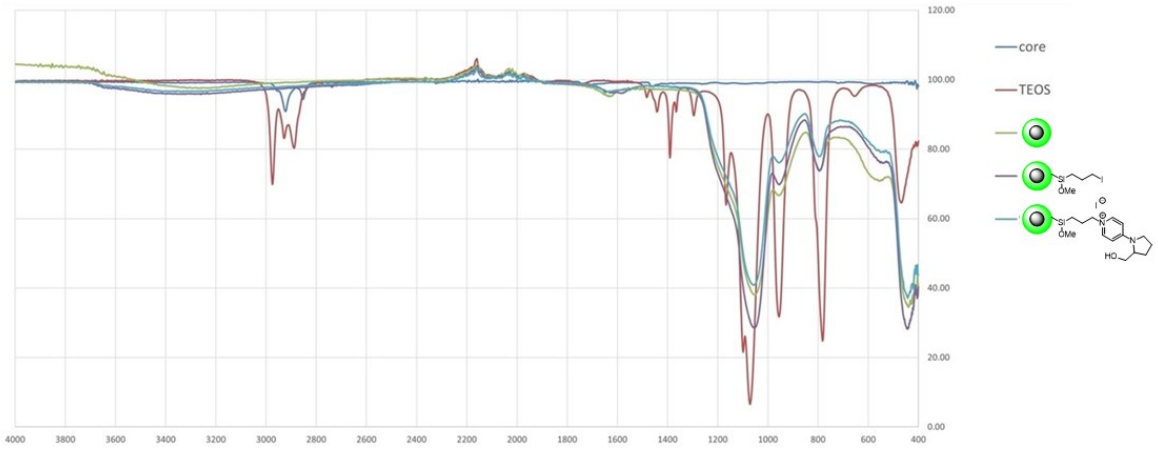

Figure 19 Comparison of the IR spectra acquired during the synthesis of nanocatalysts **27**.

Conversely, the IR spectra acquired both after the post-grafting and the immobilization of the catalytically active species steps, resulted uninformative being each other undistinguishable because of the huge silica signals overlapping, thus hiding the signals of MNPs functional groups. For this reason, it has been necessary to use other analytic techniques to confirm the success of the functionalization of the core-shell MNPs surfaces.

In particular, to know the elemental composition of the MNPs surfaces, it has been used the XPS, which allowed to confirm the presence of the elements that were expected. The XPS analyses have been performed by Sebastiano Mantovani and Dr. Alessandro Kovtun in Bologna at the ISOF-CNR. As shown in Figure 20, in all the samples, the elements in the cores are not detectable, because this technique allows the elemental analysis of just few nanometres of depth. The core-shell MNPs spectra (A and D) confirmed the presence of just silica and oxygen as components of the MNPs surfaces. Instead, by observing the spectra of post-grafted nanoparticles (B and E), it is possible to identify the signals of iodine and carbon, and so to confirm the success of the functionalization with the iodo-propylic linker. Furthermore, in the nanocatalysts spectra (C and F) it is possible to notice the presence of nitrogen, which confirmed the presence of the catalytic species on the surface. In these spectra it is also possible to observe how the iodine signals have lost intensity, if compared with spectra B and E.

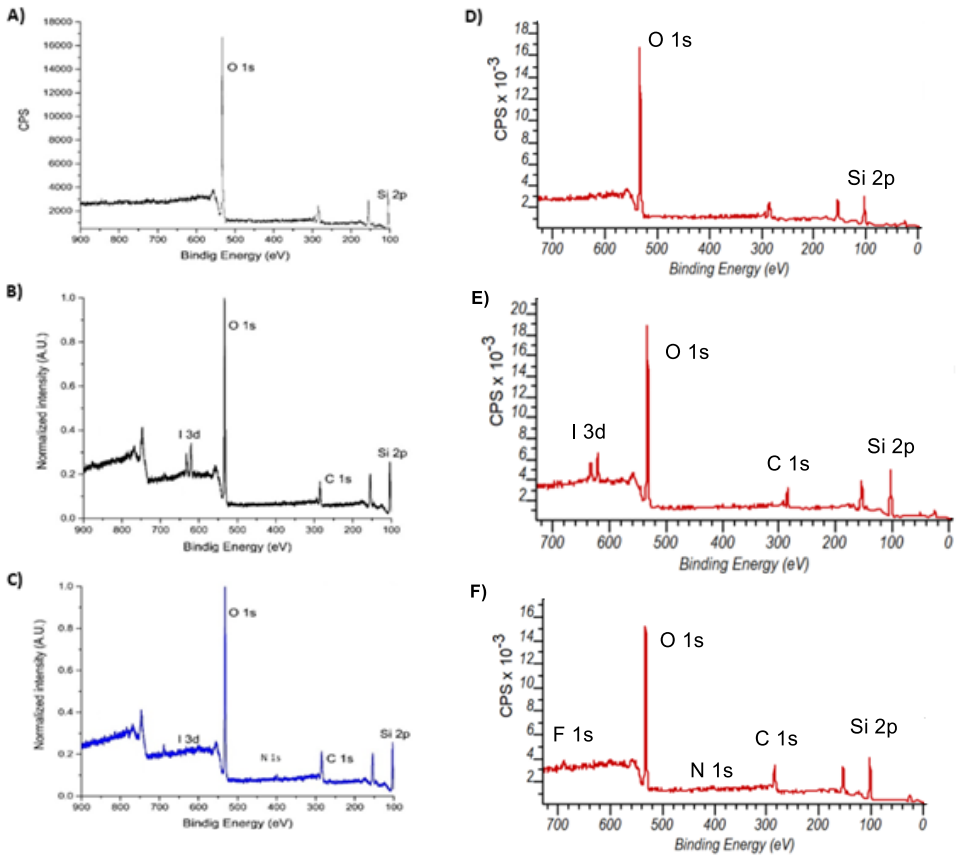

Figure 20 XPS spectra of: A) core-shell MNPs with $CoFe_2O_4$ cores; B) post-grafted MNPs with $CoFe_2O_4$ cores; C) nanocatalyst **27b**; D) core-shell MNPs with Fe_3O_4 cores; E) post-grafted MNPs with Fe_3O_4 cores; C) nanocatalyst **27a**.

XPS spectra provided quali-quantitative information regarding the MNPs surface composition. On the contrary, the quantification of the catalytically active sites bonded on their surfaces, *i.e.* the catalyst loading, have been achieved through EA measurements. By applying the formula Eq. 3, it has been possible to calculate the catalyst loading on the prepared MNPs, which it was 0.19 mmol/g, both in the case of nanocatalyst **27a** and **27b**.

After the composition analyses, the prepared materials have been also characterized in terms of dimension, morphology and functionality.

In order to obtain information about the dimensions and morphology, some TEM images have been acquired by Dr. Roberto Balboni in Bologna at the IMM-CNR. In this way it was possible to confirm the core-shell structure and to have information about the size of the prepared nanocatalysts. In Figure 21 have been reported the TEM images acquired after each step of nanocatalysts syntheses. All the MNPs

show a core-shell structure, in which it is possible to discriminate the two diverse compositions because of the different electron absorption, which means a diverse contrast in the pictures.

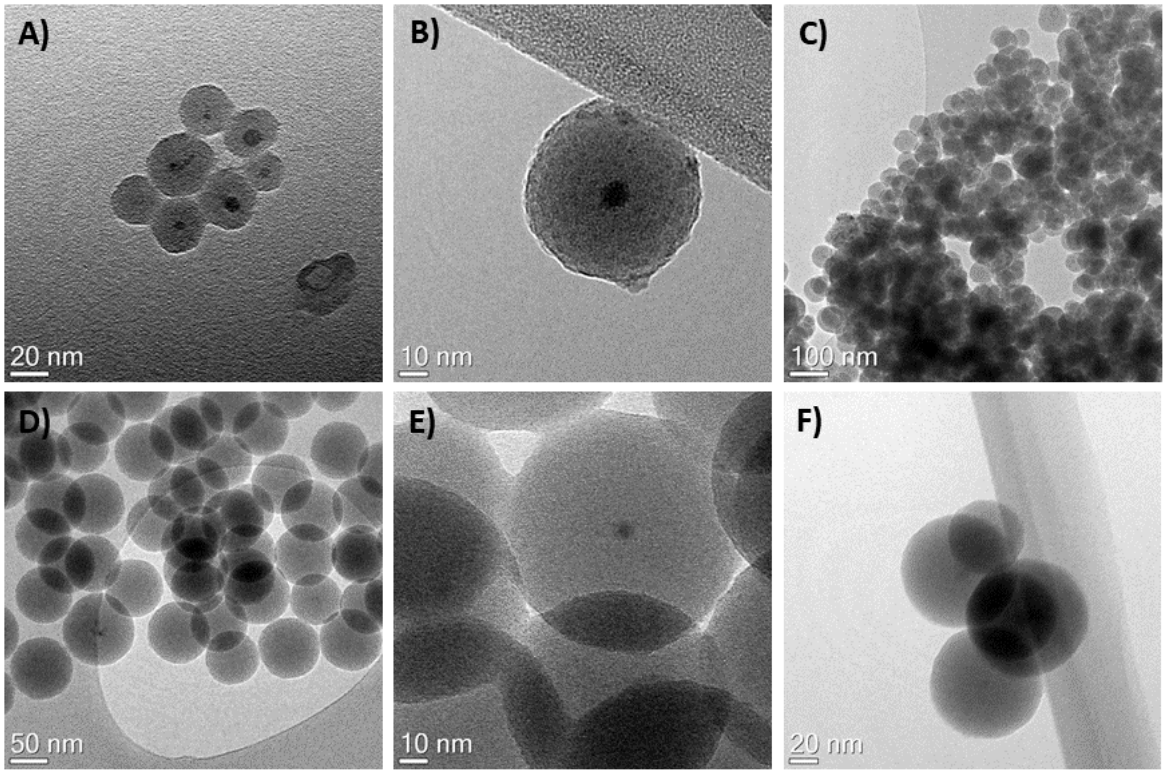

Figure 21 TEM images of: A) core-shell MNPs with $CoFe_2O_4$ cores; B) post-grafted MNPs with $CoFe_2O_4$ cores; C) nanocatalyst **27b**; D) core-shell MNPs with Fe_3O_4 cores; E) post-grafted MNPs with Fe_3O_4 cores; C) nanocatalyst **27a**.

By looking at the TEM images, it is possible to notice a difference in terms of aggregation between the samples with Fe_3O_4 cores and the samples with $CoFe_2O_4$ cores: the MNPs with cobalt-ferrite cores appear more aggregated if compared with the others. This effect was due to the different solvent used for the preparation of the two samples for the analyses, *i.e.* cyclohexane for the cobalt-ferrite MNPs and ethanol for the magnetite MNPs. The pointed-out solvent effect on the aggregation of the nanoparticles was also taken in account during the choice for the solvent to use during the test of nanocatalysts on the model reaction, where ethanol has been used as solvent for the reaction to avoid the MNPs aggregation (see Section 5.2.3).

From a functional point of view, the prepared nanocatalysts have been characterized through magnetic measurements, which have been performed at the

Nanostructured Magnetic materials laboratory[8] of the ISM-CNR in Roma, under the supervision of Prof. Davide Peddis. From the results obtained during the magnetic measurements, it was possible to exclude the presence of aggregates in the two materials, because they showed the peculiar features of superparamagnetic nanoparticles [93], *i.e.* zero coercivity and zero remnant magnetization. As shown in Figure 22, these properties, measured in both sample **27a** and **27b**, didn't show significant variations in terms of saturation magnetization (Ms) after the functionalization steps (Ms = 50(2) Am^2Kg^{-1} of bare magnetite). The same observations have been reported for the nanocatalyst with cobalt-ferrite cores. Also in this case, from the magnetic analyses it has been confirmed that the prepared materials were superparamagnetic nanoparticles which didn't show a significative variation in Ms (Ms=77(2) Am^2Kg^{-1} of bare cobalt-ferrite) after the functionalization process.

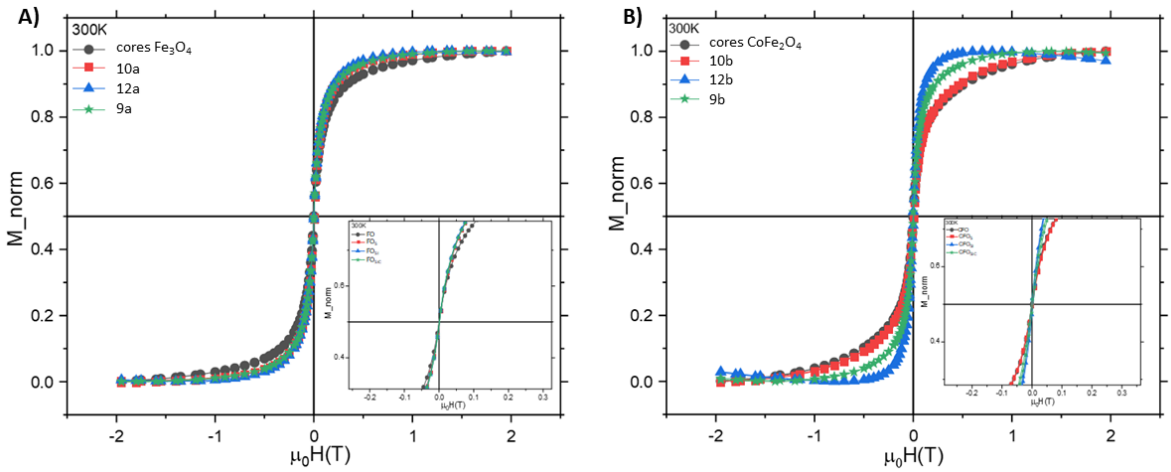

Figure 22 Magnetization dependency on the applied magnetic field, measured at 27°C, of: A) ● Fe_3O_4 cores, ■ core-shell MNPs with Fe_3O_4 cores, ▲ post-grafted MNPs with Fe_3O_4 cores and ★ nanocatalyst **27a**; **(B)** ● $CoFe_2O_4$ cores, ■ core-shell MNPs with $CoFe_2O_4$ cores, ▲ post-grafted MNPs with $CoFe_2O_4$ cores and ★ nanocatalyst **27b**. All the samples have been normalized from 0 to 1.

The results obtained also confirmed that both the presence of the silica shell and of the functional groups on the MNPs surfaces didn't affect the magnetic properties (*i.e.* saturation magnetization and inter-particles interactions) of the magnetite and

[8] www.nm2lab.com

cobalt-ferrite MNPs, confirming that the synthesis process was suitable for the preparation of the target nanocatalysts.

On the other hand, the differences encountered by comparing Ms values of the two nanocatalysts were due to the diverse intrinsic magnetic properties of the two magnetic materials.

The other fundamental information that has been extrapolated from the graphs in Figure 22 was the diverse response of the two prepared materials to the external magnetic field. It is possible to notice in the picture that nanocatalyst **27b** shows more adequate magnetic properties for TANGO purposes, with respect to the nanocatalyst **27a**. Indeed, with the same applied magnetic field, cobalt-ferrite magnetized easier and so, for this reason, it would be easier the magnetic recover (and further recycle) at the end of the catalytic role in the model reaction. However, to confirm what emerged from the magnetic measurements, both the nanocatalysts have been tested on the model reaction of carbonation of the styrene oxide.

5.2.3 Nanocatalysts' activity efficiency test on the model reaction

After the target nanocatalysts **27a** and **27b** have been successfully prepared and fully characterized, their catalytic activity has been tested on styrene oxide carbonation, chosen as a model reaction (Scheme 23).

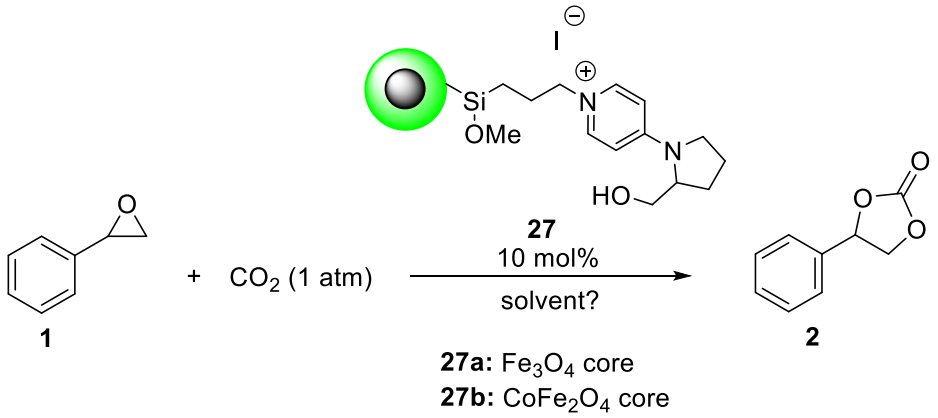

Scheme 23 Model reaction of styrene oxide carbonation using prepared nanocatalysts **27**.

The activity tests for homogeneous catalysts (see Chapter 4) have been performed by using 50 mol % of EtOH, which corresponded to a styrene oxide concentration of 6.97 M. Conversely, the efficiency tests of the prepared nanocatalysts have been performed at first in semi-heterogeneous conditions, *i.e.* heterogeneous conditions with a nanometric solid catalyst, by using a styrene oxide concentration of 0.1 M in EtOH. Using these conditions, in fact, the nanocatalysts were uniformly dispersed in EtOH. Unfortunately, after 16 hours of reaction at RT under a large excess of CO_2 (4.25 eq *vs.* SO) and vigorous stirring, the quantitative ^{1}H NMR analysis of the crude detected a 0.6 % yield of styrene carbonate.

An accurate analysis of this result, based on the hypothesis of a similar catalytic activity of nanocatalysts **27** and its corresponding homogeneous catalyst **8**, allowed us to conclude that it was necessary to operate using a higher styrene oxide concentration, in order to obtain a significative carbonate yield. Indeed, by using styrene oxide 0.1 M, the obtained yield was the best result obtainable. By using the yield of 44 % obtained with the homogeneous catalyst **8** and the concentration ratio between the model reaction with homogeneous catalyst and prepared nanocatalyst, *i.e.* 6.97 M and 0.1 M, it has been possible to calculate the expected carbonate yield in semi-heterogeneous conditions to be actually 0.6 %.

Based on these calculations, the decision to operate by using a lower amount of solvent (200 μL of Ethanol for ≃ 200 mg of MNPs), which basically brought to a solid-gas biphasic bulk reaction, was obvious. By operating in these conditions, we were able to obtain a 20 % yield of carbonate, although the presence of many side products due to the parasite reaction of EtOH with the styrene oxide.

The catalytic property which was interesting for our purpose was the ability to selectively convert styrene oxide into styrene carbonate. For this reason, to avoid side reactions, the reaction solvent has been changed into 2-methyltetrahydrofuran (Me-THF) in the further experiments, keeping the other reaction conditions unchanged. In these conditions, the model reaction catalysed by nanocatalyst **27a** or **27b** proceeded selectively until 28 % yield of carbonate. After the reaction, using the custom-made device reported in Figure 23, it was possible to magnetically recover the nanocatalysts and to recycle them in other reactions.

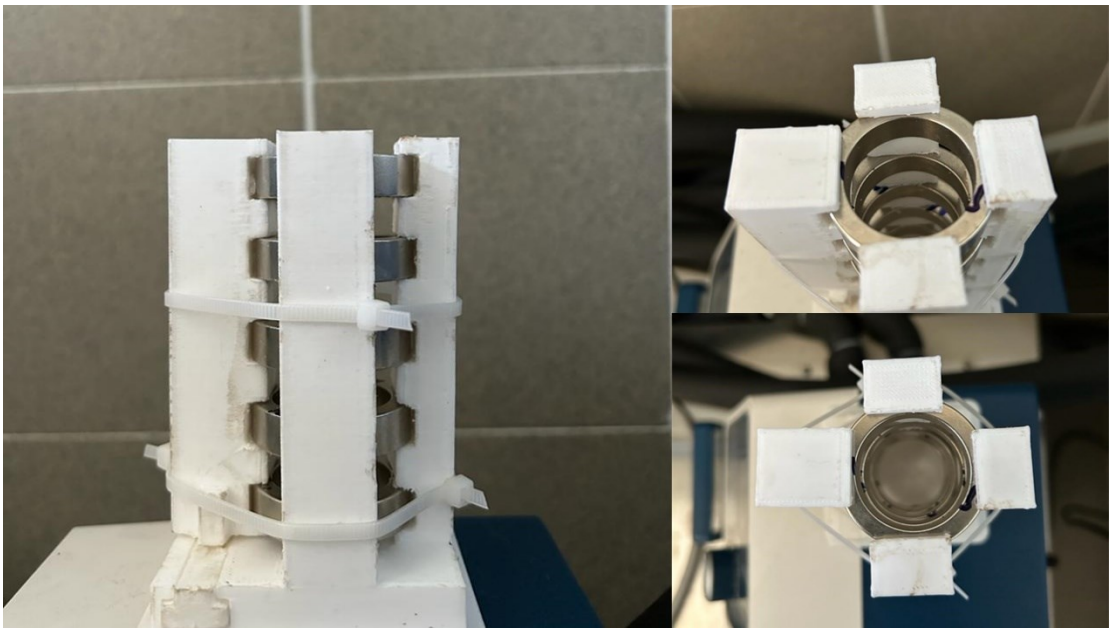

Figure 23 Custom-made device for magnetic recovery of magnetic nanocatalysts.

5.3 Experimental section

5.3.1 Materials

All the used reagents, except from the two ferrofluids, were commercially available at TCI Europe N.V., Merck or Fluorochem and they have been purchased depending on the availability and the best price. All chemicals were used without any further purification.

5.3.2 Purification Methods

After each step of the synthesis, the products have been purified by following the same procedure. The reaction mixture has been diluted with 20 mL of ethanol and moved into a centrifuge vial. The mixture has been centrifuged at 15000 rpm, for 15 minutes at RT. Then, the supernatant has been removed and the MNPs have been dispersed again in 10 mL of EtOH and sonicated until a homogeneous colloid have been obtained. The mixture has been centrifuged again at 15000 rpm, for 15 minutes at RT. The supernatant has been removed and the prepared MNPs have been dried overnight at RT.

5.3.3 Characterization methods

For the characterization of the prepared materials, several techniques have been used. The analytical techniques will be presented in the following sections (Section 5.3.3.1 - Section 5.3.3.7).

5.3.3.1 Dinamic Light Scattering (DLS) e Zeta Potential (Z_P)

To perform both the DLS and Zeta Potential analyses, a *Brookhaven NanoBrook Omni* instrument with its own software has been used.

5.3.3.2 Infrared Spectroscopy (IR)

For the acquisition of IR spectra, a Fourier Transform IR (FT-IR) spectrometer *Agilent Cary 630 FTIR* with its own software has been used.

5.3.3.3 X-ray Photoelectron Spectroscopy (XPS)

The XPS analyses have been performed by Sebastiano Mantovani and Dr. Alessandro Kovtun in Bologna at the ISOF-CNR. X-ray photoelectron spectra (XPS) were acquired by using Mg Kα excitation (XR50, Specs) and a hemispherical electron analyser (Phoibos 100, Specs). The survey and high-resolution spectra were acquired with energy resolutions of 1.4 eV and 0.9 eV, respectively, on freshly sputtered silver (Ag 3d). The spectrometer was calibrated to the Au 4f7/2 peak at 84.0 eV. Conductive carbon tape was used to fix and electrically ground the powders. Electrostatic charging effects were observed and corrected by setting C 1s signal at 285.0 eV. The spectra were fit using the CasaXPS software after Shirley's background subtraction.

5.3.3.4 Elemental Analysis (EA)

To perform the Elemental Analysis, it has been used an *Elementar UNICUBE* instrument, integrated with its own software for data elaboration. The percentage composition of each sample has been calculated by using the following formula (Eq. 4):

$$\text{Elemental composition}[\%] = \frac{\text{peak area x normalization factor}}{\text{sample weight}} \qquad \textbf{(Eq. 4)}$$

5.3.3.5 Transmission Electron Microscopy (TEM)

TEM images have been acquired by Dr. Roberto Balboni in Bologna at the IMM-CNR. To prepare the samples for the analysis, the nanoparticles with cobalt-ferrite cores have been dispersed in cyclohexane, while the MNPs with magnetite cores have been dispersed in ethanol. After the dispersion, all the sample have been sonicated. Then, the colloids have been deposed on sample holder grids for TEM observations, made of a carbon film supported by a copper grid (*Holey carbon film*). The colloids solvents have been evaporated from the samples by heating the sample holders at 50°C.

TEM observations were made using a transmission electronic microscope (TEM) FEI Tecnai F20T*,* working at an accelerating voltage of 200 kV. In these conditions, the used microscope allowed a maximum resolution of 0.24 nm. All the images have been obtained using the diffraction contrast technique, which highlighted diverse

regions of the sample depending on the atomic masses and crystalline structure. Using this technique, it was possible to point out the core-shell structure of the MNPs.

5.3.3.6 Magnetic measurements

The magnetic measurements have been performed at the *Nanostructured Magnetic materials laboratory*[9] of the ISM-CNR in Roma, under the supervision of Prof. Davide Peddis. The analyses have been performed at 27°C using vibrating-sample magnetometer (VSM), producing magnetic fields in the range ± 2 T. The powder sample was immobilized in an epoxy resin to prevent any movement of the magnetic nanoparticles (MNPs) during the measurement, and the magnetization data of all the samples were normalized from 0 to 1 for clarity reasons.

5.3.3.7 ^{1}H NMR

The ^{1}H NMR analyses to quantify the conversion in the nanocatalysts activity tests have been performed using an Agilent DD2 NMR system, equipped with a 11.7 T (500 MHz) PremiumCompact+ superconducting magnet and an Agilent OneNMR probe.

[9] www.nm2lab.com

5.3.4 Nanocatalysts synthesis

5.3.4.1 Synthesis of the magnetic cores

The syntheses and characterization of both the classes of magnetic cores, *i.e.* magnetite and cobalt-ferrite MNPs, have been performed at the *Nanostructured Magnetic materials laboratory*[10] of the University of Genova, under the supervision of Prof. Davide Peddis. The reagents used for the synthesis have been reported in the following table.

Compound	Molecular formula	Molecular weight
$Fe(acac)_3$	$FeC_{15}H_{21}O_6$	353.17 g/mol
$Co(acac)_2$	$CoC_{10}H_{14}O_4$	257.15 g/mol
Oleic acid	$C_{18}H_{34}O_2$	282.46 g/mol
Oleylamine	$C_{18}H_{37}N$	267.49 g/mol
1,2-hexadecandiol	$C_{16}H_{34}O_2$	258.44 g/mol
Dibenzyl ether	$C_{14}H_{14}O$	198.26 g/mol
1-octadecene	$C_{18}H_{36}$	252.48 g/mol

For the preparation of the Fe_3O_4 and $CoFe_2O_4$ magnetic nanoparticles (d = 8-10 nm) it has been used the following procedure. $Fe(acac)_3$ (2 mmol), $Co(acac)_2$ (1.29 mmol), oleic acid (6 mmol), oleylamine (70%, 6 mmol) and 1,2-hexadecandiol (10 mmol) have been added to a three-neck round-bottom flask containing dibenzyl ether (20 mL) under magnetic stirring. The resulting suspension have been heated to 270°C using a heating coat connected to a *Proportional Integral Derivative* (PID) for precise temperature control. In Figure 24 are reported the thermal steps of the synthesis method and it has been used as a guideline to follow the synthesis step.

First, the reaction mixture has been degassed in vacuum at 110°C for 60 minutes, then it was heated and maintained at 200°C for 120 minutes. A change in the mixture colour to dark red has been observed, suggesting the burst nucleation of the nanoparticles, according to the LaMer theory [126]. Afterwards, the temperature was increased and kept at 270°C, for 60 minutes for the particles growth. The cooled black dispersion was divided into three aliquots and the powder was precipitated by adding EtOH. Three washing cycles have been performed using sonication (10

[10] www.nm2lab.com

minutes), centrifugation (5 minutes, 5000 rpm) and by adding fresh EtOH each time the supernatant has been removed. Finally, the magnetic precipitate was redispersed in toluene and $CoFe_2O_4$ ferrofluid has been obtained. Similarly, Fe_3O_4 ferrofluid was synthetized using the same protocol with small variation in the starting reagents, *i.e.* using 3 mmol of $Fe(acac)_3$ instead of $Fe(acac)_3$ (2 mmol) and $Co(acac)_2$ (1.29 mmol) and 1-octadecene as solvent instead of dibenzyl ether [124,127,128].

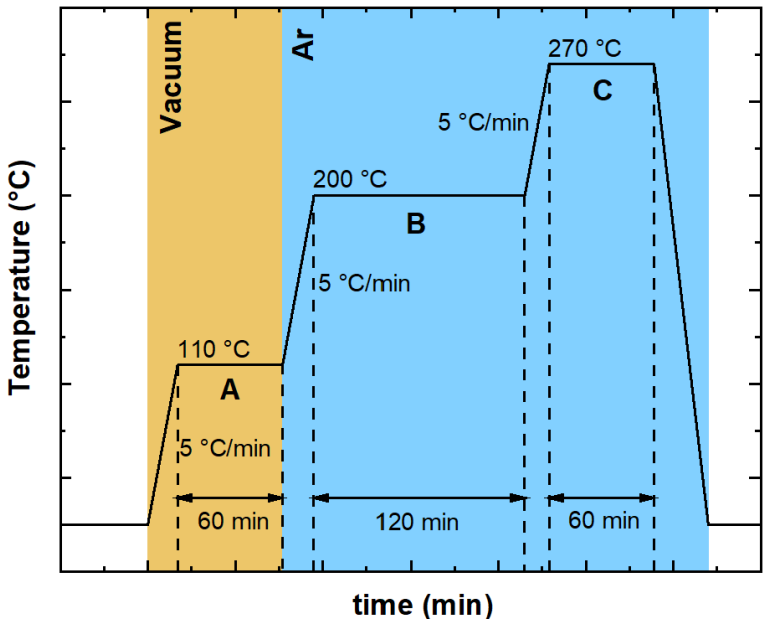

Figure 24 Thermal decomposition process.

5.3.4.2 Preparation of the ferrofluids (Fe_3O_4 or $CoFe_2O_4$ 0.8 mg/mL)

Before the synthetic elaboration of the magnetic cores, the supplied ferrofluids have been redispersed in cyclohexane, to have a solvent suitable for the further reactions. First, 3 mL of the colloid (Fe_3O_4 or $CoFe_2O_4$ 5 mg/mL) have been added to a centrifuge vial. Then, 30 mL of EtOH have been added and the mixture has been centrifuged at 15000 rpm, for 15 minutes at RT.

Furthermore, the supernatant has been removed and the MNPs have been dispersed again in 30 mL of 1:1 EtOH/Cy and sonicated until a homogeneous colloid has been obtained. The mixture has been centrifuged again at 15000 rpm, for 15 minutes at RT. The supernatant has been removed, some fresh EtOH (16 mL) has been added and the mixture was sonicated until a homogeneous colloid have been obtained. The mixture has been centrifuged again at 15000 rpm, for 15 minutes at RT. The supernatant has been removed and the MNPs have been dried overnight at RT.

After the MNPs were completely dry, they have been redispersed through sonication in cyclohexane to obtain a colloid 0.8 mg/mL. The same procedure has been used for the preparation of both Fe_3O_4 and $CoFe_2O_4$ 0.8 mg/mL in cyclohexane.

5.3.4.3 Silica coating of the magnetic cores (Fe_3O_4 or $CoFe_2O_4$) to obtain core-shell MNPs

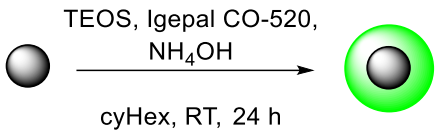

Compound	Molecular formula	Molecular weight
Magnetite MNP_s	Fe_3O_4	/
Cobalt-ferrite MNP_s	$CoFe_2O_4$	/
Igepal CO-520	$(C_2H_4O)_n \cdot C_{15}H_{24}$	/
TEOS	$C_8H_{20}O_4Si$	208.33 g/mol
Cyclohexane	C_6H_{12}	84.16 g/mol
Ammonium hydroxide	NH_4OH	35.05 g/mol

Igepal CO-520 (467 µL) and cyclohexane (4 mL) have been added to a round bottom flask. The mixture has been sonicated for 3 minutes and then stirred at 1200 rpm at RT. 350 µL of the MNPs colloid (Fe_3O_4 or $CoFe_2O_4$ 0.8 mg/mL in cyclohexane) have been added to the flask and stirred at 1200 rpm for 15 minutes. Then, TEOS (15 µL) has been added dropwise and the mixture was stirred at 600 rpm for 30 minutes. Finally, 38 µL of NH_4OH 30% in H_2O have been added dropwise and the mixture has been stirred at 600 rpm for 24 hours at RT.

After 24 hours, the product has been purified following the procedure described in Section 5.3.2 and characterized with the methods reported in Section 5.3.3. The same procedure has been used in both the case of Fe_3O_4 and $CoFe_2O_4$ cores, obtaining respectively a brown reddish powder and a black powder.

5.3.4.4 Post-grafting of the core-shell MNPs (Fe_3O_4 or $CoFe_2O_4$ cores) with (3-iodopropyl)trimethoxysilane

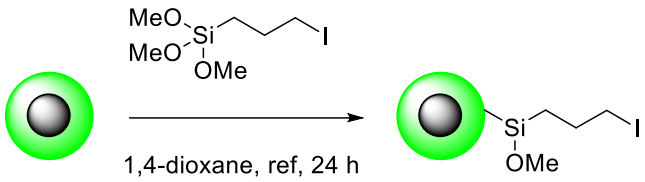

Compound	Molecular formula	Molecular weight
Core-shell MNP_s	/	/
3-iodopropyl trimethoxysilane	$C_6H_{15}IO_3Si$	290.17 g/mol
1,4-dioxane	$C_4H_8O_2$	88.11 g/mol

In a two-necks round bottom flask with a refrigerator on top, 5.9 mg of previously synthesized core-shell MNPs (Fe_3O_4 or $CoFe_2O_4$ cores) have been added as a powder. Then, 1.5 mL of 1,4-dioxane have been added and the mixture has been vigorously stirred (800 rpm) at 40°C to obtain a uniform dispersion. Afterwards, 80 µL of 3-iodopropyl trimethoxysilane (20:1 in weight with respect of MNPs) have been added and the mixture has been refluxed and stirred (800 rpm) for 24 hours.

After 24 hours, the product has been purified following the procedure described in Section 5.3.2 and characterized with the methods reported in Section 5.3.3. The same procedure has been used in both the case of Fe_3O_4 and $CoFe_2O_4$ cores, obtaining respectively a brown reddish powder and a black powder.

5.3.4.5 Post-grafting of the core-shell MNPs (Fe_3O_4 or $CoFe_2O_4$ cores) with (3-amminopropyl)triethoxysilane

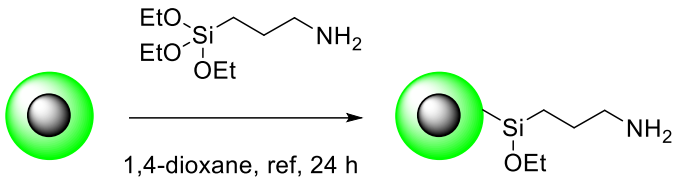

Compound	Molecular formula	Molecular weight
Core-shell MNP_s	/	/
3-amminopropyl triethoxysilane	$C_9H_{23}NO_3Si$	221.37 g/mol
1,4-dioxane	$C_4H_8O_2$	88.11 g/mol

In a two-necks round bottom flask with a refrigerator on top, 7.3 mg of previously synthesized core-shell MNPs (Fe_3O_4 or $CoFe_2O_4$ cores) have been added as a powder. Then, 2 mL of 1,4-dioxane have been added and the mixture has been vigorously stirred (800 rpm) at 40°C to obtain a uniform dispersion. Afterwards, 154 µL of 3-amminopropyl triethoxysilane (20:1 in weight with respect of MNPs) have been added and the mixture has been refluxed and stirred (800 rpm) for 24 hours.

After 24 hours, the product has been purified following the procedure described in Section 5.3.2 and characterized with the methods reported in Section 5.3.3. The same procedure has been used in both the case of Fe_3O_4 and $CoFe_2O_4$ cores, obtaining respectively a brown reddish powder and a black powder.

5.3.4.6 Immobilization of the catalytic active species on the core-shell MNPs (Fe_3O_4 or $CoFe_2O_4$ cores) to obtain nanocatalysts 27a and 27b

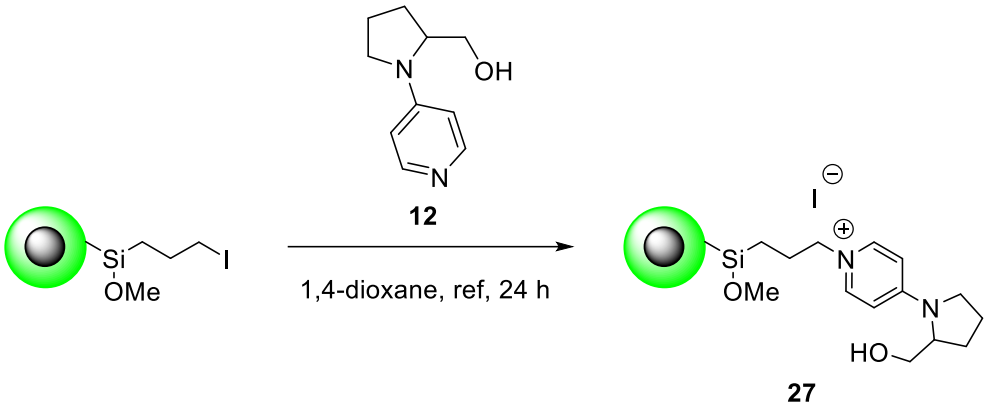

27a: Fe_3O_4 core
27b: $CoFe_2O_4$ core

Compound	Molecular formula	Molecular weight
Post-grafted core-shell MNP_s	/	/
12	$C_{10}H_{14}N_2O$	178.24 g/mol
1,4-dioxane	$C_4H_8O_2$	88.11 g/mol

In a two-necks round bottom flask with a refrigerator on top, 11.7 mg of previously synthesized core-shell MNPs post-grafted with 3-iodopropyl trimethoxysilane (Fe_3O_4 or $CoFe_2O_4$ cores) have been added as a powder. Then, 3 mL of 1,4-dioxane have been added and the mixture has been vigorously stirred (800 rpm) at 40°C to obtain a uniform dispersion. Afterwards, 11.9 mg of **12** (1.35 mmol/g, which was the calculated MNPs functionalization degree, multiplied by 5) have been added and the mixture has been refluxed and stirred (800 rpm) for 24 hours.

After 24 hours, the product has been purified following the procedure described in Section 5.3.2 and characterized with the methods reported in Section 5.3.3. The same procedure has been used in both the case of Fe_3O_4 and $CoFe_2O_4$ cores, obtaining respectively a brown reddish powder (**27a**) and a black powder (**27b**).

5.3.5 Nanocatalysts 27a and 27b efficiency tests

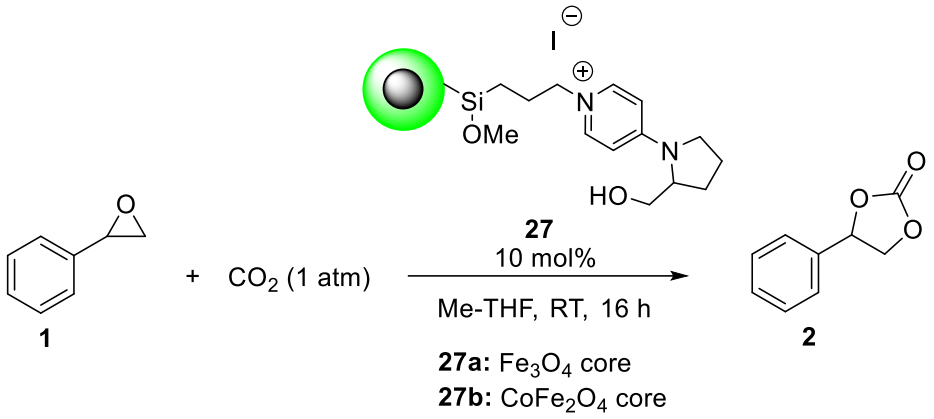

Compound	Molecular formula	Molecular weight
Styrene oxide	C_8H_8O	120.15 g/mol
27a or **27b**	/	/
2-Methyltetrahydrofuran	$C_5H_{10}O$	86.13 g/mol

In a 30 mL centrifuge vial, 40.4 µL of styrene oxide have been added. Then, 10 mol % (186 mg, calculated using the catalyst loading of 0.19 mmol/g) of previously synthesized nanocatalyst **27** (**27a** with Fe_3O_4 cores or **27b** with $CoFe_2O_4$ cores) have been added as a powder. Afterwards, 200 µL of Me-THF have been added dropwise and the vial has been closed with a pierceable rubber cap. The closed vial has been subjected to five vacuum/CO_2 cycles and finally filled with CO_2. The vial has been immersed in a sonication bath thermostated at 25°C and the mixture has been sonicated (pulsed mode) for 16 hours.

After 16 hours, 5 mL of EtOH have been added to the reaction mixture and the vial has been inserted in the custom-made device for magnetic recovery. Then, 2 mL of the supernatant has been sampled and centrifuged at 15000 rpm for 15 min to remove all the MNPs from the liquid phase. The removed MNPs have been recovered by purifying them using the procedure described in Section 5.3.2, to be able to reuse them as nanocatalysts in further reactions.

The liquid phase has been characterized through ^{1}H NMR (in $CDCl_3$) to quantify the styrene oxide conversion into styrene carbonate (28 % yield). The same procedure has been performed both by using nanocatalysts **27a** and **27b**.

^{1}H NMR (500 MHz, $CDCl_3$): a) Styrene oxide **1**: δ 7.39-7.30 (m, 5 H, AR), δ 3.88 (dd, 1 H, CH, $J_{CH\text{-}CH2}$ = 3.96 Hz, $J_{CH\text{-}CH2'}$ = 2.67 Hz), δ 3.16 (dd, 1 H, CH_2, $J_{CH2\text{-}CH2'}$ = 5.46 Hz, $J_{CH2\text{-}CH}$ = 4.16 Hz), δ 2.82 (dd, 1 H, CH_2', $J_{CH2'\text{-}CH2}$ = 5.50 Hz, $J_{CH2'\text{-}CH}$ = 2.58 Hz); b) Styrene carbonate **2**: δ 7.46-7.36 (m, 5 H, AR), δ 5.68 (t, 1 H, CH, $J_{CH\text{-}CH2}$ = $J_{CH\text{-}CH2'}$ = 8.01 Hz), δ 4.81 (t, 1 H, CH_2, $J_{CH2\text{-}CH2'}$ = $J_{CH2\text{-}CH}$ = 8.40 Hz), δ 4.35 (t, 1 H, CH_2', $J_{CH2'\text{-}CH2}$ = $J_{CH2'\text{-}CH}$ = 8.29 Hz).

5.4 Conclusions

The goal of the research reported in this chapter was to prepare two core-shell magnetic nanocatalysts, having magnetite or cobalt-ferrite cores, and to test their catalytic activities in the styrene oxide carbonation, our model reaction.

First of all, it has been possible to ideate and optimize a synthetic strategy to allow the preparation of the target nanocatalysts that involved three steps: a) silica coating of the magnetic cores; b) post-grafting with the immobilization of a iodo-propylic linker on the MNPs surfaces; c) immobilization of the catalytically active species, which was established to be the most performant for the model reaction (see Chapter 4), on the surface of the core-shell MNPs. Using this strategy, two magnetic nanocatalysts, the first one with magnetite (Fe_3O_4) cores (**27a**) and the other one with cobalt-ferrite ($CoFe_2O_4$) cores (**27b**), have been successfully prepared (Figure 25).

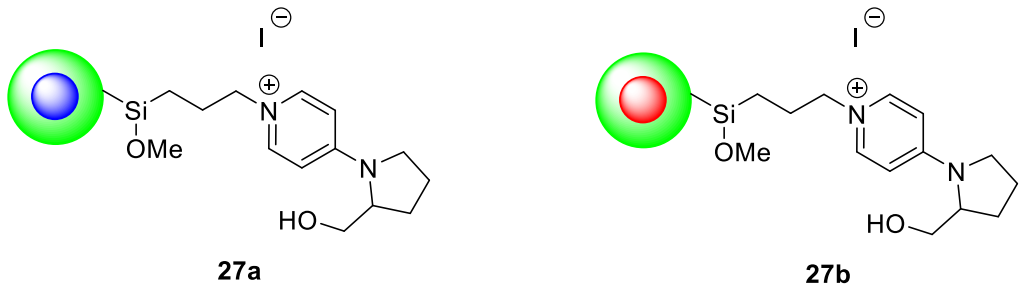

Figure 25 Prepared nanocatalysts **27a** (magnetite core, in blue) and **27b** (cobalt-ferrite core, in red).

The complete functional and morphological characterization of the prepared nanocatalysts, which has been performed integrating several analytic techniques, allowed to confirm the success of the syntheses of the core-shell MNPs and to calculate the catalyst loading on the nanoparticles surface to be 0.19 mmol/g.

Furthermore, all the synthesized nanoparticles resulted to be superparamagnetic, confirming that: a) the silica shell around the core was thin enough to keep the magnetic properties of the MNPs and to allow the magnetic recovery; b) the prepared materials were nanoparticles and not aggregates.

The catalytic efficiency of the synthesized nanocatalysts has been then tested on the model reaction, obtaining 28 % of styrene oxide selective conversion into styrene carbonate in 16 hours, in optimized reaction conditions, using both the

nanocatalysts. It is well known that epoxides carbonations are deeply affected by the temperature and, for this reason, the further step of this project will be to create a set-up in which it will be possible to test the MNPs activity at higher temperature.

Finally, another important field to explore it will be to use the prepared nanocatalysts in microdroplets conditions, integrating aerosol advantages with the easy magnetic recovery of the superparamagnetic nanocatalysts. However, to be able to pursue this objective in an efficient way, it will be necessary to design and assemble an aerosol batch reactor which allow to work with a very little amount of both catalyst and solvent.

6. Continuous flow aerosol exploitation for the styrene carbonate conversion into styrene oxide

6.1 Introduction and aim of the research

In this chapter it has been reported the research work performed during my three months staying at CIPT Lab of KU Leuven (Diepenbeek campus, Belgium) under the supervision of Prof. Mumin Enis Leblebici.

Professor Leblebici's group is mainly focused on the resolution of chemical engineering problems: reactors building and optimization for several purposes, simulations and modeling. Among many activities, a part of the group works on CO_2 capture and reutilization approaches (CCU). In addition, Prof. Leblebici's group has experience in the field of continuous flow microdroplets reactions, since in the past they have worked on photochemical sulfoxidations in aerosol [87].

For all these reasons, I decided to spend my period abroad at CIPT Lab, to extend my knowledge in the aerosol field and widen my skills working in a chemical engineering environment. Basically, what has been done was to adapt and optimize to the needs of this study a continuous-flow aerosol reactor, previously built by Annelot Van den Bogaert, and to finally exploit it in the styrene carbonation. As already discussed in the previous chapters of this thesis, the chosen model reaction was a biphasic gas-liquid reaction, which requires a catalytic system to properly work. A wide catalysts variety has been used to this purpose, among which there are the catalysts already explored in bulk reactions in the previous chapters, but many of them operates at high temperature and/or high pressure values. In addition, most of the catalysts used for this objective were complex and, for this reason, expensive and difficult to be prepared in large scale.

The chosen catalyst for this research was triethylammonium iodide (Et_3NH^+ I^-), quoted in the literature as efficient, cheap and easy-to-prepare (*in situ*) [10].

The performances of the envisaged catalyst in the carbonation model reaction have been reported in the literature by testing it on several epoxides carbonations using mild conditions (p = 1 bar, T = 40°C), no solvent, 10 mol % of catalyst and the reaction required 24 hours to obtain a 87-99% yield of carbonate (Scheme 24) [47].

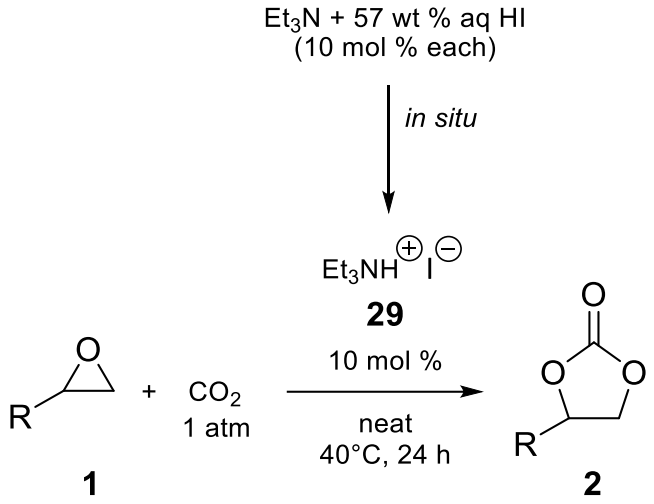

Scheme 24 Reported scheme for several epoxides carbonations reactions using triethylammonium iodide as a catalyst [47].

Considering that the abovementioned reaction needs 24 hours to give good yields, it was fundamental to try to increase as much as possible the aerosol microdroplets residence time, to allow carbon dioxide to dissolve in the liquid and react as long as possible. Indeed, continuous-flow (CF) aerosol wasn't the most convenient solution for this specific purpose, while batch aerosol set-up was impossible to be built at CIPT Lab. For this reason, the CF reactor has been adapted as much as possible for this research goal and the variation of several parameters has been investigated to identify the most efficient conditions to convert styrene oxide into styrene carbonate.

6.2 Discussion of the results

The custom-made set-up described in section 6.3.3, has been exploited for the research purpose. The optimized conditions to obtain styrene carbonate in aerosol have been explored by changing one by one all the parameters, *i.e.* styrene oxide concentration in methanol, catalyst amount, gas flow rate and liquid flow rate. For each parameter, the exploration led to the identification of the best performing conditions. It wasn't possible to work at higher temperature and so to explore the influence of the temperature on the reaction performances because of the geometry of the set-up.

The first explored parameter was the initial styrene oxide concentration leading to the highest styrene oxide conversion into styrene carbonate. Accordingly, all performed runs were periodically sampled and analyzed by HPLC (see section 6.3.5). Results of this initial optimization are shown in the following Figure 26 and they referred to reactions in which all the other parameters were the same: small reaction chamber (56 mL), 2 L/min gas flow rate (which was the maximum flow rate with the available MFC) and 10 mol % of catalyst *vs.* SO. The experiments have been performed using four different liquid flow rates, in order to confirm that the trend was always the same.

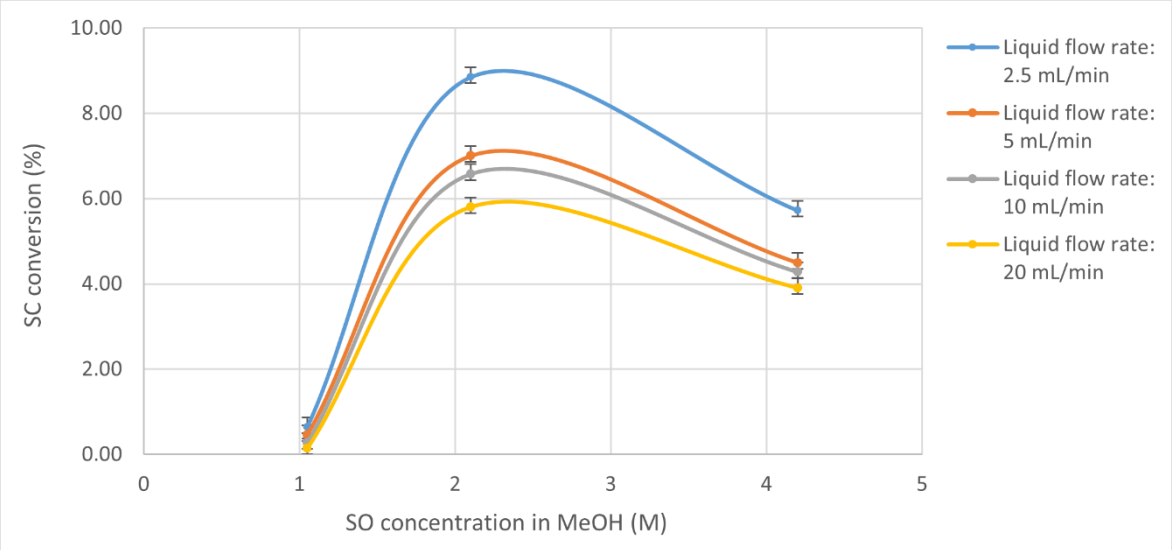

Figure 26 Obtained results for the identification of the most performant SO concentration in MeOH; used conditions: small reaction chamber (56 mL), 2 L/min gas flow rate and 10 mol % of catalyst *vs.* SO.

The concentrations of SO which have been explored were 1.05 M, 2.10 M and 4.20 M. By looking at the graph in Figure 26 it is possible to see that, at each liquid flow

rate, to the increase of the of styrene oxide concentration corresponded an increased conversion into the desired compound up to a maximum. Further increase of the SO concentration negatively affected its conversion. It has been speculated that the explanation of this unexpected behavior can be attributed to the fact that if the reaction mixture was too concentrated, there wasn't a sufficient amount of MeOH to allow enough CO_2 to dissolve in each microdroplet, and so the SC yield was affected because the reaction couldn't proceed properly. Anyhow, this hypothesis needs to be demonstrated with experimental data. Using the performed experiments, the optimized concentration of styrene oxide has been identified to be 2.10 M and this concentration has been used for all the further experiments.

The second parameter which had to be optimized was the catalyst amount. Using constant conditions (small reaction chamber of 56 mL, SO 2.10 M in MeOH, gas flow rate of 50 mL/min and liquid flow rate of 2.5 mL/min), the performances of several catalyst concentrations, *i.e.* 10 mol %, 20 mol %, 30 mol %, 50 mol % and 100 mol %, have been explored. In the following Figure 27 it is possible to observe a linear dependence of the SO conversion into SC in function of the amount of catalyst.

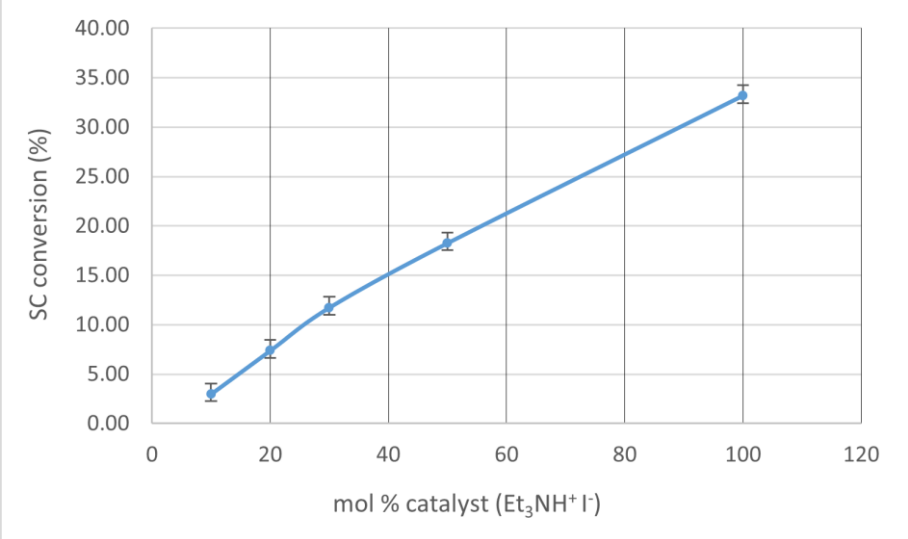

Figure 27 SO conversion into SC *vs.* catalyst amount graph as a confirmation of the absence of mass transfer limitation in aerosol.

The trend of the graph was expected, and it confirmed the absence of mass transfer limitation phenomena in this aerosol system. In fact, in case of mass transfer limitation occurring, the curve had to present a plateau, this mirroring the fact that by increasing the catalyst amount, at a certain point, the conversion is not affected

anymore, because the rate determining step is the absorption rate of CO_2 in the microdroplets.

Once the absence of mass transfer limitation has been confirmed, the same obtained data have been evaluated in terms of turnover number (TON), which has been calculated as the ratio between the moles of SC obtained and the moles of catalyst added to the reaction mixture. Looking at the graph in Figure 28 it was possible to identify 30 mol % of catalyst as the most promising amount of catalyst to use.

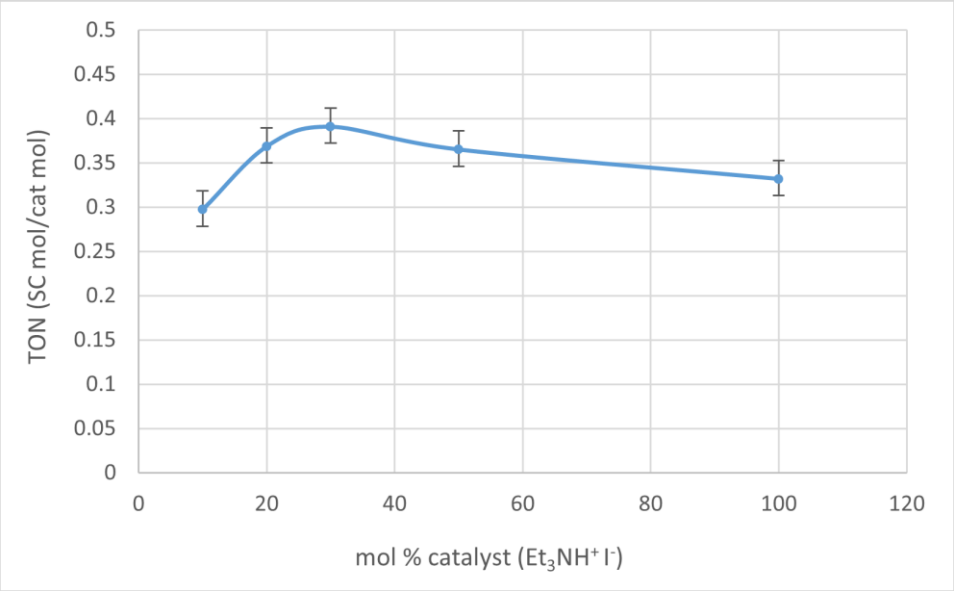

Figure 28 TON (SC mol/cat mol) *vs.* catalyst amount.

Using these data, the optimized concentration of catalyst has been chosen and this concentration, *i.e.* 30 mol % *vs.* SO, and it was used for all the further experiments.

The third exploration aimed to determine how the gas flow rate and the liquid flow rate were able to affect the obtaining of styrene carbonate. In Figure 29 are reported the data obtained by performing the reactions in the small reaction chamber (56 mL), using a 2.10 M reaction mixture with a 30 mol % of catalyst. How it is possible to see by looking at the curves reported in the graph, by increasing the gas flow rate, the conversion increased because the excess of CO_2 was larger and so, due to a faster CO_2 redissolution, more gas was available to be redissolved in the liquid microdroplets up to its thermodynamic limit. Instead, by increasing the liquid flow rate, the behavior was the opposite, *i.e.* SO conversion into SC decreased.

Considering the two different trends observed by changing liquid and gas flow rates, the optimized parameters chosen were 2.5 mL/min liquid flow rate (the smallest value possible) and 2 L/min gas flow rate (the highest possible).

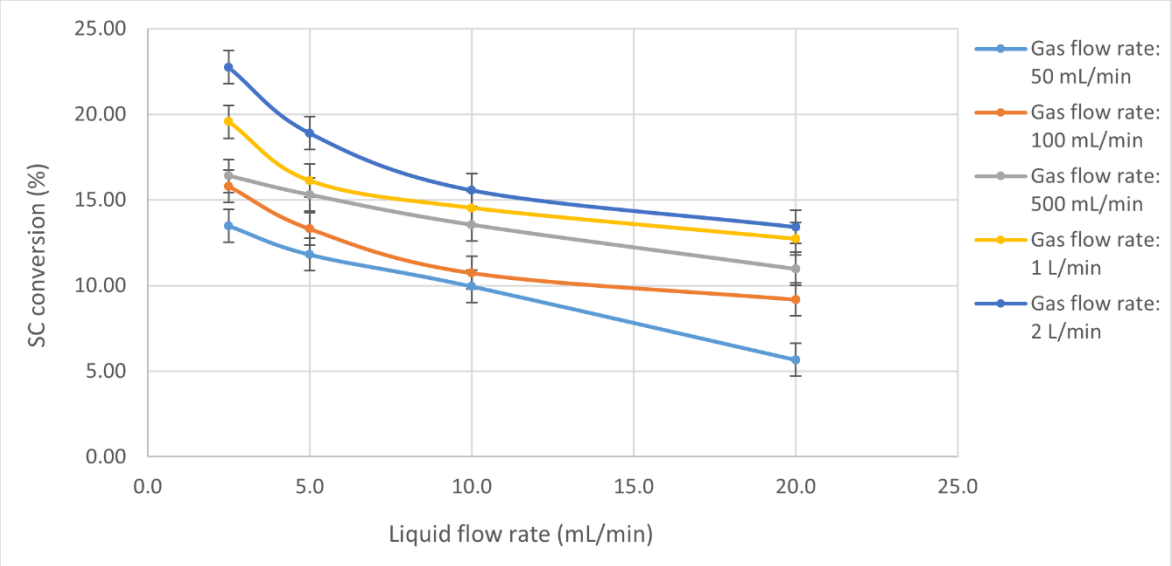

Figure 29 Influence on the conversion into styrene carbonate of the gas flow rate and the liquid flow rate.

The gas and the liquid flow rates also affect the microdroplets dimensions, as it has been previously reported in the literature for other set-ups [87], but unfortunately, in this system, it wasn't possible to measure the microdroplets diameter for safety reason and, because of that, the influence of the flow rates on the microdroplets dimensions and the consequent impact on the substrate conversion have not been evaluated.

All these optimized parameters have been used to perform the experiments in two different reaction chambers, to be able to evaluate the influence of the microdroplets residence time, which is defined as the ratio between the volume of the reactor and the gas flow rate [87], on the carbonate yield.

In Figure 30 it has been reported a picture of the experimental set-up in which is highlighted the 56 mL reaction chamber, which has been changed with a bigger one (100 mL) for some experiments.

Figure 30 Experimental set-up with 56 mL aerosol chamber (yellow circle).

The reaction carried out with the 56 mL aerosol chamber and the other optimized conditions (SO 2.10 M in MeOH, 30 mol % of catalyst, liquid flow rate of 2.5 mL/min, gas flow rate of 2 L/min) led to a conversion of styrene oxide into its corresponding carbonate of 23 ± 1 % (calculated microdroplets residence time of 1.68 seconds), while the reaction performed in the same optimized conditions but by using the 100 mL aerosol chamber led to a 28 ± 1 % of conversion (calculated microdroplets residence time of 3 seconds). Both the reaction chambers are visible in Figure 31.

Figure 31 The two different aerosol chambers used: 100 mL aerosol chamber on the left and 56 mL aerosol chamber on the right.

These results confirmed that by increasing the volume of the reaction chamber, the microdroplets residence time increased and so the conversion increased too.

Nonetheless, the expected relation between the residence time and the conversion, *i.e.* a linear dependency, hasn't been confirmed in our set-up, suggesting that the diverse geometries of the aerosol chamber (Figure 31) played a fundamental role in affecting the performances of the system.

6.3 Experimental section

6.3.1 Materials

Styrene oxide (>98%) and hydriodic acid (57% in water) were purchased from TCI Europe N.V.; methanol (HPLC grade, ≥99.9%) and triethylamine (≥99.0% technical) were purchased from VWR chemicals. All chemicals were used without any further purification.

6.3.2 Reaction mixtures preparation

According to the procedure decribed by Y. Kumatabara *et al.* [47], in a 250 mL flask containing 100 mL of MeOH, styrene oxide has been added to reach the desired concentration (1.05 M, 2.10 M or 4.20 M) while the mixture has been magnetically stirred at RT. Then, Et_3N has been added dropwise (10 mol %, 20 mol %, 30 mol %, 50 mol % or 100 mol % *vs.* styrene oxide). The reaction mixture has been cooled to 0°C and HI has been added dropwise (same amount of Et_3N, *i.e.* 10 mol %, 20 mol %, 30 mol %, 50 mol % or 100 mol % *vs.* styrene oxide). The homogeneous reaction mixture has been stirred for 5 minutes at 0°C, allowing the *in situ* formation of the catalyst $Et_3NH^+ I^-$.

6.3.3 Experimental set-up

The experimental set-up shown in Figure 30 has been self-assembled. Each component of the set-up was introduced for a specific purpose, allowing the reactor to be functional to perform the continuous flow aerosol reactions of our interest. In Figure 32 has been reported a scheme of the set-up.

In details, an ultrasonic nozzle (USN, Ultrasonic processor UP200St coupled to S26d18-S nebulizer sonotrode, bought from Hielscher Ultrasonics GmbH) has been connected to a liquid (reaction mixture) reservoir, to allow the nebulization. The flask cointaining the reaction mixture has been connected to a previously calibrated membrane pump (SIMDOS 10, bought from KNF), which is able to operate in the range 1 mL/min-100 mL/min flow rate. The pump has been then connected to the USN to ensure a liquid supply to the USN which is controlled in terms of flow rate.

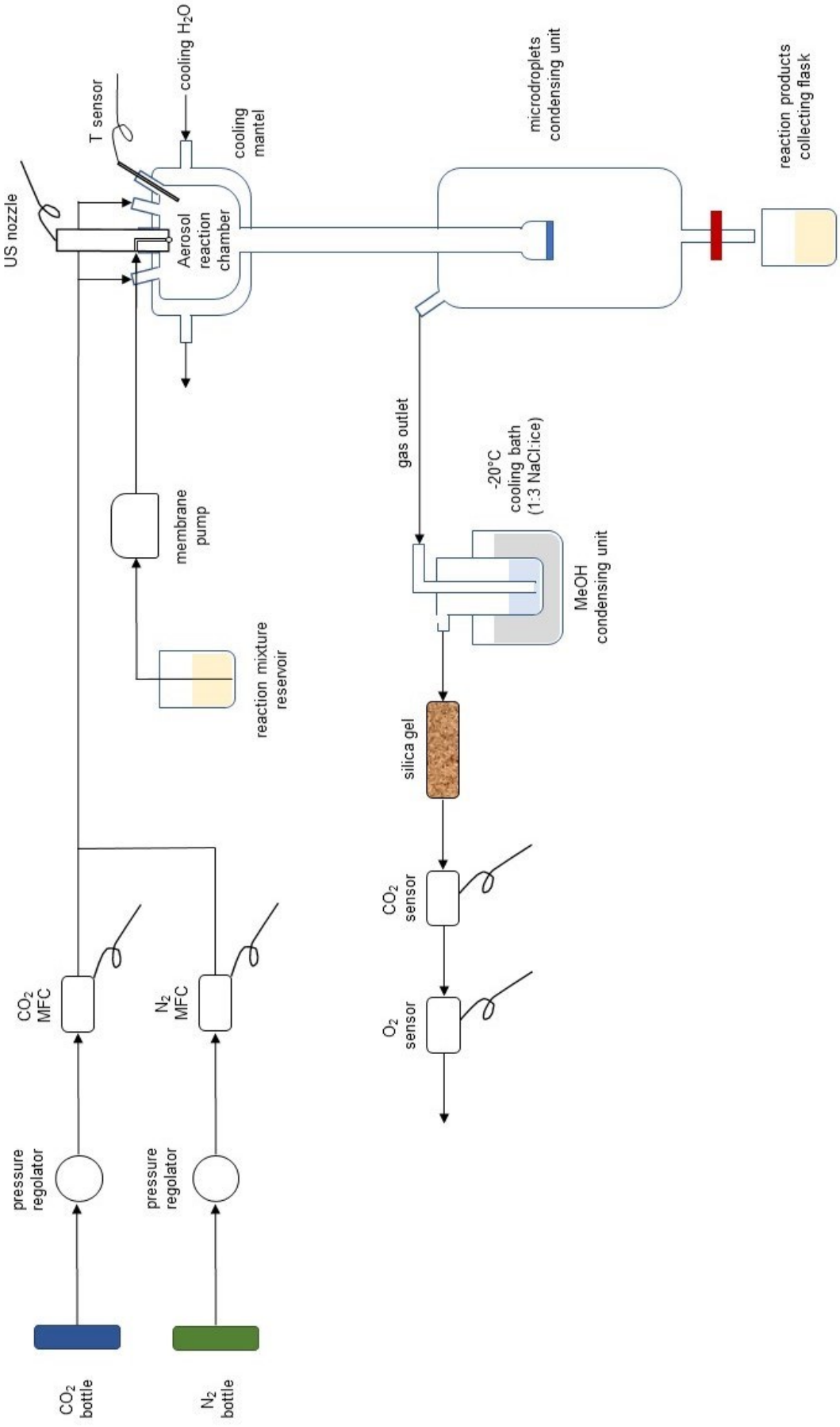

Figure 32 The self-assembled experimental set-up.

How it is possible to see in the set-up scheme, the USN nebulized the reaction mixture in the aerosol reaction chamber, which had a volume of 56 mL or 100 mL, depending on the experiment.

In this chamber it is also possible to observe the presence of a temperature sensor, which made possible to monitor the temperature during the experiments, and two connections with N_2 and CO_2 supplies. The gases supply had to be regulated and, for this reason, each of the two gas bottles (both nitrogen and carbon dioxide) have been connected to mass-flow controllers (Bronkhorst EL-FLOW Select with a range of 2 L/min for N_2 and Bronkhorst EL-FLOW Prestige with a range of 2 L/min for CO_2). In this set-up the operating gas pressure was always of 1 atm. It was also possible to use tap water to cool down the reaction chamber in case of exothermic reactions, but this tool has not been used during the experiments because it wasn't necessary.

In the bottom part of the reaction chamber, it has been placed a glass tube with a glass filter at the end. This part of the set-up was necessary to condensate the microdroplets, after they have been sprayed, in order to collect the liquid reacted mixture. Indeed, it is possible to identify, in the bottom part of the scheme, a tap which allowed the operator to pick up the liquid phase in a collecting flask or in a vial for the further samples analyses.

The gas phase outlet has been connected to several components, each of them having a specific role. First of all, there was a bubbler immersed in a cooling bath at -20°C (1:3 NaCl:ice) to allow the condensation of the amount of MeOH which was in the gas phase. This condensing unit was necessary, otherwise the MeOH in the gas flow interfered with the CO_2 sensor, which is based on IR signals. A silica gel trap has been inserted to avoid the humidity in the gas flow to reach both CO_2 and O_2 sensor and avoid damages to them. The carbon dioxide sensor allowed the monitoring of the consumption of CO_2 during the reactions. Instead, the O_2 sensor, which was coupled with an Arduino, was placed in the set-up just for safety reasons. In fact, because oxygen is a flamable gas, it was very important, in every moment, to be sure that there was no oxygen in the gas flow.

6.3.4 Reaction procedures

In order to perform each of the aerosol reactions, the entire set-up has been filled with CO_2 using the desired gas flow rate. Subsequently, water was first sprayed to clean the liquid pump, the tubes and the reactor. Then, methanol was sprayed to wash from water the system and then finally the previously prepared reaction mixture has been sprayed. The samples were collected after the reaction from the bottom of the set-up (see section 6.3.3) after at least 1 minute of nebulization, to be sure to collect the reaction mixture and not traces of the solvents used to wash the set-up. All the samples have been then analyzed through HPLC (section 6.3.5) to quantify the obtained conversion in terms of amount of styrene carbonate.

6.3.5 HPLC analysis for the evaluation of the conversion

High Performance Liquid Chromatography (HPLC, Agilent 1100 Series) has been used for the evaluation of the conversion in each sample. In order to be able to calculate the conversion after the reactions, a calibration curve of both styrene oxide and styrene carbonate was necessary.

For this reason, first of all, five standard solutions at different concentrations containing both the analytes have been prepared (SO 0.25 mM + SC 0.25 mM in MeOH, SO 0.50 mM + SC 0.50 mM in MeOH, SO 1.00 mM + SC 1.00 mM in MeOH, SO 1.25 mM + SC 1.25 mM in MeOH, SO 1.50 mM + SC 1.50 mM in MeOH). The five solutions have been analyzed using a previous optimized method (column: Synergi H18-041891, flow: 1.1 mL/min, RT, water:ACN 1:1, 14 min, detector wavelenght: 216 nm, SO Rt = 7.65, SC Rt = 5.50), obtaining the graph in Figure 33.

At the end of each reaction, the collected samples have been diluted 1:1000 and analyzed through HPLC. Using the reported calibration curve, it was possible to calculate the conversion value for each of the reaction conditions, which have been all performed in quadruplicate and the reported data in Section 6.2 are the averages with the relative errors calculated as standard errors.

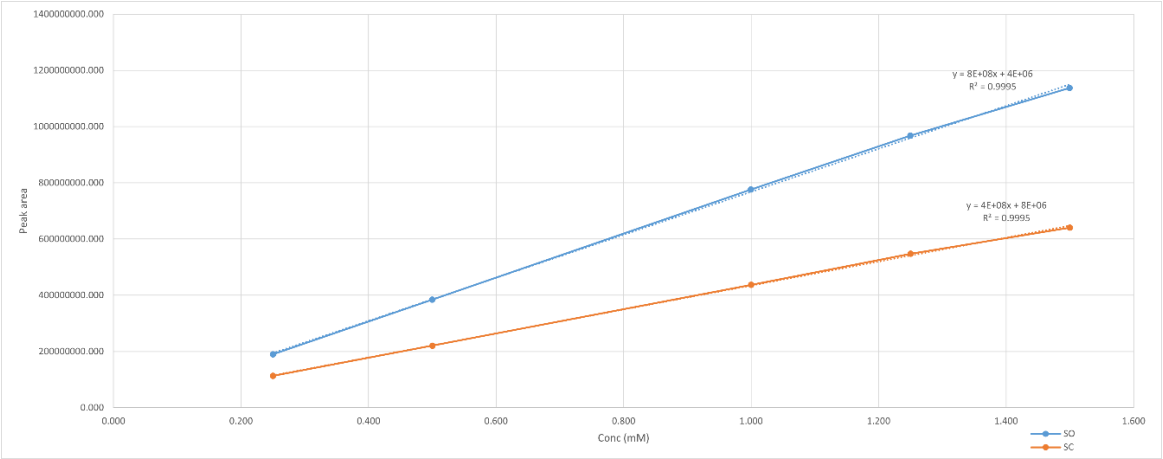

Figure 33 Calibration curve for styrene oxide (SO) and styrene carbonate (SC).

6.4 Conclusions

The described research work had the goal to demonstrate the validity of CF aerosol to quickly perform reactions which normally need 24 hours and temperatures higher than RT to occur.

The aerosol set-up used for this exploration was custom-made and self-assembled. Each component has been added or optimized in the first phase of the research, to obtain a reactor with all the components needed which perfectly worked for the purpose.

Using this set-up, several parameters have been explored to identify the optimized reaction conditions by evaluating the influence of all the variables involved. First of all, it has been obtained that the optimal concentration of the reaction mixture was 2.10 M styrene oxide in MeOH with 30 mol % of catalyst (Et_3NH^+ I^-). Then, the influence of the gas flow rate and the liquid flow rate on the performances have been evaluated, obtaining that the best gas flow rate with which operating was 2 L/min (the highest one) and the best liquid flow rate was 2.5 mL/min (the lowest one).

Using all the optimized conditions the best result obtained was 23 ± 1 % of **1** conversion in **2** using the small reactor and 28 ± 1 % of conversion using the bigger one. These results confirmed our hypothesis of dependency of the conversion on the microdroplets residence time, but it also suggested a high influence of the reactor geometry on the residence time, because of the absence of a linear correlation. Indeed, an estimation of the residence time has been calculated by dividing the reactor volume by the used gas flow rate (2 L/min), obtaining 1.68 seconds of residence time by using the 56 mL reaction chamber and 3 seconds by using the 100 mL reaction chamber. These results are very promising if compared with classical batch reaction which normally proceeds very slow.

Furthermore, the validity of aerosol as a method to perform reactions has been confirmed by demonstrating the absence of mass-transfer limitation phenomena in this system, overcoming the kinetic limit in gas-liquid heterogeneous systems.

7. Final conclusions

In the scenario described in the Introduction, it was fundamental to find new CCU strategies to exploit carbon dioxide in the zero-waste insertion into epoxides to obtain carbonates. The research work reported in this thesis aimed to identify and study new implemented approaches for process intensification of cyclic carbonates synthesis, using mild conditions and performing, sustainable and efficient methodologies. Guided by the principles of Green Chemistry, the final aim of this thesis was, therefore, to explore new optimized processes that maximize the efficiency of the conversion of epoxides into cyclic carbonates exploiting CO_2 as a feedstock, and to recover and recycle the used catalyst at the end of the reaction.

In Chapter 3 a research work in batch aerosol has been reported. The goal was to explore the kinetics of the model reaction in microdroplets conditions *vs*. normal bulk reactions, to demonstrate the advantages of aerosol in enhancing the efficiency of biphasic transformations, overcoming mass-transfer limitations. The carbonation of styrene oxide, in fact, has been selected as a model reaction in the realm of CO_2-utilization strategies, which are considered a fundamental research topic nowadays, and it was herein performed by using a potassium iodide/triethylene glycol (KI/TEG) complex to catalyse the obtaining of styrene carbonate (Scheme 25).

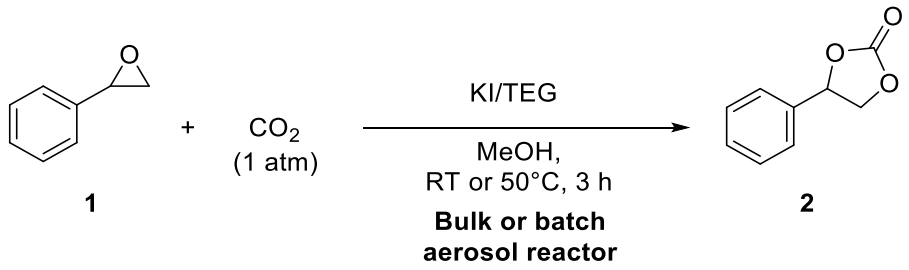

Scheme 25 Reaction studied in the research work reported in Chapter 3.

The batch approach used allowed a lower CO_2 consumption during the experiments, if compared to a continuous flow process. The custom-made aerosol set-up has demonstrated to be efficient for our purpose, affording a twofold acceleration in microdroplets conditions *vs.* sonicated bulk, both at 25°C and 50°C. Furthermore, the experiments at 50°C confirmed the dependency of the model reaction on the temperature, affording a higher yield when the reaction was performed at higher temperature.

Subsequently, in Chapter 6, the validity of also continuous flow aerosol as a useful tool to improve the process efficiency has been studied. The home-made CF aerosol set-up was exploited to quickly perform reactions which normally need 24 hours and temperatures higher than RT to occur. Since the reactor was self-assembled, each component was optimized in the first phase of the research, to obtain a reactor with all the components needed which perfectly worked for the purpose. The catalyst used, in this case, was a very cheap and easy to prepare ionic liquid, because the process required a very large amount of reacting mixture. A lot of parameters were involved while performing reactions in this kind of custom-made reactor and, for this reason, each of them has been studied and optimized, and they have been reported in Scheme 26.

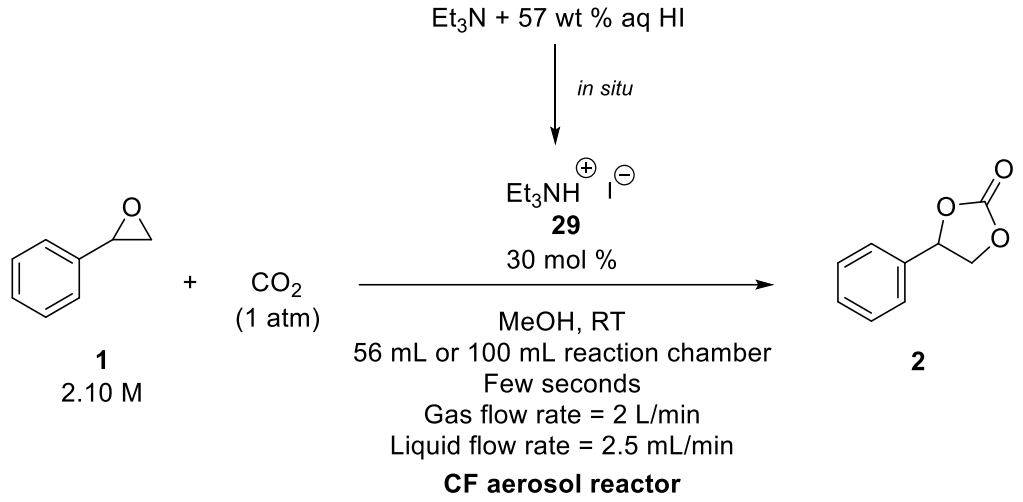

Scheme 26 CF aerosol reaction explored in Chapter 6.

Using all the optimized conditions, the best result obtained was 23 % of conversion of **1** in **2** using the 56 mL reactor and 28 % of conversion using the bigger one. These results confirmed the dependency of the conversion on the microdroplets residence time, but it also suggested a high influence of the reactor geometry on the residence time, leading to a non-linear correlation between the two variables. The residence time of the microdroplets, *i.e.* the reaction time, was calculated to be 1.68 seconds in the 56 mL reaction chamber and 3 seconds in the 100 mL one. These results are very promising if compared with classical batch reaction, which normally proceeds very slow. Furthermore, the validity of aerosol as a method to perform reactions has been confirmed by demonstrating the absence of mass-transfer

limitation phenomena in this system, overcoming the kinetic limit in gas-liquid heterogeneous systems.

A very important output is that microdroplets conditions can be applied to a wide range of reactions, using batch or continuous flow processes depending on the circumstances. Continuous flow aerosol can give very fast reactions, but it requires a lot of reactive mixture which can be easy to be prepared and cheap. On the contrary, batch aerosol is more suitable for a reaction that requires a longer contact time between the two phases or when the catalyst used is precious, *i.e.* expensive or difficult to obtain. Anyway, what was clear from the experiments performed is that aerosol chemistry is able to enhance styrene carbonate formation from its corresponding epoxide and CO_2, thus paving the way for the application of microdroplets conditions to the whole realm of biphasic gas-liquid transformations.

In the literature a very wide range of catalysts that can be exploited for the styrene carbonate synthesis are reported. Nonetheless, some new ionic liquids which can be exploited as organocatalysts have been prepared. As it is depicted in Scheme 27, the preparation and the use of five different ionic liquids as organocatalysts for the styrene oxide conversion into styrene carbonate have been studied in Chapter 4.

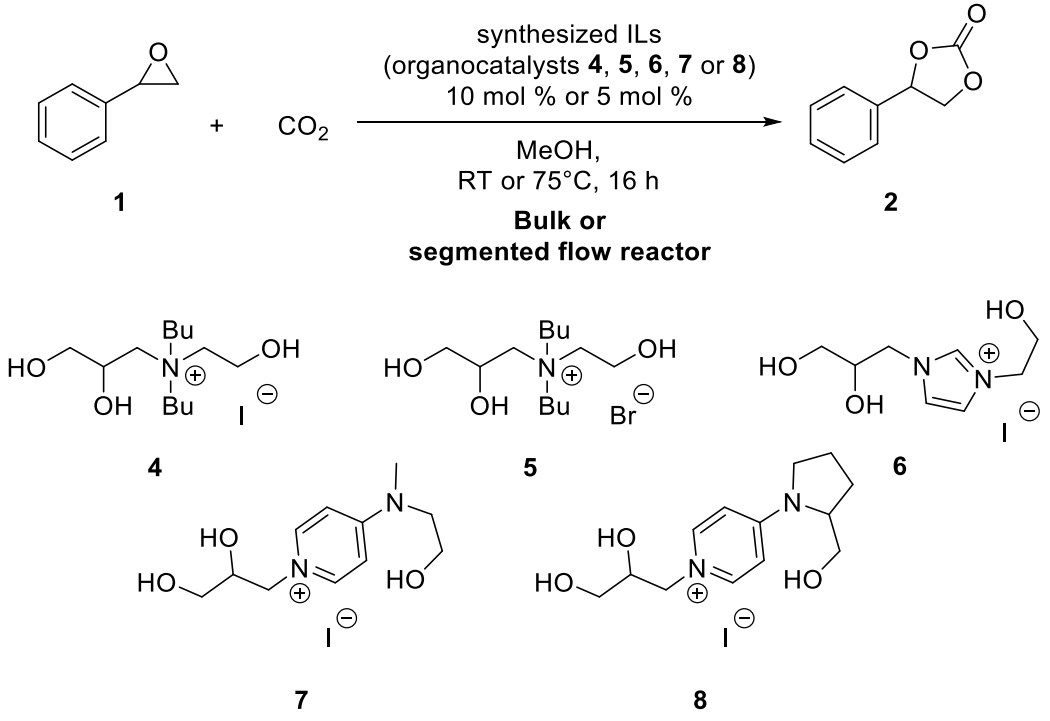

Scheme 27 Reaction studied in Chapter 4.

The five catalysts have been synthesized and tested on the model reaction. Furthermore, more of them can be designed and prepared, inspired by the ones that have been synthesized in this thesis work. In fact, keeping in mind the features that can confer to an ionic liquid suitable properties to be exploited as organocatalyst in reaction with CO_2, the range of new compounds that can be synthesized is very wide.

The ionic liquid **8** has shown the best catalytic efficiency, producing styrene carbonate quantitatively at 75°C in 16 hours, and, for this reason, it has been exploited to obtain a collection of six cyclic carbonates from their corresponding epoxides (Figure 34) in good or excellent yields, expanding the scope of the research.

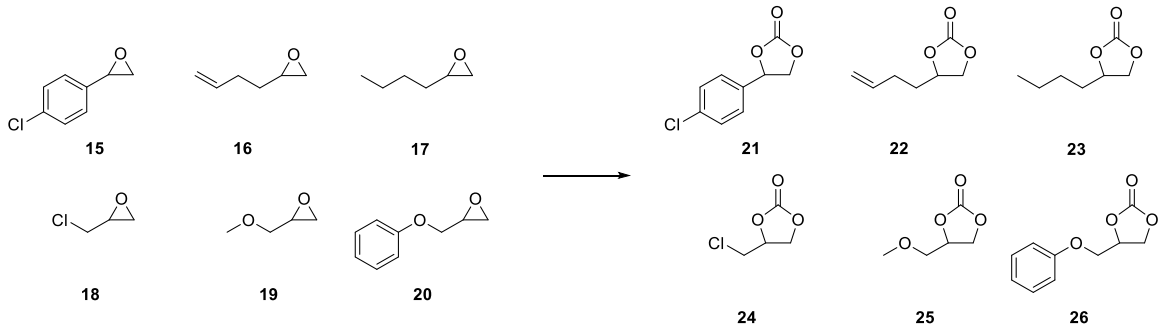

Figure 34 Substrates and products of the scope extension performed in Chapter 4.

Considering the main interest in the development of efficient methodologies for the intensification of gas-liquid reactions, the selected organocatalyst has been used to promote the synthesis of cyclic carbonates in segmented flow conditions, with the detection of significant improvements in terms of reaction rate and productivity passing from a bulk reactor to flow chemistry. Traditional flow chemistry demonstrated to be a very useful tool for the process intensification of biphasic gas-liquid transformation, giving an increase of the process productivity up to 17 times, if compared with bulk process.

These very promising results paved the way for the further exploration of the bifunctional catalyst **8** in semi-heterogeneous conditions reported in Chapter 5. In fact, the catalytically active moiety of the previously identified best performing ionic liquid has been immobilized on silica core-shell magnetic nanoparticles, to obtain nanocatalysts for the styrene oxide carbonation in semi-heterogeneous conditions. Two classes of nanocatalysts (with magnetite or cobalt-ferrite cores) have been

prepared, allowing an easy magnetic recovery at the end of the reaction, with the simple application of a static magnetic field. In fact, magnetic nanocatalysts can be considered a very promising technology to recycle and reduce wastes as much as possible: despite their synthesis requires a moderate effort, once they have been prepared, they are very stable and they can be used in semi-heterogeneous catalysis and easily recycled through a static magnetic field.

Among the two prepared materials, cobalt-ferrite has been identified as the most suitable cores material, because of the higher saturation magnetization shown during the magnetic measurements. The catalytic performances of the prepared nanocatalysts have been evaluated on the model reaction in a classic bulk reactor (Scheme 28), obtaining 28 % of styrene oxide selective conversion into styrene carbonate in 16 hours.

It is well known that carbonates of epoxides are deeply affected by the temperature and, for this reason, it could be very interesting to create a set-up which allows to test the MNPs activity at higher temperature.

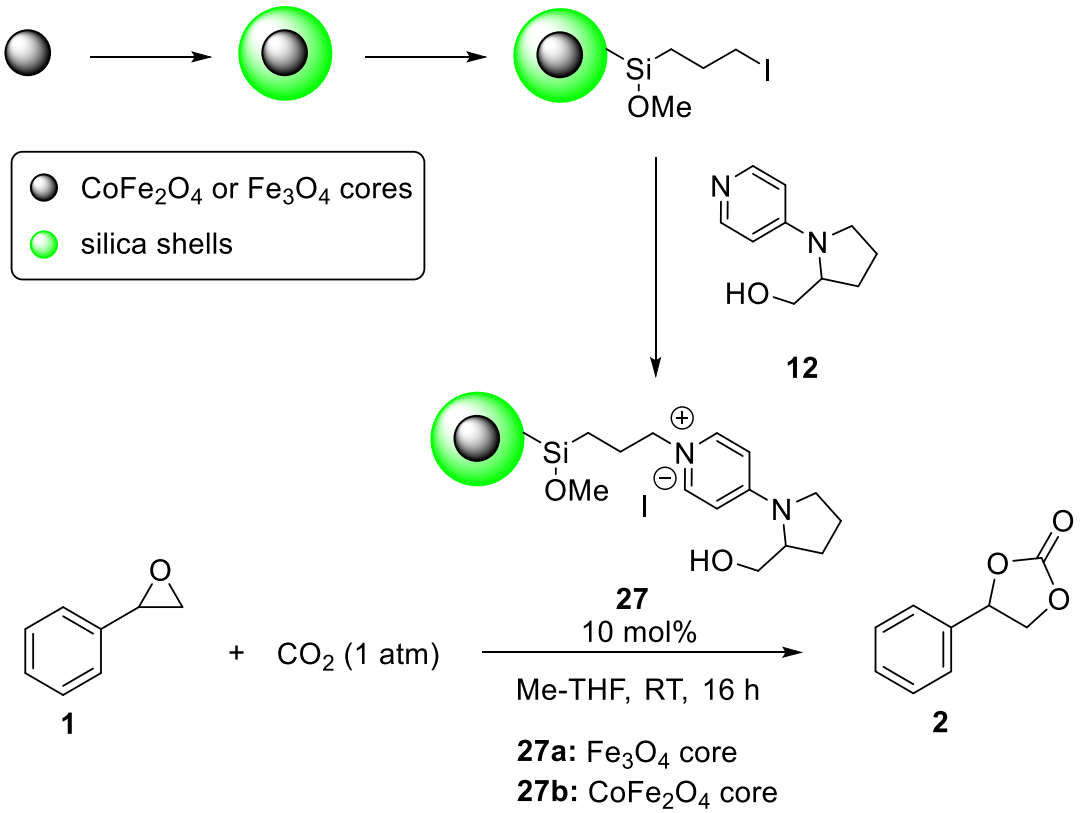

Scheme 28 Styrene carbonate synthesis in semi-heterogeneous conditions, studied in Chapter 5.

To conclude, in the depicted scenario, considering the advantages of using aerosol reactors, semi-heterogeneous magnetic catalysts and the related literature, it appears to be very promising to exploit the integration of aerosol advantages with the easy magnetic recovery of the superparamagnetic nanocatalysts, which can synergistically cooperate, to improve the speed, selectivity and productivity in gas-liquid reactions. An example of this could be the use of the prepared nanocatalysts in a small-scale batch aerosol reaction, to test their catalytic efficiency on the styrene carbonate synthesis. However, to be able to pursue this objective in an efficient way, it will be necessary to design and assemble an aerosol batch reactor which will allow to work with a very little amount of both catalyst and solvent.

List of acronyms

AAF	Apparent acceleration factor
ACN	Acetonitrile
AcOH	Acetic acid
AF	Acceleration factor
AR	Aromatic
BPR	Back-pressure regulator
CCS	Carbon capture and storage
CCU	Carbon capture and utilization
$CDCl_3$	Deuterated chloroform
CF	Continuous flow
CIPT	Centre for industrial process technology
CNR	(Italian) National research council
$Co(acac)_2$	Cobalt(II) acetylacetonate
CO_2	Carbon dioxide
$CoFe_2O_4$	Cobalt-ferrite
COFs	Covalent organic structures
COSY	Correlated spectroscopy
CSTR	Continuous stirred tank reactor
CSTR	Continuous stirred tank reactor
CV	Column volume
Cy	Cyclohexane
DCM	dichloromethane
DIPEA	N,N-Diisopropylethylamine
DLS	Dynamic light scattering
DMF	Dimethyl formamide
DMSO	Dimethyl sulfoxide
EA	Elemental analysis
ESI	Electrospray ionization
ESSI	Electrosonic spray ionization
ESSL	European severe storms laboratory
ESWD	European severe weather database
Et_3N	Triethylamine
$Et_3NH^+I^-$	Triethylammonium iodide

EtOAc	Ethyl acetate
EtOH	Ethanol
FC	Flow chemistry
$Fe(acac)_3$	Iron(III) acetylacetonate
Fe_3O_4	Magnetite
FEP	Fluoropolymer
FTIR	Fourier transform infrared spectroscopy
H_2O	Water
HCl	Hydrochloric acid
HI	Hydriodic acid
HMBC	Heteronuclear multiple bond correlation
HPLC	High performance liquid chromatography
HRMS	High resolution mass spectrometry
HSQC	Heteronuclear single quantum coherence
ICP	Inductively coupled plasma
IL	Ionic liquid
IMM	Institute for microelectronics and microsystems
IR	Infrared
ISM	Institute of structure of matter
ISOF	Institute of organic synthesis and photoreactivity
K_2CO_3	Potassium carbonate
KI	Potassium iodide
KU	Katholieke universiteit
LC	Liquid chromatography
LiI	Lithium iodide
MeOH	Methanol
Me-THF	2-methyl tetrahydrofuran
MFC	Mass-flow controller
MNPs	Magnetic nanoparticles
MS	Mass spectrometry
Ms	Saturation magnetization
NaOH	Sodium hydroxide
NATO	North Atlantic treaty organization
NH_4OH	Ammonium hydroxide

NMR	Nuclear magnetic resonance
P	Productivity
PFR	Plug flow reactor
PID	Proportional integral derivative
POPs	Porous polymers
rpm	Round per minute
Rt	Retention time
RT	Room temperature
SA	Surface area
SC	Styrene carbonate
SO	Styrene oxide
SPS	Science for peace and security
SS-NMR	Solid state nuclear magnetic resonance
TANGO	Technology against climate change to mitigate CO_2 environmental security threats
TEG	Triethylene glycol
TEM	Transmission electron microscopy
TEOS	Tetraethyl orthosilicate
THF	Tetrahydrofuran
TOF	Turnover frequency
TON	Turnover number
UN	Ultrasonic nebulization/nebulizer
USN	Ultrasonic nozzle
V	Volume
VSM	Vibrating-sample magnetometer
XPS	X-ray photoelectron spectroscopy
Z_P	Zeta potential

Bibliography

1. *The Hindu Kush Himalaya Assessment, Mountains, Climate Change, Sustainability and People*; Wester, P., Mishra, A., Mukherji, A., Shrestha, A., Eds.; 2019; ISBN 9783319922874.

2. Richmond, A.; Heimel, N.; Galgano, F. Modeling Environmental Security in Sub-Saharan Africa. *The Geographical Bulletin* **2012**, *53*, 21–38.

3. Dalby, S. Climate Change. *Rusi J* **2013**, *158*, 34–43, doi:10.1080/03071847.2013.807583.

4. Song, C. Global Challenges and Strategies for Control, Conversion and Utilization of CO2 for Sustainable Development Involving Energy, Catalysis, Adsorption and Chemical Processing. *Catal Today* **2006**, *115*, 2–32, doi:10.1016/j.cattod.2006.02.029.

5. Zhang, H.; Kong, X.; Cao, C.; Pang, G.; Shi, Y. An Efficient Ternary Catalyst ZnBr2/K2CO3/[Bmim]Br for Chemical Fixation of CO2 into Cyclic Carbonates at Ambient Conditions. *J Co2 Util* **2016**, *14*, 76–82, doi:10.1016/j.jcou.2016.03.001.

6. Gao, W.; Liang, S.; Wang, R.; Jiang, Q.; Zhang, Y.; Zheng, Q.; Xie, B.; Toe, C.Y.; Zhu, X.; Wang, J.; et al. Industrial Carbon Dioxide Capture and Utilization: State of the Art and Future Challenges. *Chem Soc Rev* **2020**, *49*, 8584–8686, doi:10.1039/d0cs00025f.

7. Yang, Y.; Lee, J.-W. Toward Ideal Carbon Dioxide Functionalization. *Chem Sci* **2019**, *10*, 3905–3926, doi:10.1039/c8sc05539d.

8. Shaikh, R.R.; Pornpraprom, S.; D'Elia, V. Catalytic Strategies for the Cycloaddition of Pure, Diluted and Waste CO2 to Epoxides under Ambient Conditions. *Acs Catal* **2017**, doi:10.1021/acscatal.7b03580.

9. Yan, S.-S.; Fu, Q.; Liao, L.-L.; Sun, G.-Q.; Ye, J.-H.; Gong, L.; Bo-Xue, Y.-Z.; Yu, D.-G. Transition Metal-Catalyzed Carboxylation of Unsaturated Substrates with CO2. *Coordin Chem Rev* **2018**, *374*, 439–463, doi:10.1016/j.ccr.2018.07.011.

10. Guo, L.; Lamb, K.J.; North, M. Recent Developments in Organocatalysed Transformations of Epoxides and Carbon Dioxide into Cyclic Carbonates. *Green Chem* **2020**, *23*, 77–118, doi:10.1039/d0gc03465g.

11. P, S.; Mandal, S.K. From CO 2 Activation to Catalytic Reduction: A Metal-Free Approach. *Chem Sci* **2020**, *11*, 10571–10593, doi:10.1039/d0sc03528a.

12. Bui, M.; Adjiman, C.S.; Bardow, A.; Anthony, E.J.; Boston, A.; Brown, S.; Fennell, P.S.; Fuss, S.; Galindo, A.; Hackett, L.A.; et al. Carbon Capture and Storage (CCS): The Way Forward. *Energ Environ Sci* **2018**, *11*, 1062–1176, doi:10.1039/c7ee02342a.

13. Guo, W.; Gómez, J.E.; Cristòfol, À.; Xie, J.; Kleij, A.W. Catalytic Transformations of Functionalized Cyclic Organic Carbonates. *Angew. Chem. Int. Ed.* **2018**, *57*, 13735–13747, doi:10.1002/anie.201805009.

14. Besse, V.; Camara, F.; Voirin, C.; Auvergne, R.; Caillol, S.; Boutevin, B. Synthesis and Applications of Unsaturated Cyclocarbonates. *Polym Chem-uk* **2013**, *4*, 4545–4561, doi:10.1039/c3py00343d.

15. Pyo, S.-H.; Persson, P.; Mollaahmad, M.A.; Sörensen, K.; Lundmark, S.; Hatti-Kaul, R. Cyclic Carbonates as Monomers for Phosgene- and Isocyanate-Free Polyurethanes and Polycarbonates. *Pure Appl Chem* **2011**, *84*, 637–661, doi:10.1351/pac-con-11-06-14.

16. Pescarmona, P.P.; Taherimehr, M. Challenges in the Catalytic Synthesis of Cyclic and Polymeric Carbonates from Epoxides and CO 2. *Catal Sci Technol* **2012**, *2*, 2169–2187, doi:10.1039/c2cy20365k.

17. Assen, N. von der; Sternberg, A.; Kätelhön, A.; Bardow, A. Environmental Potential of Carbon Dioxide Utilization in the Polyurethane Supply Chain. *Faraday Discuss* **2015**, *183*, 291–307, doi:10.1039/c5fd00067j.

18. Fukuoka, S.; Kawamura, M.; Komiya, K.; Tojo, M.; Hachiya, H.; Hasegawa, K.; Aminaka, M.; Okamoto, H.; Fukawa, I.; Konno, S. A Novel Non-Phosgene Polycarbonate Production Process Using by-Product CO 2 as Starting Material. *Green Chem* **2003**, *5*, 497–507, doi:10.1039/b304963a.

19. Beattie, C.; North, M.; Villuendas, P. Proline-Catalysed Amination Reactions in Cyclic Carbonate Solvents. *Molecules* **2011**, *16*, 3420–3432, doi:10.3390/molecules16043420.

20. Schäffner, B.; Schäffner, F.; Verevkin, S.P.; Börner, A. Organic Carbonates as Solvents in Synthesis and Catalysis. *Chem Rev* **2010**, *110*, 4554–4581, doi:10.1021/cr900393d.

21. Xu, K. Nonaqueous Liquid Electrolytes for Lithium-Based Rechargeable Batteries. *Chem Rev* **2004**, *104*, 4303–4418, doi:10.1021/cr030203g.

22. Zhang, S.S. A Review on Electrolyte Additives for Lithium-Ion Batteries. *J Power Sources* **2006**, *162*, 1379–1394, doi:10.1016/j.jpowsour.2006.07.074.

23. Clements, J.H. Reactive Applications of Cyclic Alkylene Carbonates. *Ind Eng Chem Res* **2003**, *42*, 663–674, doi:10.1021/ie020678i.

24. Mindemark, J.; Mogensen, R.; Smith, M.J.; Silva, M.M.; Brandell, D. Polycarbonates as Alternative Electrolyte Host Materials for Solid-State Sodium Batteries. *Electrochem Commun* **2017**, *77*, 58–61, doi:10.1016/j.elecom.2017.02.013.

25. Duval, A.; Avérous, L. Cyclic Carbonates as Safe and Versatile Etherifying Reagents for the Functionalization of Lignins and Tannins. *Acs Sustain Chem Eng* **2017**, *5*, 7334–7343, doi:10.1021/acssuschemeng.7b01502.

26. Büttner, H.; Longwitz, L.; Steinbauer, J.; Wulf, C.; Werner, T. Recent Developments in the Synthesis of Cyclic Carbonates from Epoxides and CO2. *Top Curr Chem* **2017**, *375*, 50, doi:10.1007/s41061-017-0136-5.

27. Cokoja, M.; Wilhelm, M.E.; Anthofer, M.H.; Herrmann, W.A.; Kühn, F.E. Synthesis of Cyclic Carbonates from Epoxides and Carbon Dioxide by Using Organocatalysts. *Chemsuschem* **2015**, *8*, 2436–2454, doi:10.1002/cssc.201500161.

28. Martín, C.; Fiorani, G.; Kleij, A.W. Recent Advances in the Catalytic Preparation of Cyclic Organic Carbonates. *Acs Catal* **2015**, *5*, 1353–1370, doi:10.1021/cs5018997.

29. Comerford, J.W.; Ingram, I.D.V.; North, M.; Wu, X. Sustainable Metal-Based Catalysts for the Synthesis of Cyclic Carbonates Containing Five-Membered Rings. *Green Chem* **2014**, *17*, 1966–1987, doi:10.1039/c4gc01719f.

30. Alves, M.; Grignard, B.; Mereau, R.; Jerome, C.; Tassaing, T.; Detrembleur, C. Organocatalyzed Coupling of Carbon Dioxide with Epoxides for the Synthesis of

Cyclic Carbonates: Catalyst Design and Mechanistic Studies. *Catal Sci Technol* **2017**, *7*, 2651–2684, doi:10.1039/c7cy00438a.

31. Dabral, S.; Schaub, T. The Use of Carbon Dioxide (CO2) as a Building Block in Organic Synthesis from an Industrial Perspective. *Adv. Synth. Catal.* **2019**, *361*, 223–246, doi:10.1002/adsc.201801215.

32. Yang, C.; Chen, Y.; Xu, P.; Yang, L.; Zhang, J.; Sun, J. Facile Synthesis of Zinc Halide-Based Ionic Liquid for Efficient Conversion of Carbon Dioxide to Cyclic Carbonates. *Mol Catal* **2020**, *480*, 110637, doi:10.1016/j.mcat.2019.110637.

33. Calmanti, R.; Sargentoni, N.; Selva, M.; Perosa, A. One-Pot Tandem Catalytic Epoxidation—CO2 Insertion of Monounsaturated Methyl Oleate to the Corresponding Cyclic Organic Carbonate. *Catalysts* **2021**, *11*, 1477, doi:10.3390/catal11121477.

34. Xu, A.; Chen, Z.; Jin, L.; Chu, B.; Lu, J.; He, X.; Yao, Y.; Li, B.; Dong, L.; Fan, M. Quaternary Ammonium Salt Functionalized MIL-101-NH2(Cr) as a Bifunctional Catalyst for the Cycloaddition of CO2 with Epoxides to Produce Cyclic Carbonates. *Appl Catal Gen* **2021**, *624*, 118307, doi:10.1016/j.apcata.2021.118307.

35. Cai, X.; Tolvanen, P.; Virtanen, P.; Eränen, K.; Rahkila, J.; Leveneur, S.; Salmi, T. Kinetic Study of the Carbonation of Epoxidized Fatty Acid Methyl Ester Catalyzed over Heterogeneous Catalyst HBimCl-NbCl5/HCMC. *Int. J. Chem. Kinet.* **2021**, *53*, 1203–1219, doi:10.1002/kin.21526.

36. Li, X.; Sun, J.; Xue, M.; Yin, J. Catalytic Conversion of CO2 by Supported Ionic Liquid Prepared with Supercritical Fluid Deposition in a Continuous Fixed-Bed Reactor. *J Co2 Util* **2022**, *64*, 102168, doi:10.1016/j.jcou.2022.102168.

37. Wang, Y.; Liu, Y.; Su, Q.; Li, Y.; Deng, L.; Dong, L.; Fu, M.; Liu, S.; Cheng, W. Poly(Ionic Liquid) Materials Tailored by Carboxyl Groups for the Gas Phase-Conversion of Epoxide and CO2 into Cyclic Carbonates. *J Co2 Util* **2022**, *60*, 101976, doi:10.1016/j.jcou.2022.101976.

38. Sun, J.; Zhang, S.; Cheng, W.; Ren, J. Hydroxyl-Functionalized Ionic Liquid: A Novel Efficient Catalyst for Chemical Fixation of CO2 to Cyclic Carbonate. *Tetrahedron Lett* **2008**, *49*, 3588–3591, doi:10.1016/j.tetlet.2008.04.022.

39. Comin, E.; Aquino, A.S.; Favero, C.; Mignoni, M.L.; Souza, R.F. de; Souza, M.O. de; Pergher, S.B.C.; Campos, C.X. da S.; Bernardo-Gusmão, K. Cyclic Carbonate Synthesis via Cycloaddition of CO2 and Epoxides Catalysed by Beta Zeolites Containing Alkyl Imidazolium Ionic Liquids Used as Structure-Directing Agents. *Mol Catal* **2022**, *530*, 112624, doi:10.1016/j.mcat.2022.112624.

40. Hernández, E.; Santiago, R.; Moya, C.; Navarro, P.; Palomar, J. Understanding the CO2 Valorization to Propylene Carbonate Catalyzed by 1-Butyl-3-Methylimidazolium Amino Acid Ionic Liquids. *J Mol Liq* **2021**, *324*, 114782, doi:10.1016/j.molliq.2020.114782.

41. Wu, Y.; Chen, Z.; Zhang, X.; Chen, J.; Wang, Y.; Xu, J. Kinetic Study of CO2 Fixation into Propylene Carbonate with Water as Efficient Medium Using Microreaction System. *Chinese J Chem Eng* **2022**, *50*, 247–253, doi:10.1016/j.cjche.2022.05.019.

42. Shannon, M.S.; Bara, J.E. Properties of Alkylimidazoles as Solvents for CO2 Capture and Comparisons to Imidazolium-Based Ionic Liquids. *Ind Eng Chem Res* **2011**, *50*, 8665–8677, doi:10.1021/ie200259h.

43. Peng, J.; Deng, Y. Cycloaddition of Carbon Dioxide to Propylene Oxide Catalyzed by Ionic Liquids. *New J Chem* **2001**, *25*, 639–641, doi:10.1039/b008923k.

44. Girard, A.-L.; Simon, N.; Zanatta, M.; Marmitt, S.; Gonçalves, P.; Dupont, J. Insights on Recyclable Catalytic System Composed of Task-Specific Ionic Liquids for the Chemical Fixation of Carbon Dioxide. *Green Chem* **2014**, *16*, 2815–2825, doi:10.1039/c4gc00127c.

45. Li, W.; Cheng, W.; Yang, X.; Su, Q.; Dong, L.; Zhang, P.; Yi, Y.; Li, B.; Zhang, S. Synthesis of Cyclic Carbonate Catalyzed by DBU Derived Basic Ionic Liquids. *Chinese J Chem* **2018**, *36*, 293–298, doi:10.1002/cjoc.201700747.

46. Motokura, K.; Itagaki, S.; Iwasawa, Y.; Miyaji, A.; Baba, T. Silica -Supported Aminopyridinium Halides for Catalytic Transformations of Epoxides to Cyclic Carbonates under Atmospheric Pressure of Carbon Dioxide. *Green Chem.* **2009**, *11*, 1876–1880, doi:10.1039/b916764c.

47. Kumatabara, Y.; Okada, M.; Shirakawa, S. Triethylamine Hydroiodide as a Simple Yet Effective Bifunctional Catalyst for CO2 Fixation Reactions with Epoxides

under Mild Conditions. *ACS Sustain. Chem. Eng.* **2017**, *5*, 7295–7301, doi:10.1021/acssuschemeng.7b01535.

48. Rostami, A.; Mahmoodabadi, M.; Ebrahimi, A.H.; Khosravi, H.; Al-Harrasi, A. An Electrostatically Enhanced Phenol as a Simple and Efficient Bifunctional Organocatalyst for Carbon Dioxide Fixation. *ChemSusChem* **2018**, *11*, 4262–4268, doi:10.1002/cssc.201802028.

49. Kaneko, S.; Shirakawa, S. Potassium Iodide–Tetraethylene Glycol Complex as a Practical Catalyst for CO2 Fixation Reactions with Epoxides under Mild Conditions. *Acs Sustain Chem Eng* **2017**, *5*, 2836–2840, doi:10.1021/acssuschemeng.7b00324.

50. Butera, V.; Detz, H. Cyclic Carbonate Formation from Epoxides and CO2 Catalyzed by Sustainable Alkali Halide–Glycol Complexes: A DFT Study to Elucidate Reaction Mechanism and Catalytic Activity. *Acs Omega* **2020**, *5*, 18064–18072, doi:10.1021/acsomega.0c01572.

51. Metcalfe, I.S.; North, M.; Villuendas, P. Influence of Reactor Design on Cyclic Carbonate Synthesis Catalysed by a Bimetallic Aluminium(Salen) Complex. *J. CO2 Util.* **2013**, *2*, 24–28, doi:10.1016/j.jcou.2013.07.001.

52. Décultot, M.; Ledoux, A.; Fournier-Salaün, M.-C.; Estel, L. Solubility of CO2 in Methanol, Ethanol, 1,2-Propanediol and Glycerol from 283.15 K to 373.15 K and up to 6.0 MPa. *J. Chem. Thermodyn.* **2019**, *138*, 67–77, doi:10.1016/j.jct.2019.05.003.

53. Petropoulos, J.H.; Havredaki, V.I. On the Fundamental Concepts Underlying Henry-Law Adsorption and Adsorbed Gas Transport in Porous Solids. *J Chem Soc Faraday Transactions 1 Phys Chem Condens Phases* **1986**, *82*, 2531–2545, doi:10.1039/f19868202531.

54. Lévesque, F.; Seeberger, P.H. Highly Efficient Continuous Flow Reactions Using Singlet Oxygen as a “Green” Reagent. *Organic letters* **2011**, *13*, 5008–5011, doi:10.1021/ol2017643.

55. Ioannou, G.I.; Montagnon, T.; Kalaitzakis, D.; Pergantis, S.A.; Vassilikogiannakis, G. A Novel Nebulizer-Based Continuous Flow Reactor: Introducing the Use of Pneumatically Generated Aerosols for Highly Productive Photooxidations. *ChemPhotoChem* **2017**, *1*, 173–177, doi:10.1002/cptc.201600054.

56. Fallah-Araghi, A.; Meguellati, K.; Baret, J.-C.; Harrak, A.E.; Mangeat, T.; Karplus, M.; Ladame, S.; Marques, C.M.; Griffiths, A.D. Enhanced Chemical Synthesis at Soft Interfaces: A Universal Reaction-Adsorption Mechanism in Microcompartments. *Physical Review Letters* **2014**, *112*, 3–5, doi:10.1103/physrevlett.112.028301.

57. Cooks, R.G.; Yan, X. Mass Spectrometry for Synthesis and Analysis. *Annual Review of Analytical Chemistry* **2018**, *11*, 1–28, doi:10.1146/annurev-anchem-061417-125820.

58. Yan, X. Emerging Microdroplet Chemistry for Synthesis and Analysis. *Int J Mass Spectrom* **2021**, *468*, 116639, doi:10.1016/j.ijms.2021.116639.

59. Wei, Z.; Li, Y.; Cooks, R.G.; Yan, X. Accelerated Reaction Kinetics in Microdroplets: Overview and Recent Developments. *Annu. Rev. Phys. Chem.* **2020**, *71*, 31–51, doi:10.1146/annurev-physchem-121319-110654.

60. Urbani, D.; Rovegno, C.; Massi, A.; Leblebici, M.E.; Kayahan, E.; Polo, E.; Dambruoso, P. Efficiency in CO2-Utilization Strategies: The Case of Styrene Carbonate Synthesis in Microdroplets Conditions. *J Co2 Util* **2023**, *67*, 102328, doi:10.1016/j.jcou.2022.102328.

61. Martinez, A.S.; Hauzenberger, C.; Sahoo, A.R.; Csendes, Z.; Hoffmann, H.; Bica, K. Continuous Conversion of Carbon Dioxide to Propylene Carbonate with Supported Ionic Liquids. *Acs Sustain Chem Eng* **2018**, *6*, 13131–13139, doi:10.1021/acssuschemeng.8b02627.

62. Bui, T.Q.; Konwar, L.J.; Samikannu, A.; Nikjoo, D.; Mikkola, J.-P. Mesoporous Melamine-Formaldehyde Resins as Efficient Heterogeneous Catalysts for Continuous Synthesis of Cyclic Carbonates from Epoxides and Gaseous CO2. *Acs Sustain Chem Eng* **2020**, *8*, 12852–12869, doi:10.1021/acssuschemeng.0c03123.

63. Zanda, N.; Sobolewska, A.; Alza, E.; Kleij, A.W.; Pericàs, M.A. Organocatalytic and Halide-Free Synthesis of Glycerol Carbonate under Continuous Flow. *Acs Sustain Chem Eng* **2021**, *9*, 4391–4397, doi:10.1021/acssuschemeng.1c01060.

64. Hou, J.; Ee, A.; Cao, H.; Ong, H.; Xu, J.; Wu, J. Visible-Light-Mediated Metal-Free Difunctionalization of Alkenes with CO2 and Silanes or C(Sp3)−H Alkanes. *Angew. Chem. Int. Ed.* **2018**, *57*, 17220–17224, doi:10.1002/anie.201811266.

65. Wu, X.; Wang, M.; Xie, Y.; Chen, C.; Li, K.; Yuan, M.; Zhao, X.; Hou, Z. Carboxymethyl Cellulose Supported Ionic Liquid as a Heterogeneous Catalyst for the Cycloaddition of CO2 to Cyclic Carbonate. *Appl Catal Gen* **2016**, *519*, 146–154, doi:10.1016/j.apcata.2016.04.002.

66. Sathe, A.A.; Nambiar, A.M.K.; Rioux, R.M. Synthesis of Cyclic Organic Carbonates via Catalytic Oxidative Carboxylation of Olefins in Flow Reactors. *Catal Sci Technol* **2016**, *7*, 84–89, doi:10.1039/c6cy01974a.

67. Rigo, D.; Calmanti, R.; Perosa, A.; Selva, M.; Fiorani, G. Diethylene Glycol/NaBr Catalyzed CO2 Insertion into Terminal Epoxides: From Batch to Continuous Flow. *Chemcatchem* **2021**, *13*, 2005–2016, doi:10.1002/cctc.202002010.

68. Wu, Y.; Chen, A.; Liu, X.; Xu, J.; Wang, Y.; Mumford, K.; Stevens, G.W.; Fei, W. Kinetic Study of Highly Efficient CO2 Fixation into Propylene Carbonate Using a Continuous-Flow Reactor. *Chem Eng Process - Process Intensif* **2021**, *159*, 108235, doi:10.1016/j.cep.2020.108235.

69. North, M.; Villuendas, P.; Young, C. A Gas-Phase Flow Reactor for Ethylene Carbonate Synthesis from Waste Carbon Dioxide. *Chem European J* **2009**, *15*, 11454–11457, doi:10.1002/chem.200902436.

70. Zhao, Y.; Yao, C.; Chen, G.; Yuan, Q. Highly Efficient Synthesis of Cyclic Carbonate with CO 2 Catalyzed by Ionic Liquid in a Microreactor. *Green Chem* **2012**, *15*, 446–452, doi:10.1039/c2gc36612f.

71. Wu, Y.; Ding, Y.; Xu, J.; Wang, Y.; Mumford, K.; Stevens, G.W.; Fei, W. Efficient Fixation of CO2 into Propylene Carbonate with [BMIM]Br in a Continuous-Flow Microreaction System. *Green Energy Environ* **2021**, *6*, 291–297, doi:10.1016/j.gee.2020.04.016.

72. Kozak, J.A.; Wu, J.; Su, X.; Simeon, F.; Hatton, T.A.; Jamison, T.F. Bromine-Catalyzed Conversion of CO2 and Epoxides to Cyclic Carbonates under Continuous Flow Conditions. *J Am Chem Soc* **2013**, *135*, 18497–18501, doi:10.1021/ja4079094.

73. Zhang, X.; Su, D.; Xiao, L.; Wu, W. Immobilized Protic Ionic Liquids: Efficient Catalysts for CO2 Fixation with Epoxides. *J Co2 Util* **2017**, *17*, 37–42, doi:10.1016/j.jcou.2016.11.005.

74. Rehman, A.; Fernández, A.M.L.; Resul, M.F.M.G.; Harvey, A. Kinetic Investigations of Styrene Carbonate Synthesis from Styrene Oxide and CO2 Using a Continuous Flow Tube-in-Tube Gas-Liquid Reactor. *J Co2 Util* **2018**, *24*, 341–349, doi:10.1016/j.jcou.2018.02.001.

75. Seo, H.; Katcher, M.H.; Jamison, T.F. Photoredox Activation of Carbon Dioxide for Amino Acid Synthesis in Continuous Flow. *Nat Chem* **2017**, *9*, 453–456, doi:10.1038/nchem.2690.

76. Wang, T.; Wang, W.; Lyu, Y.; Chen, X.; Li, C.; Zhang, Y.; Song, X.; Ding, Y. Highly Recyclable Polymer Supported Ionic Liquids as Efficient Heterogeneous Catalysts for Batch and Flow Conversion of CO 2 to Cyclic Carbonates. *Rsc Adv* **2017**, *7*, 2836–2841, doi:10.1039/c6ra26780g.

77. James, B.R.; Boissonnault, J.A.; Wong-Foy, A.G.; Matzger, A.J.; Sanford, M.S. Structure Activity Relationships in Metal–Organic Framework Catalysts for the Continuous Flow Synthesis of Propylene Carbonate from CO 2 and Propylene Oxide. *Rsc Adv* **2018**, *8*, 2132–2137, doi:10.1039/c7ra13245j.

78. Zanda, N.; Primitivo, L.; Chaudhari, M.; Kleij, A.W.; Pericàs, M.À. Organocatalytic N -Formylation of Amines by CO 2 in Batch and Continuous Flow. *Org Chem Front* **2022**, doi:10.1039/d2qo01711c.

79. Wu, J.; Kozak, J.A.; Simeon, F.; Hatton, T.A.; Jamison, T.F. Mechanism-Guided Design of Flow Systems for Multicomponent Reactions: Conversion of CO 2 and Olefins to Cyclic Carbonates. *Chem Sci* **2014**, *5*, 1227–1231, doi:10.1039/c3sc53422g.

80. Zanda, N.; Zhou, L.; Alza, E.; Kleij, A.W.; Pericàs, M.À. Continuous Organocatalytic Flow Synthesis of 2-Substituted Oxazolidinones Using Carbon Dioxide. *Green Chem* **2022**, *24*, 4628–4633, doi:10.1039/d2gc00503d.

81. Johnson, M.D.; May, S.A.; Kopach, M.E.; Groh, J.M.; Braden, T.; Shankarraman, V.; Merritt, J.M. Chemical Engineering in the Pharmaceutical Industry. **2019**, 367–385, doi:10.1002/9781119600800.ch16.

82. Seo, H.; Nguyen, L.V.; Jamison, T.F. Using Carbon Dioxide as a Building Block in Continuous Flow Synthesis. *Adv. Synth. Catal.* **2019**, *361*, 247–264, doi:10.1002/adsc.201801228.

83. Rehman, A.; Saleem, F.; Javed, F.; Ikhlaq, A.; Ahmad, S.W.; Harvey, A. Recent Advances in the Synthesis of Cyclic Carbonates via CO2 Cycloaddition to Epoxides. *J Environ Chem Eng* **2021**, *9*, 105113, doi:10.1016/j.jece.2021.105113.

84. Chaudhuri, A.; Kuijpers, K.P.L.; Hendrix, R.B.J.; Shivaprasad, P.; Hacking, J.A.; Emanuelsson, E.A.C.; Noël, T.; Schaaf, J. van der Process Intensification of a Photochemical Oxidation Reaction Using a Rotor-Stator Spinning Disk Reactor: A Strategy for Scale Up. *Chem Eng J* **2020**, *400*, 125875, doi:10.1016/j.cej.2020.125875.

85. Yan, X.; Lai, Y.-H.; Zare, R.N. Preparative Microdroplet Synthesis of Carboxylic Acids from Aerobic Oxidation of Aldehydes. **2018**, *9*, 5207–5211, doi:10.1039/c8sc01580e.

86. Ioannou, G.I.; Montagnon, T.; Kalaitzakis, D.; Pergantis, S.A.; Vassilikogiannakis, G. Synthesis of Cyclopent-2-Enones from Furans Using a Nebulizer-Based Continuous Flow Photoreactor. *Organic & Biomolecular Chemistry* **2017**, *15*, 10151–10155, doi:10.1039/c7ob02557b.

87. Kayahan, E.; Urbani, D.; Dambruoso, P.; Massi, A.; Braeken, L.; Gerven, T.V.; Leblebici, M.E. Overcoming Mass and Photon Transfer Limitations in a Scalable Reactor: Oxidation in an Aerosol Photoreactor. *Chem Eng J* **2021**, *408*, 127357, doi:10.1016/j.cej.2020.127357.

88. Huang, K.-H.; Wei, Z.; Cooks, R.G. Accelerated Reactions of Amines with Carbon Dioxide Driven by Superacid at the Microdroplet Interface. *Chem. Sci.* **2020**, *12*, 2242–2250, doi:10.1039/d0sc05625a.

89. Li, C.; Ma, C.; Wang, F.; Xi, Z.; Wang, Z.; Deng, Y.; He, N. Preparation and Biomedical Applications of Core–Shell Silica/Magnetic Nanoparticle Composites. *J Nanosci Nanotechno* **2012**, *12*, 2964–2972, doi:10.1166/jnn.2012.6428.

90. Joo, S.H.; Park, J.Y.; Tsung, C.-K.; Yamada, Y.; Yang, P.; Somorjai, G.A. Thermally Stable Pt/Mesoporous Silica Core–Shell Nanocatalysts for High-Temperature Reactions. *Nat Mater* **2009**, *8*, 126–131, doi:10.1038/nmat2329.

91. Sun, Y.; Duan, L.; Guo, Z.; DuanMu, Y.; Ma, M.; Xu, L.; Zhang, Y.; Gu, N. An Improved Way to Prepare Superparamagnetic Magnetite-Silica Core-Shell Nanoparticles for Possible Biological Application. *J Magn Magn Mater* **2005**, *285*, 65–70, doi:10.1016/j.jmmm.2004.07.016.

92. Astruc, D.; Lu, F.; Aranzaes, J.R. Nanoparticles as Recyclable Catalysts: The Frontier between Homogeneous and Heterogeneous Catalysis. *Angewandte Chemie International Edition* **2005**, *44*, 7852–7872, doi:10.1002/anie.200500766.

93. Cannas, C.; Musinu, A.; Piccaluga, G.; Fiorani, D.; Peddis, D.; Rasmussen, H.K.; Mørup, S. Magnetic Properties of Cobalt Ferrite–Silica Nanocomposites Prepared by a Sol-Gel Autocombustion Technique. *J Chem Phys* **2006**, *125*, 164714, doi:10.1063/1.2354475.

94. Meng, X.; Ju, Z.; Zhang, S.; Liang, X.; Solms, N. von; Zhang, X.; Zhang, X. Efficient Transformation of CO 2 to Cyclic Carbonates Using Bifunctional Protic Ionic Liquids under Mild Conditions. *Green Chem* **2019**, *21*, 3456–3463, doi:10.1039/c9gc01165j.

95. Galvan, M.; Selva, M.; Perosa, A.; Noè, M. Toward the Design of Halide- and Metal-Free Ionic-Liquid Catalysts for the Cycloaddition of CO2 to Epoxides. *Asian J Org Chem* **2014**, *3*, 504–513, doi:10.1002/ajoc.201402044.

96. Sheldon, R.A. Fundamentals of Green Chemistry: Efficiency in Reaction Design. *Chemical Society Reviews* **2012**, *41*, 1437–1451, doi:10.1039/c1cs15219j.

97. Luo, K.; Li, J.; Cao, Y.; Liu, C.; Ge, J.; Chen, H.; Zare, R.N. Reaction of Chloroauric Acid with Histidine in Microdroplets Yields a Catalytic Au–(His) 2 Complex. *Chem Sci* **2020**, *11*, 2558–2565, doi:10.1039/c9sc06221a.

98. Wei, Z.; Wleklinski, M.; Ferreira, C.; Cooks, R.G. Reaction Acceleration in Thin Films with Continuous Product Deposition for Organic Synthesis. *Angewandte Chemie International Edition* **2017**, *56*, 9386–9390, doi:10.1002/anie.201704520.

99. Poletti, L.; Rovegno, C.; Carmine, G.D.; Vacchi, F.; Ragno, D.; Brandolese, A.; Massi, A.; Dambruoso, P. Efficiency in Carbon Dioxide Fixation into Cyclic Carbonates: Operating Bifunctional Polyhydroxylated Pyridinium Organocatalysts in Segmented Flow Conditions. *Molecules* **2023**, *28*, 1530, doi:10.3390/molecules28041530.

100. Shi, T.-Y.; Wang, J.-Q.; Sun, J.; Wang, M.-H.; Cheng, W.-G.; Zhang, S.-J. Efficient Fixation of CO 2 into Cyclic Carbonates Catalyzed by Hydroxyl-Functionalized Poly(Ionic Liquids). *Rsc Adv* **2013**, *3*, 3726–3732, doi:10.1039/c3ra21872d.

101. Sun, J.; Wang, J.; Cheng, W.; Zhang, J.; Li, X.; Zhang, S.; She, Y. Chitosan Functionalized Ionic Liquid as a Recyclable Biopolymer -Supported Catalyst for Cycloaddition of CO 2. *Green Chem* **2012**, *14*, 654–660, doi:10.1039/c2gc16335g.

102. Sun, J.; Han, L.; Cheng, W.; Wang, J.; Zhang, X.; Zhang, S. Efficient Acid–Base Bifunctional Catalysts for the Fixation of CO2 with Epoxides under Metal- and Solvent-Free Conditions. *Chemsuschem* **2011**, *4*, 502–507, doi:10.1002/cssc.201000305.

103. Sun, J.; Cheng, W.; Fan, W.; Wang, Y.; Meng, Z.; Zhang, S. Reusable and Efficient Polymer-Supported Task-Specific Ionic Liquid Catalyst for Cycloaddition of Epoxide with CO2. *Catal Today* **2009**, *148*, 361–367, doi:10.1016/j.cattod.2009.07.070.

104. Sun, J.; Ren, J.; Zhang, S.; Cheng, W. Water as an Efficient Medium for the Synthesis of Cyclic Carbonate. *Tetrahedron Lett* **2009**, *50*, 423–426, doi:10.1016/j.tetlet.2008.11.034.

105. Gou, H.; Ma, X.; Su, Q.; Liu, L.; Ying, T.; Qian, W.; Dong, L.; Cheng, W. Hydrogen Bond Donor Functionalized Poly(Ionic Liquid)s for Efficient Synergistic Conversion of CO 2 to Cyclic Carbonates. *Phys Chem Chem Phys* **2020**, *23*, 2005–2014, doi:10.1039/d0cp06041k.

106. Wu, Y.; Ding, Y.; Xu, J.; Wang, Y.; Mumford, K.; Stevens, G.W.; Fei, W. Efficient Fixation of CO2 into Propylene Carbonate with [BMIM]Br in a Continuous-Flow Microreaction System. *Green Energy Environ* **2021**, *6*, 291–297, doi:10.1016/j.gee.2020.04.016.

107. Sela, T.; Vigalok, A. Organic Synthesis “on Water” vs “on Liquids”: A Comparative Analysis. *Org Lett* **2014**, *16*, 1964–1967, doi:10.1021/ol500518n.

108. Acevedo, O.L.; Andrews, R.S. Synthesis of Propane-2,3-Diol Combinatorial Monomers. *Tetrahedron Lett* **1996**, *37*, 3931–3934, doi:10.1016/0040-4039(96)00745-9.

109. Pereira, M.P.; Martins, R. de S.; Oliveira, M.A.L. de; Bombonato, F.I. Amino Acid Ionic Liquids as Catalysts in a Solvent-Free Morita–Baylis–Hillman Reaction. *Rsc Adv* **2018**, *8*, 23903–23913, doi:10.1039/c8ra02409j.

110. Bajwa, J.S.; Anderson, R.C. A Highly Regioselective Conversion of Epoxides to Halohydrins by Lithium Halides. *Tetrahedron Lett* **1991**, *32*, 3021–3024, doi:10.1016/0040-4039(91)80676-w.

111. Massi, A.; Cavazzini, A.; Zoppo, L.D.; Pandoli, O.; Costa, V.; Pasti, L.; Giovannini, P.P. Toward the Optimization of Continuous-Flow Aldol and Î±-Amination Reactions by Means of Proline-Functionalized Silicon Packed-Bed Microreactors. *Tetrahedron letters* **2011**, *52*, 619–622, doi:10.1016/j.tetlet.2010.11.157.

112. Bortolini, O.; Caciolli, L.; Cavazzini, A.; Costa, V.; Greco, R.; Massi, A.; Pasti, L. Silica-Supported 5-(Pyrrolidin-2-Yl)Tetrazole : Development of Organocatalytic Processes from Batch to Continuous-Flow Conditions. *Green Chem* **2012**, *14*, 992–1000, doi:10.1039/c2gc16673a.

113. Bortolini, O.; Cavazzini, A.; Giovannini, P.P.; Greco, R.; Marchetti, N.; Massi, A.; Pasti, L. A Combined Kinetic and Thermodynamic Approach for the Interpretation of Continuous-Flow Heterogeneous Catalytic Processes. *Chem European J* **2013**, *19*, 7802–7808, doi:10.1002/chem.201300181.

114. Greco, R.; Caciolli, L.; Zaghi, A.; Pandoli, O.; Bortolini, O.; Cavazzini, A.; Risi, C.D.; Massi, A. A Monolithic 5-(Pyrrolidin-2-Yl)Tetrazole Flow Microreactor for the Asymmetric Aldol Reaction in Water–Ethanol Solvent. *React Chem Eng* **2015**, *1*, 183–193, doi:10.1039/c5re00017c.

115. Ragno, D.; Carmine, G.D.; Brandolese, A.; Bortolini, O.; Giovannini, P.P.; Massi, A. Immobilization of Privileged Triazolium Carbene Catalyst for Batch and Flow Stereoselective Umpolung Processes. *Acs Catal* **2017**, *7*, 6365–6375, doi:10.1021/acscatal.7b02164.

116. Warias, R.; Zaghi, A.; Heiland, J.J.; Piendl, S.K.; Gilmore, K.; Seeberger, P.H.; Massi, A.; Belder, D. An Integrated Lab-on-a-chip Approach to Study Heterogeneous Enantioselective Catalysts at the Microscale. *Chemcatchem* **2018**, *10*, 5382–5385, doi:10.1002/cctc.201801637.

117. Warias, R.; Ragno, D.; Massi, A.; Belder, D. A Visible-Light-Powered Polymerization Method for the Immobilization of Enantioselective Organocatalysts into Microreactors. *Chem European J* **2020**, *26*, 13152–13156, doi:10.1002/chem.202002063.

118. Risi, C.D.; Bortolini, O.; Brandolese, A.; Carmine, G.D.; Ragno, D.; Massi, A. Recent Advances in Continuous-Flow Organocatalysis for Process Intensification. *React Chem Eng* **2020**, *5*, 1017–1052, doi:10.1039/d0re00076k.

119. Ragno, D.; Leonardi, C.; Carmine, G.D.; Bortolini, O.; Brandolese, A.; Risi, C.D.; Massi, A. Regiodivergent Isosorbide Acylation by Oxidative N-Heterocyclic Carbene Catalysis in Batch and Continuous Flow. *Acs Sustain Chem Eng* **2021**, *9*, 8295–8305, doi:10.1021/acssuschemeng.1c02765.

120. Bortolini, O.; Fantin, G.; Fogagnolo, M.; Giovannini, P.P.; Massi, A.; Pacifico, S. Thiazolium-Catalyzed Intermolecular Stetter Reaction of Linear and Cyclic Alkyl α-Diketones. *Organic & Biomolecular Chemistry* **2011**, *9*, 8437, doi:10.1039/c1ob06480k.

121. Leonardi, C.; Brandolese, A.; Preti, L.; Bortolini, O.; Polo, E.; Dambruoso, P.; Ragno, D.; Carmine, G.D.; Massi, A. Expanding the Toolbox of Heterogeneous Asymmetric Organocatalysts: Bifunctional Cyclopropenimine Superbases for Enantioselective Catalysis in Batch and Continuous Flow. *Adv. Synth. Catal.* **2021**, *363*, 5473–5485, doi:10.1002/adsc.202100757.

122. Westphal, H.; Warias, R.; Becker, H.; Spanka, M.; Ragno, D.; Gläser, R.; Schneider, C.; Massi, A.; Belder, D. Unveiling Organocatalysts Action – Investigating Immobilized Catalysts at Steady-State Operation via Lab-on-a-Chip Technology. *Chemcatchem* **2021**, *13*, 5089–5096, doi:10.1002/cctc.202101148.

123. Westphal, H.; Warias, R.; Weise, C.; Ragno, D.; Becker, H.; Spanka, M.; Massi, A.; Gläser, R.; Schneider, C.; Belder, D. An Integrated Resource-Efficient Microfluidic Device for Parallelised Studies of Immobilised Chiral Catalysts in Continuous Flow via Miniaturized LC/MS-Analysis. *React Chem Eng* **2022**, *7*, 1936–1944, doi:10.1039/d2re00153e.

124. Cannas, C.; Musinu, A.; Ardu, A.; Orrù, F.; Peddis, D.; Casu, M.; Sanna, R.; Angius, F.; Diaz, G.; Piccaluga, G. CoFe 2 O 4 and CoFe 2 O 4 /SiO 2 Core/Shell Nanoparticles: Magnetic and Spectroscopic Study. *Chem Mater* **2010**, *22*, 3353–3361, doi:10.1021/cm903837g.

125. Rahimi, J.; Mirmohammadi, S.S.; Maleki, A. Trihydrazinotriazine-Grafting Fe3O4/SiO2 Core-Shell Nanoparticles with Expanded Porous Structure for Organic

Reactions. *Front Chem Sci Eng* **2021**, *15*, 1008–1020, doi:10.1007/s11705-020-1996-8.

126. Mer, V.K.L. Nucleation in Phase Transitions. *Industrial Eng Chem* **1952**, *44*, 1270–1277, doi:10.1021/ie50510a027.

127. Peddis, D.; Cannas, C.; Musinu, A.; Ardu, A.; Orrù, F.; Fiorani, D.; Laureti, S.; Rinaldi, D.; Muscas, G.; Concas, G.; et al. Beyond the Effect of Particle Size: Influence of CoFe2O4 Nanoparticle Arrangements on Magnetic Properties. *Chem Mater* **2013**, *25*, 2005–2013, doi:10.1021/cm303352r.

128. Peddis, D.; Orrù, F.; Ardu, A.; Cannas, C.; Musinu, A.; Piccaluga, G. Interparticle Interactions and Magnetic Anisotropy in Cobalt Ferrite Nanoparticles: Influence of Molecular Coating. *Chem Mater* **2012**, *24*, 1062–1071, doi:10.1021/cm203280y.